LIQUID CROSS-FLOW-INDUCED VIBRATIONS OF A TUBE-ARRAY

by

© DIMITRIS KOROYANNAKIS, B.A.Sc. (Eng.) Hons.

A Thesis

Submitted to the School of Graduate Studies

in Partial Fulfilment of the Requirements

for the Degree

Master of Engineering

McMaster University

December 1980

TO MY KIND PARENTS

MASTER OF ENGINEERING (1980) McMaster University
(Mechanical Engineering) Hamilton, Ontario

TITLE: Liquid Cross-Flow-Induced Vibration of a Tube-array

AUTHOR: Dimitris Koroyannakis, B.A.Sc. (Eng.) Hons.
University of Wales
University College,
Cardiff

SUPERVISOR: Dr. D.S. Weaver

NUMBER OF PAGES: (xi),165

ABSTRACT

Modern tube and shell heat exchangers designed with the existing standards may be susceptible to damage as a result of excessive tube vibrations caused by the shell-side flow. The present study was undertaken to further our understanding of the liquid cross-flow-induced vibrations of a tube array of contemporary interest.

An experimental facility to study these phenomena was designed and built. The experiments were conducted using this specially designed water tunnel having a 305 x 305 mm working section. The tube bundle was a parallel-triangular array with pitch to diameter ratio of 1.375. The array was 6 rows deep with 5 tubes in each row. Ten tubes at the centre of the array were designed to be flexibly mounted. The natural frequency and damping of these tubes could be controlled over a range of values. The rest of the tubes were rigidly fixed in the test section.

The critical velocity for instability of tubes located in the third and fourth rows was established and the stability for the array was determined. The present results indicate that extrapolation of the stability boundary proposed from results obtained in wind tunnels, for arrays of the same geometry yield unconservative predictions. A study of the flow velocity power spectra indicate that no flow periodicity could be detected in the flow before the critical velocity was reached.

Detuning of adjacent tubes was proven to have little effect on the stability threshold of a tube located in the third row.

The results of the present study were compared with data in the published literature. It is seen that the present results lie below the majority of the proposed stability boundaries.

ACKNOWLEDGEMENTS

The author wishes to express his sincere gratitude to his friend and supervisor Dr. D.S. Weaver for suggesting the problem. His constant encouragement and advice, often extended beyond the scope of this work, are greatly appreciated.

The author is also grateful to the late Dr. S. El Shammaa for the use of his computer software.

The kind help and advice of the Departmental technicians, Mr. Dave Schick and Mr. Frank Drieman are gratefully acknowledged. Thanks are also due to Ms. Betty Anne Bedell for her excellent typing of the manuscript.

The financial support provided through the Natural Science and Engineering Research Council Operating Grant A 8284 is greatly appreciated.

TABLE OF CONTENTS

LIST OF FIGURES

CHAPTER 1

INTRODUCTION

Flow-induced vibration problems in heat exchangers have increased considerably in recent years as contemporary designs tend to become more energy efficient demanding larger size equipment, higher operating flows and temperatures, the use of exotic heat transport fluids, etc. A number of recent publications [2], [68], [69] have described field experiences in which heat exchanger equipment failures due to excessive vibrations have been recorded. These vibrations are often the result of an effort to increase the equipment performance by increasing the mass flow. The use of modern high strength materials together with smaller diameter tubes result in a reduction of structural rigidity which aggravates the problem. Such vibrations cause fretting and fatigue failure in the tubes at the tube sheets and baffles as well as mid-span leaks due to tube-to-tube clashing.

Failures can often result in the mixing of shell-side and tube-side fluids, creating contamination hazards. The cost of heat transfer fluids alone, such as the heavy water used in the Canadian CANDU reactors for example, makes such failures unacceptable. Repairs of these failures are often very expensive. Specialized repair techniques are usually required, such as remote operations, in view of the hostile radioactive environment in which this equipment operates.

Capital losses are also encountered due to the production loss while repairs are in progress.

In a recent study published by Ontario Hydro [69], covering a five year period (1975-1979), heat exchangers contributed 3% of the nuclear generating stations' incapability factor, while the value for all causes was 20.7%. In 1979 alone, heat exchangers accounted for 4.9% while the value for all causes was 20.6%. This amounts to 2,300 G.W.h. lost production out of 9,800 G.W.h. for all causes, or 23.5% of the lost production was due to heat exchanger problems. This percentage was considered too high, considering the quantity and complexity of all other equipment in modern nuclear power stations, and the improvement of heat exchanger performance is currently considered a high priority target calling for more fundamental work to understand the phenomena involved.

Flow-induced vibrations continue to occur because their prevention is usually a secondary design criterion. In addition, our knowledge of the involved mechanisms is still far from sufficient to allow us to design successfully in all cases. In view of the enormous costs involved during repair shut-downs, very little is learned of the nature of the mechanisms involved when a remedy "solution" is attempted to eliminate an existing problem. It also appears that there is poor communication with other engineering fields where flow-induced vibration problems are commonly encountered.

During the last decade, a considerable technical literature in the area of flow-induced vibration has developed.

The large variety of array patterns, tube bundle sizes and proposed excitation mechanisms have resulted in considerable confusion, while a large number of questions remain unanswered. A number of literature reviews [2], [3], [12], [14] have been published in an effort to clarify the state of knowledge and indicate the potentially important areas for future research activities.

It is now generally accepted that there are four basic mechanisms causing vibrations:

(a) Flow periodicity resonances,

(b) Acoustic resonance,

(c) Response to turbulent buffeting, and

(d) Fluidelastic excitation.

The first three mechanisms result in forced vibration by the flow field, while the fourth more important mechanism is of a self-excited nature. At sufficiently high flow velocities, the tubes develop an instability called fluidelastic whirling and severe damage may result in a relatively short time.

The research of Connors [34] was the first to establish the nature of the fluidelastic mechanism on a single row of circular cylinders. Connors established a fluidelastic stability boundary based on an elementary theory and on wind tunnel tests to determine quasi-static fluid force coefficients. Connors' work was further generalized by Blevins [35] and, despite the absence of solid experimental data, his theory formed the basis for the design against fluidelastic excitation

in heat exchangers. However more recent experimental evidence questioned the validity of Connors' theory as applied to tube arrays. One of Blevins' assumptions was that fluid forces on a tube are only dependent on the relative displacements of the two nearest tubes. Weaver and Grover [38] have shown, using wind tunnel tests, that this is not true, i.e., a single tube can become unstable in a rigid tube bank. Similarly Weaver and Grover [38] have shown that the reduced velocity depended on damping to the power of 0.21 rather than 0.5 as implied by Connors' theory. A number of other questions were raised relating to the validity of Connors' theory for tube arrays and are discussed in more detail in the second chapter of the present study. When a heavy fluid such as water for example, is used as the shell-side fluid, parameters like the "added" mass and fluid coupling which can be neglected in gas flows, become very significant. In view of the significant scatter in the data reported in the literature, the question whether the presently existing stability criteria can accurately predict the stability boundary of any given tube array still remains.

The purpose of the present study is to develop an experimental facility and a representative model of a tube array to permit the investigation of the various mechanisms involved in liquid cross-flow-induced vibrations in tube arrays.

Of particular interest are:

(a) The stability threshold of the array.

(b) The tubes' frequency response and flow periodicity measurements.

(c) The effect of detuning all adjacent tubes on the stability threshold of a tube in the array.

(d) A comparison of these results with those of similar arrays in gas flows.

It is hoped that the present research and development will provide a facility for future experiments and help improve our understanding of the complex phenomena involved with liquid cross-flow-induced vibration mechanisms of tube arrays of contemporary interest.

CHAPTER 2

LITERATURE SURVEY OF FLOW INDUCED VIBRATION

Flow induced vibration problems of structures involve the mutual interaction among the elastic and inertial forces of the structure and the fluid forces. The exact determination of the nature of the interaction and the magnitude of the fluid forces is often difficult, since flow-induced vibration phenomena are relatively complex and diverse and, often the excitation mechanisms are not well understood. This field finds its applications in the areas of tube vibrations, in heat exchangers and steam generators [1], [2], [3], in problems related to vibration and fretting in nuclear fuel assemblies [4], vibrations of hydraulic components and structures [5], [6] and in the areas of naval and space science [7], [8]. Wind effects on buildings and structures [7] is another area in which flow-induced vibrations are of importance.

The technical literature in the field is expanding rapidly and is scattered throughout a wide variety of journals due to the diverse nature of the flow-induced vibration phenomena. A few general papers [10], [11] have been written attempting to classify the hydroelastic instability phenomena by their common flow instability mechanisms. However most of the flow-induced vibrations can be characterized as (a) dynamic response, (b) self-controlled and (c) self excited vibrations.

Dynamic response problems are forced vibrations induced

by turbulence or pressure fluctuations in the flow or by fluid impact. Response of tall buildings to ground boundary layer turbulence or aircraft response to wind gusts are problems of practical interest. Their solutions rely on the use of statistical techniques to determine the force field. Once the forcing function is known the analysis is relatively straightforward. Additional examples are the response of aircraft panels to jet noise. The dynamic response of a pipe transporting fluids, the dynamic response of a marine vehicle which operates at the interface between air and water and is subjected to complex and difficult to analyze loading conditions, etc. These motions are usually random in nature and a necessary condition for this class of response problems is that the motion of the structure has no appreciable effect on the fluid forces.

In self-controlled vibrations, some periodicity exists in the flow. If this periodicity coincides with one of the natural frequencies of the structure, resonance will occur. As a result the vibration of the structure builds up to the point where the magnitude and the frequency of the fluid forces are now controlled by the motion of the structure. Hence a dynamic feedback mechanism develops. The velocity range in which the periodicity in the flow is controlled by the motion of the structure is called the "lock-in" region and is affected by the structural damping. The most common source of periodicity in the flow is the vortex-shedding phenomenon. The shedding of a vortex, in the wake of a bluff body, results from the separation of a

free shear layer from each side of it. Vortex-shedding can also cause acoustic resonance which results in structural loading and noise generation. The most obvious examples of this class of vibration are the vibrations of smokestacks, submarine periscopes, turbine blade vibrations, etc. In all these problems, mutual interaction exists between inertial and elastic forces of the structure, with an already existing flow periodicity. Such vibrations can be prevented by additional stiffening or damping of the structure as well as by some geometrical change which would destroy the periodicity in the flow.

Self-excited vibrations are produced when the motion of the structure itself results in periodicty of the fluid forces which in turn amplify the structure's motion. These vibrations are distinguished from those of the self-controlled type in that the periodicty in the fluid forces disappears in the absence of structural motion. Examples of self-excited vibrations are the oscillations of gate seals, vibration of vertical lift gates, and the hydroelastic vibration of swing check valves.

In the field of dynamic aeroelasticity, problems such as the "flutter" of plates and shells and the galloping of transmission lines are typical examples of self-excited vibrations. Both self-controlled and self-excited vibrations are termed as fluidelastic vibrations since they involve the mutual interaction of elastic and inertial forces with the fluid forces.

The development of mathematical models for the analysis of fluid-structure interaction problems concentrates on the

following disciplines:

(a) theory of elasticity,

(b) theory of fluid mechanics,

(c) mechanical vibrations and,

(d) mathematical stability theory.

The determination of the so called structural operators, inertial operators, and fluid dynamic operators becomes necessary for the formulation of the equations of fluidelasticity. The adequacy of formulating these equations depends on the degree to which the mechanism itself is understood.

The major difficulty of fluidelasticity is focussed around the determination of the fluid dynamic operators because of the often nonlinear and/or stochastic nature of these operators.

Since only in a limited number of simplified and usually idealized problems we are able to obtain exact solutions for our mathematical models, it becomes essential that we employ experimental methods to determine the solution of fluid-elastic phenomena encountered in modern designs and which do not yield to analytical solutions. Dimensional analysis and similitude theory are often used to analyze very complex phenomena and are of considerable help in setting up experiments.

The needed experimental information is usually in the form of fluid-dynamic coefficients, stability thresholds, pressure distribution, flow-visualization, velocity profiles, amplitude-frequency-phase of oscillations, etc.

To study the response and stability of such dynamic models, we commonly employ wind tunnels, water tunnels, two-phase

flow loops, etc. An example to demonstrate the combination of various flow regimes and possible simultaneous existence of all different types of excitation mechanisms of flow-induced vibrations in a single component is presented below.

The flow regime within a recirculating type steam generator, of a typical CANDU-PHW nuclear power station, such as the one shown in Fig.(2.1) can be complex. Heavy water flow inside the tubes varies from 5% steam quality to subcooled liquid. The tubes are subjected to liquid cross-flow in the preheater section and in the recirculated water entrance region near the tubesheet. Within the tube bundle the shell side flow is mostly axial. It is liquid at the bottom and gradually becomes two-phase, reaching 15-20% steam quality at the top. Two-phase cross flow is predominant in the "U" bend tube region. In heat exchangers the tubes are often subjected to cross-flow particularly near inlets and outlets where flow velocities are generally high. Thus it can be seen that depending on the flow consideration, vibration problems in steam generators and/or heat exchangers can be induced by (a) internal axial (pipe) flow, (b) external axial flow, (c) cross-flow single or two-phase flow and (d) annular and leakage flow.

In very few cases is the fluid stream a truly axial or cross flow; nevertheless, for most studies in the field, the idealization that the flow is purely axial or normal to the cylinder array is made. This is fully justifiable for the purposes of research into the phenomena involved.

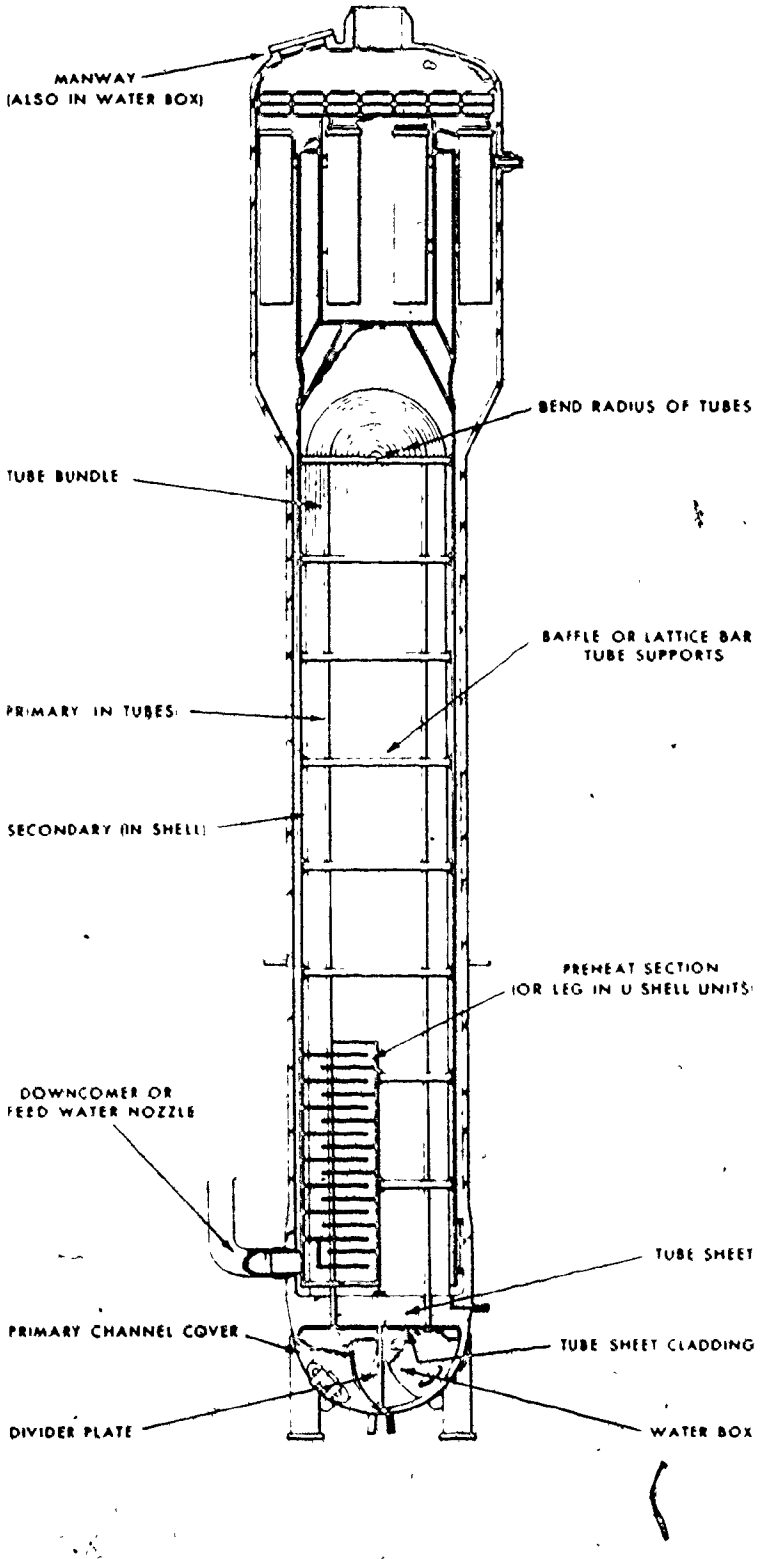

Figure 2.1: Typical Nuclear Steam Generator.

The concern of the present study is focussed on the contained liquid cross-flow configuration of the type common in heat exchangers and steam generators, rather than on cylindrical arrays subjected to atmospheric or oceanic flows. A short review of the major contributions to the advancement of the state of the art is presented first, while the various vibration regimes and fluidelastic phenomena are identified and discussed briefly.

The literature on flow-Induced vibrations on circular cylinders in cross-flow is vast. There have been several reviews of the state of the art [2], [3], [12], [13], [14] and a number of international conferences [1], [6], [15] in recent years which contain a large number of papers which make it clear that a great deal of research is being conducted in the field. The dynamical behaviour of an array of cylinders in cross-flow is at the present considered to have four distinct manifestations. These are:

(1) Various kinds of resonance conditions may arise between the frequency f_{fp} of some flow periodicity (attributed to "vortex-shedding" by some investigators) and a structural natural frequency, f_n.

(2) Similar resonance conditions may arise due to acoustic resonance, i.e., when some acoustical frequency of the containing vessel, f_a, coincides with a fluid excitation source. Considerable noise is generated and structural failures can occur if this acoustic frequency also coincides with a structural natural frequency, f_n.

In both the above cases the response of an array would exhibit a peak in the plot of the vibration amplitude versus flow velocity, similar to an essentially linear system about resonance.

(3) The response of the array to turbulence buffeting. In this case, with increasing flow velocity, the vibration amplitude increases due to the increasing turbulence in the flow.

(4) Fluidelastic instability mechanisms. Such instabilities will generally develop at sufficiently high flow velocities where large amplitude motions may be expected to occur. The amplitude of vibration increases sharply with flow velocity, apparently only limited by tube-to-tube clashing.

It should be noted that the first three mechanisms result in vibration forced by the flow field, while the last mechanism is a self-excited type of vibration.

Excitation Mechanisms in Bundles of Circular Cylinder in Cross-Flow

2.1 Flow Periodicities of a Single Cylinder and Cylinder Arrays.

The generation of the acoustical notes created when the wind passed the taut wires of the Aeolian harp were noticed since ancient times. In the fifteenth century, Leonardo da Vinci produced a sketch of a row of vortices in the wake of a bamboo rod exposed in a water stream [17] . These phenomena are

attributed to the vortex shedding phenomenon.

When a fluid flows past a cylindrical obstacle, the wake behind it, in certain Reynolds number ranges contains a number of vortices in a regular pattern. The vortices appear alternately on each side of the cylinder and are washed away in the wake when they reach a certain size. When the vortex reaches its maximum size and just before it detaches itself from the cylinder, the velocity of the flow past that side of the cylinder is maximum and hence, by Bernoulli's Law, the pressure on that side is a minimum. The cylinder thus experiences an alternating force in a direction perpendicular to that of the flow.

In 1878 Strouhal, based on observations only, related the frequency of this vortex-shedding to the "wind" speed and the "wire" thickness in the following way:

$$S = \frac{f_s \, d}{V}$$

S: Strouhal number dimensionless,

f_s: frequency of vortex-shedding,

d: diameter of circular cylindrical body,

V: flow velocity of undisturbed stream.

The periodicity of the wake of a cylinder was associated with vortex formation by Benard in 1908 and with the formation of a stable street of staggered vortices by von Karman in 1912. This was the first theoretical investigation of the subject, and it is so important that the vortex wake is now referred to

as the Karman Wake [17].

Vortex-shedding can cause large vibration amplitudes only when the shedding frequency f_s, is close to the natural frequency, f_n, of the tube. If this happens, the shedding frequency and the cylinder natural frequency can become synchronized, to the point that the cylinder's motion controls the vortex-shedding frequency.

In this "lock-in" region, the frequency of shedding remains constant as the flow velocity increases until, at some point depending on amplitude, the control is lost. The amplitude then decays and the vortex-shedding frequency "jumps" to coincide with its fixed body value. The nature of the vortex-shedding phenomenon is strongly dependent on the Reynolds number, as is explained below.

The flow developments past a stationary cylinder are shown in figure (2.2). At extremely low Reynolds number (<5) there is no flow separation as shown in figure (2.2(a)) which results in a symmetrical pressure distribution along the tube length. Increasing the Reynolds number ($5 < Re \leq 40$), the streamlines widen and a fixed symmetric pair of "Föppl" vortices appear immediately behind the cylinder as shown in figure (2.2(b)). This vortex pair remains attached to the cylinder. Further increase in the Reynolds number ($40 < Re \leq 90$) causes an elongation of the "Föppl" vortices and unsteady shedding into the wake. At Reynolds numbers of about ($90 < Re \leq 150$), there is a stable laminar vortex wake in which vortices are alternately shed and convected downstream at a velocity less than the free stream

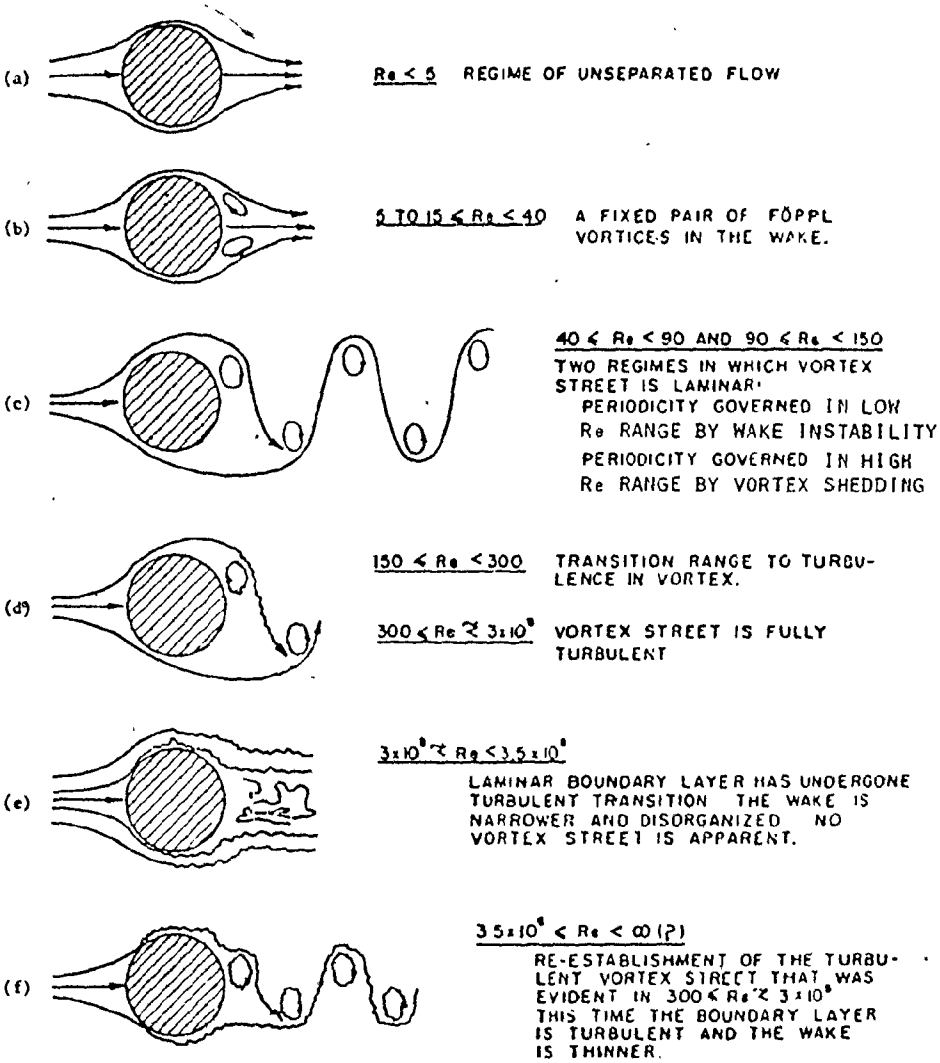

Figure 2.2: Regimes of fluid flow across a circular cylinder (from ref. 18)

velocity (figure (2.2(c)).

As the Reynolds number is increased in the range of 150-300, a laminar-to-turbulent transition begins in the free shear layers before breaking away into the street, as shown in figure (2.2(d)). At a Reynolds number of about 300 and up to 3×10^5, the vortex street is fully turbulent. In the range of 3×10^5 to 3.5×10^6 a transition to turbulence in the cylinder boundary layer occurs and there is no well defined vortex street in this region as shown in figure (2.2(e)). Finally as the Reynolds number is increased beyond 3.5×10^6, the turbulent vortex street forms and the wake is narrower as shown in figure (2.2(f)).

The variation of Strouhal number with Reynolds number for a single cylinder has been studied by a number of researchers [18], [19]. It was found that over the Reynolds number range of 300 to 2×10^5 remained constant with a value of about 0.21.

At the transition Reynolds numbers, the shedding frequency is defined in terms of the dominant frequency of a broad band of shedding frequencies. The relationship of the Strouhal number versus Reynolds number for circular cylinders is shown in figure (2.3).

The flow characteristics within a tube bundle are much more complicated than for an isolated single cylinder. As a result the variation of Strouhal number should be also dependent on the geometry of the array, if the vortex-shedding phenomenon occurs in such flow manifestations.

Grover [60] refers to the various array arrangements,

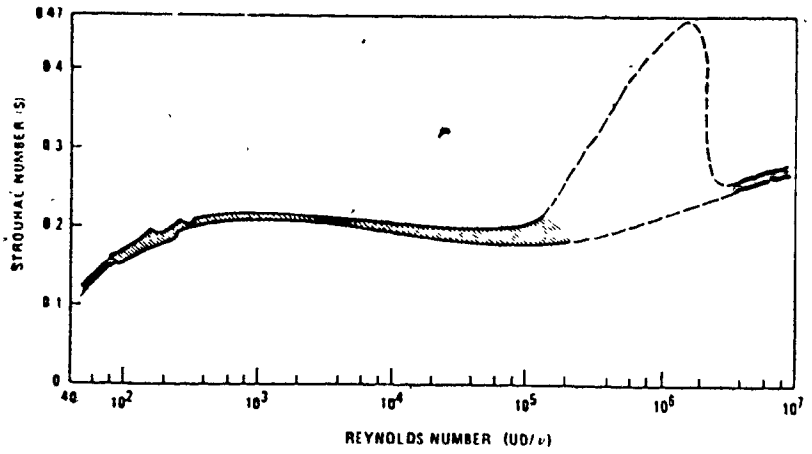

Figure 2.3: The Strouhal-Reynolds number relationship for circular cylinders. (from ref. I8)

considering two general classes; the in-line and the staggered arrays. The four most common types of tube patterns are shown in figure (2.4).

The in-line patterns can be subdivided into the "square" and "parallel-triangle" and the out-of-line or staggered patterns into the "rotated-square" and normal or perpendicular-triangle. These patterns represent the most common geometries in actual applications.

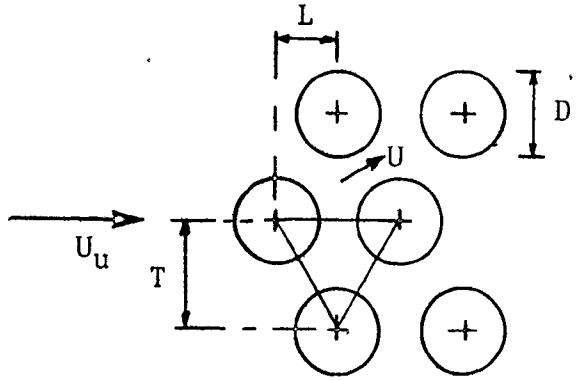

St: Transverse spacing ratio: T/D.
S_1: Longitudinal spacing ratio: L/D.
P : Pitch ratio: $(T^2+L^2)^{0.5}/D$

Figure 2.5: Definition diagram for cylinder arrays.

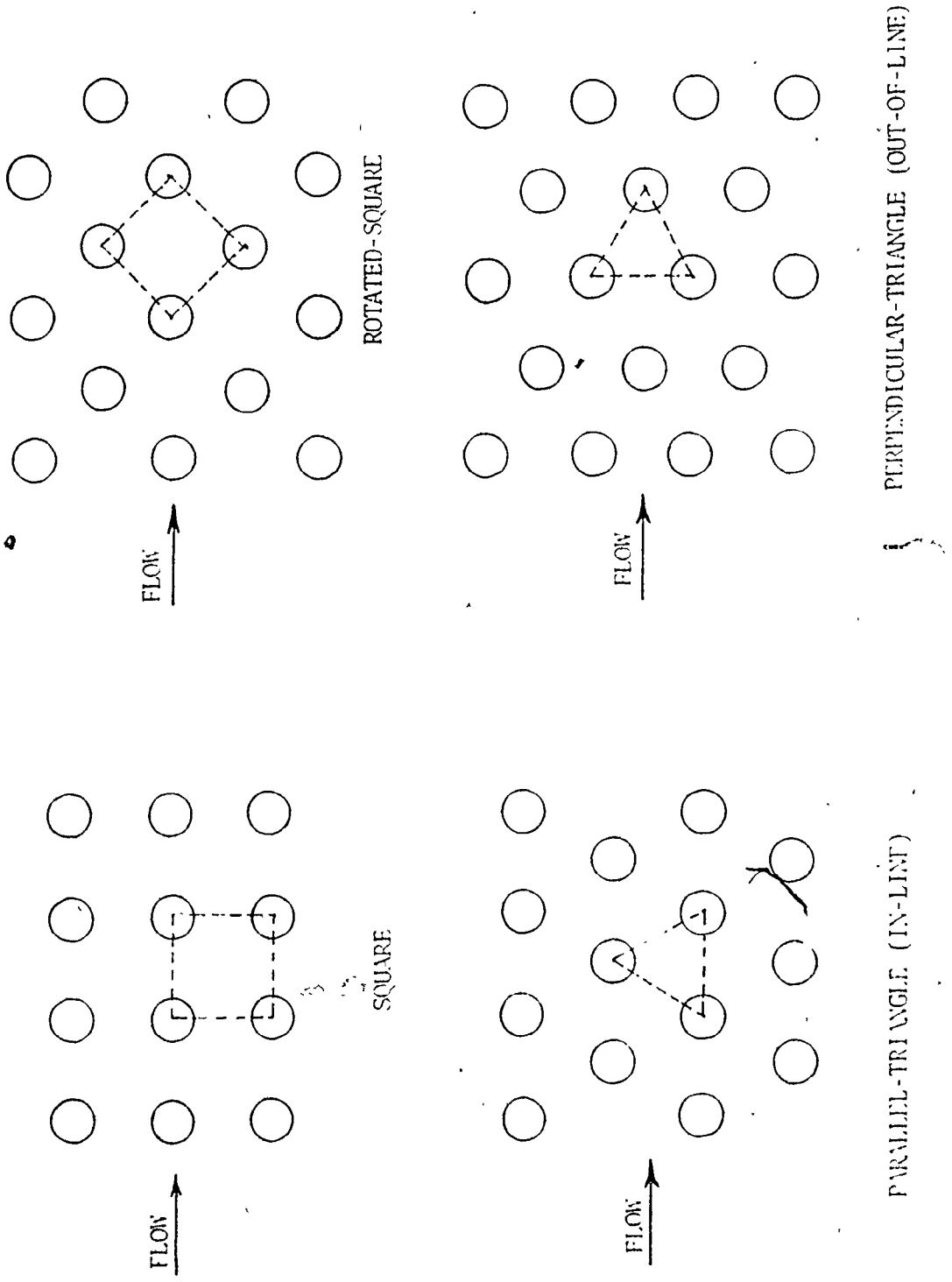

Figure 2.4: Commonly used tube arrays.

Attention should be paid to the author's definition of longitudinal pitch when referring to the original literature as these may vary. In the present study the definition followed is as shown in figure (2.5).

The question whether or not classical, well-formed von Karman vortices can exist within a tube array remains in dispute. As early as 1959 Putman [20] considered that the vibration problems in cylinder arrays in cross-flow was caused mainly by the vortex-shedding phenomenon, and a lot of effort was devoted since, on measuring the Strouhal number as a function of the geometry of the array.

Chen [19] has published sketches of possible ways for vortex streets to form in tube arrays but it is not clear how he obtained them. Also it is not clear how these patterns depend on the flow Reynolds number. The question of whether the shedding is in phase over the tube array is not clear. According to Chen [19] it can be if an acoustic resonance is present. This might be true as acoustic resonance can completely organize the flow.

It becomes rather difficult to visualize the formation of the classical vortices in a closely spaced array, where there is insufficient space for the shear layers to develop and "roll up". To overcome this difficulty, a number of alternative physical mechanisms, such as the ones proposed recently by Chen ([21], [22]) and named as "jet switch" and "jet instability" models have been developed. These mechanisms are yet to be verified by experimental evidence.

The effort to predict Strouhal numbers for vortex-shedding, in both in-line and staggered tube arrays, as a function of tube spacings, resulted in the charts published by Fitz-Hugh [24] and Chen [25].

A comparison diagram of the two sets of Strouhal numbers charts for different layouts is shown in figure (2.6). The spacing parameters are as defined in figure (2.5) and the flow velocity is defined as

$$U = U_u \, [s_t/(s_t-1)]$$

where:

U_u is the undisturbed upstream flow velocity.

It becomes obvious that large discrepancies exist between the two sets of data. The major difference occurs with the very large values of Strouhal number predicted by Chen as the transverse spacing ratio approaches the value of 1. It should also be noted that in the data on which Chen's and Fitz-Hugh's Strouhal numbers are based, it was not clear if there was acoustic resonance or not.

Although the existence of vortex shedding deep inside a tube array is in doubt, Pettigrew et al. [14] reported that observed vortex shedding resonance at least at the first few rows. Grover and Weaver [26] observed discrete periodicity in the flow at low Reynolds number inside a tube array corresponding to a Strouhal number of 0.83. At higher Reynolds numbers they observed that the increased turbulence levels suppress the vorticity phenomenon.

An alternative mechanism causing flow periodicities is suggested in the literature by Owen [23]. He is of the opinion

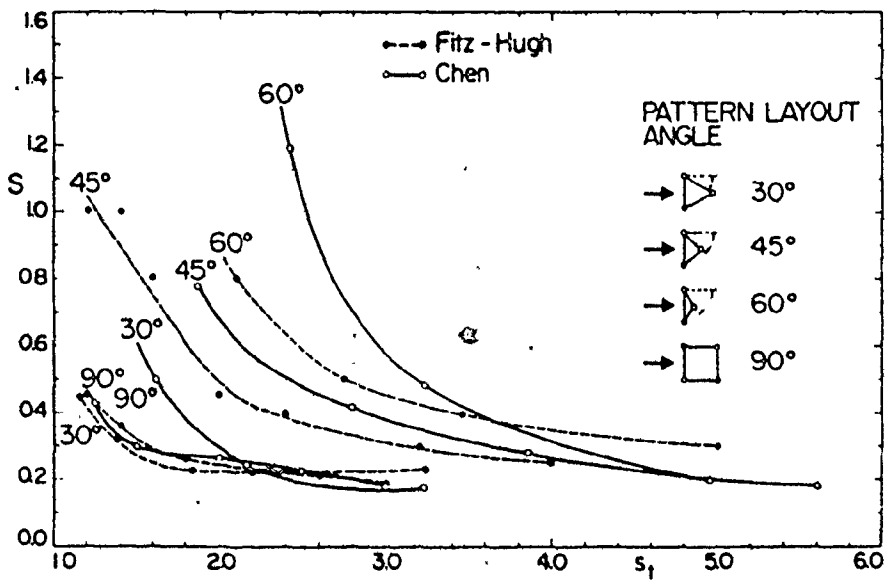

Figure 2.6: Comparison of Strouhal number between Fitz-Hugh and Chen plots. (from ref. 2).

that at high Reynolds numbers, deep in a tube array, the flow is completely turbulent and discrete periodicity cannot exist. Instead a periodic peak in the turbulent energy spectrum is suggested. This frequency is predicted by Owen to be:

$$(f_b D/U)\ s_\ell s_t = 3.05\ (1-1/s_t)^2 + 0.28$$

where

f_b: is the peak of the turbulent spectrum

s_ℓ, s_t: are the longitudinal and transverse spacing ratios as defined in figure (2.5).

Similarly to Chen's and Fitz-Hught's "vortex-shedding" Strouhal number computations, Owens' buffeting Strouhal number can be computed for different array geometries. The comparison of the different data is shown in figure (2.7).

We can easily observe that Owens' data will (in contrast with Chen's data) result in very small values of Strouhal numbers as the transverse spacing ratio tends to the unity value, which is in line with Owens' reservations concerning the validity of his formula for small spacings. From a practical point of view the two different suggested mechanisms appear to lead at same Strouhal numbers, outside the limiting case of $S_t \to 1$.

At present, beyond the observation of the existence of some apparent periodicity in the velocity and power spectra, in the absence of tube motion, we are not in a position to resolve the dispute between the predominance of either mechanism in real flows.

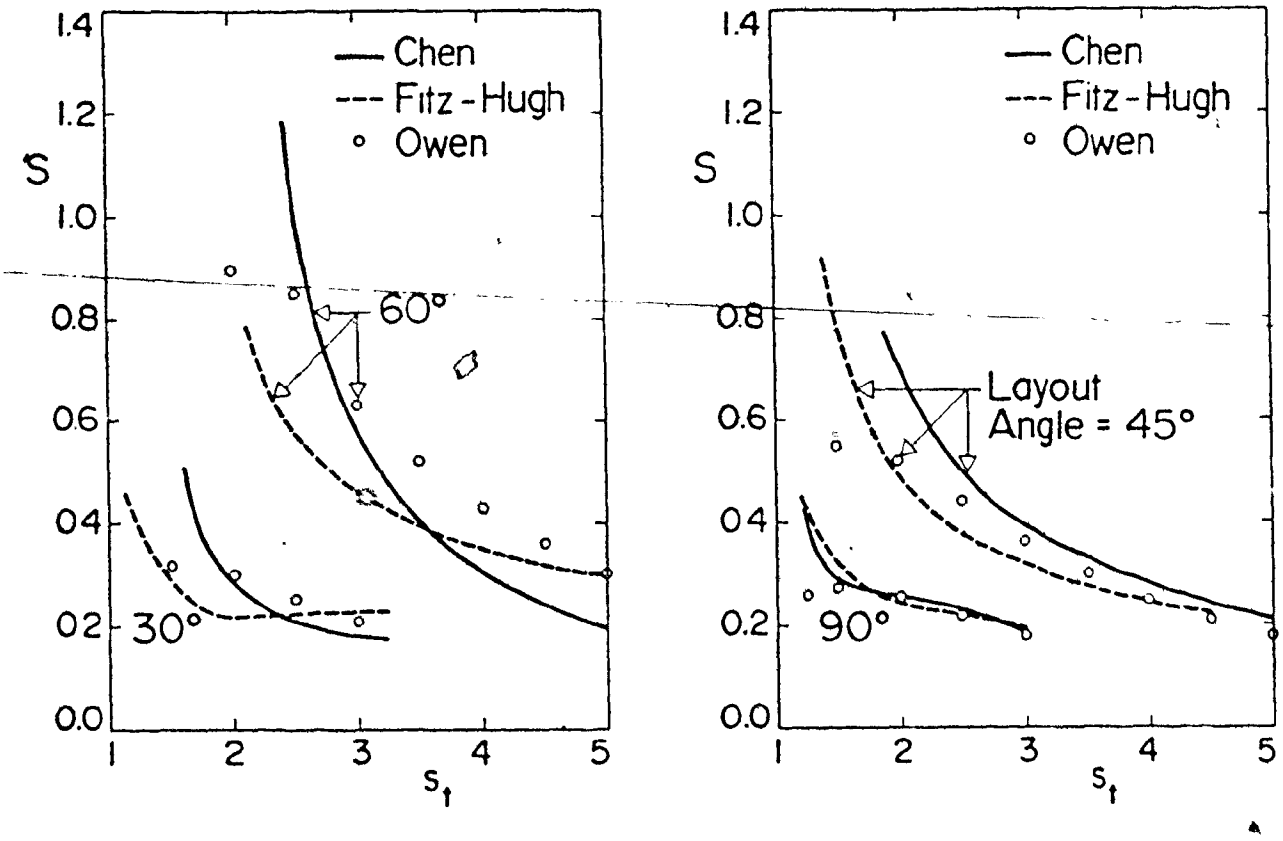

Figure 2.7: Vortex shedding Strouhal numbers according to Fitz-Hugh and Chen compared to Owen's buffeting frequency Strouhal number. (from ref.2)

From the designer's point of view, one may use the charts presented in figure (2.7) to ensure that the natural frequency of the designed tubes is not close to the frequency of the periodicity that may exist in the design flow velocity, independently of the mechanisms that cause this periodicity. It should also be noted that due to the large discrepancies between the published charts, especially at small spacing ratios, these charts should not become the only design guidelines.

2.2 Acoustical Resonances

The presence of acoustical vibrations in a heat exchanger can cause serious problems. The phenomenon manifests itself as a resonance between the natural frequency, f_a, of a standing acoustical wave in the vessel containing the tube array and the frequency, f_{fp} of a flow periodicity present in the flow.

This resonance provides a mechanism of energy transfer from the flow to acoustical wave motion. This results in intense sound amplification and large pressure fluctuations on the containing walls. Furthermore, the acoustical vibration appears to have a correlating effect on the flow periodicity, enhancing the energy content of the frequency of this flow periodicity. Acoustical coupling can become a dominant resonance mechanism and can occur deep in a tube array. Although the resultant sound can be very intense, vibration of the array tubes themselves is not required.

The acoustic resonance phenomenon is associated mainly with gas flows. In water flows, the speed of sound is higher while equipment dimensions are smaller and operating velocities are

lower. As a result the frequency, f_a, of an acoustic wave is higher while the frequency of the flow periodicity, f_{fp}, is lower. Therefore it is unlikely that resonaces will occur.

In the literature this type of excitation is associated by Chen [19] and Funakawa [27] with vortex-shedding "lock-in" phenomena. Whether acoustic resonance is possible due to fluidelastic excitation of the tubes is still unknown.

Chen and Young [28] proposed a guideline relationship for in-line arrays. Acoustical resonances will not occur if

$$\frac{R_e}{S_{fp}} (1-1/s_t)^2 (1/s_\ell) < 2{,}000$$

where

Re: Reynolds number

S_{fp}: Strouhal number of the flow periodicity

s_t, s_ℓ: Transverse and longitudinal spacing ratios of the array (figure (2.5)).

The destructive potential of an acoustic resonance becomes obvious when the acoustic frequency, f_a, coincides with the tube natural frequency, f_n. If a triple frequency coincidence occurs, i.e.,

$$f_a \simeq f_{fp} \simeq f_n$$

then the heat exchanger can be destroyed completely in a few hours, as is shown by Paidoussis ([2], case 34). In order to avoid acoustic coupling Chen recommended the insertion of detuning baffles along the flow direction in heat exchangers,

while Zdravkovich [29] suggests that the acoustic resonance will be minimized, if some tubes in the tube array are omitted so that the regular flow pattern will be disturbed.

2.3 Turbulent Buffeting

As it was described earlier, the flow deep in a tube array can be considered as being fully turbulent. The energy associated with the turbulent pressure fluctuations in the flow is distributed over a wide range of frequencies. The tubes extract energy from the fluctuating pressure field, selectively from a frequency band around their natural frequency. The tubes are acting somewhat like a shaped band-pass filter. The turbulent buffeting excitation mechanism gives rise to a behaviour similar to that associated with a randomly forced, damped vibration.

The vibration amplitude levels, under this excitation, are usually small and it has been traditional to consider these fluctuating forces as not posing any serious problems, provided that resonance is avoided, since their magnitude is considerably smaller than the steady drag force, imposed on the tubes. This is a sound assumption provided that the tube natural frequency, f_n, and the frequency, f_{fp}, of any possible flow periodicity are well separated, otherwise fatigue may occur even in the absence of resonance.

In the literature Brunn and Davies [30] reported some quantitative data. Their observations indicated that there is little influence of the upstream turbulence on the wake region, which reinforces Owens' [23] observations that the turbulence

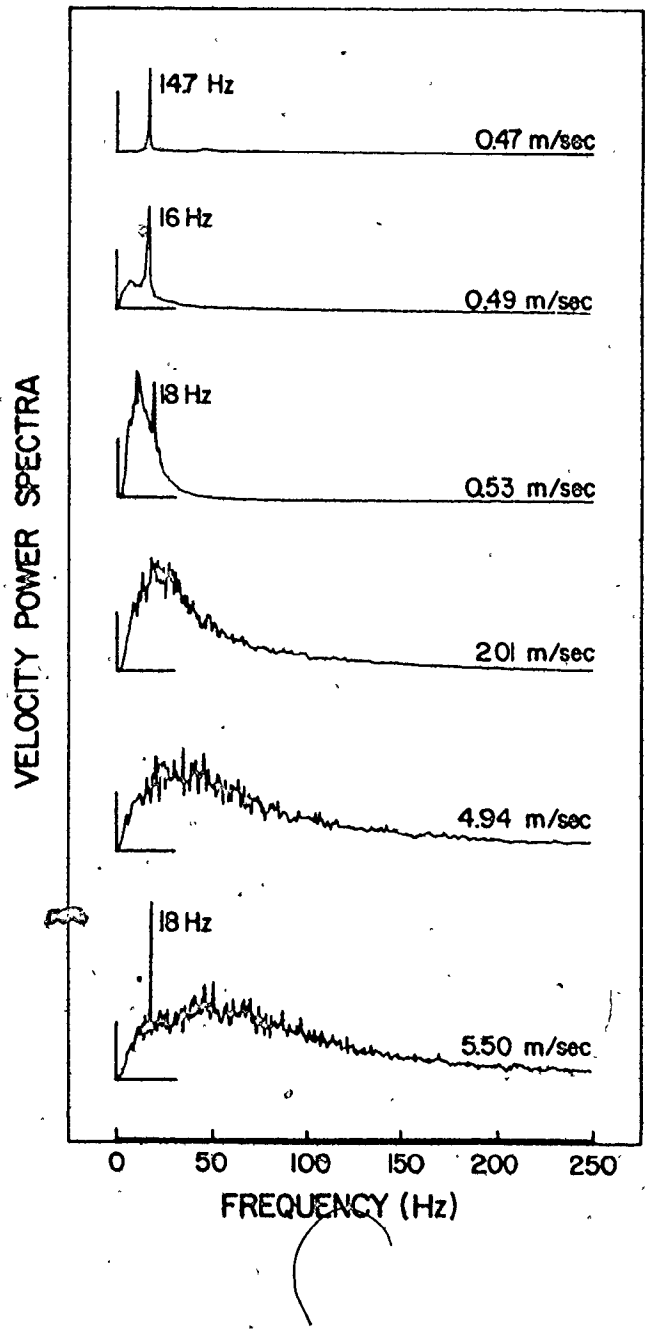

Figure 2.8: Velocity power spectra of an in-line array. (from ref.27)

deep inside a tube array, is due to the wake interaction rather than any upstream turbulence carried to the wake.

Nicolet et al. [31] suggested that for the non-resonant areas the forced vibration amplitude due to the turbulent pressure fluctuations is proportional to $U^{3/2}$ for values of the reduced velocity ($U/f_n D$) larger than 4.

For liquid flows Pettigrew et al. [14] reported that the vibration amplitude is proportional to the dynamic head ($1/2\ \rho\ U^2$), as long as the motion of the tube does not affect the turbulent fluid forces. For two-phase flows the same authors reported that the vibration amplitude is proportional to the reference gap mass flux. They also provided methods for calculating the forced vibration amplitude. Finally figure (2.8) shows the variation of the velocity power spectra published by Weaver and Lever [32] for an in-line array. It can be seen that the initially observed flow periodicity at 0.47 m/sec velocity of 14.7 Hz is increasing with flow velocity until turbulence takes over this periodicity at a velocity of about 2 m/sec. The resonance present at the higher velocity of 5.5 m/s is imposed on the flow from the tubes' motion (tube natural frequency 18 Hz) which are dynamically unstable due to the fluidelastic instability of the array at such high velocities.

2.4 Fluidelastic Instability

Tube vibrations at flow velocities considerably higher than those predicted by the previously mentioned mechanisms have been reported to have occurred in a number of heat exchangers.

These vibrations are of large amplitude and can result in severe damage in a short period of time. Unlike the flow periodicity response mechanisms reported earlier, the tube amplitude keeps on building up with increasing flow rate until it is limited by some form of the system non-linearities. This type of vibration is typical of the self-excited type, which is a motion-dependent mechanism, and is called fluidelastic instability mechanism. The possibility of such a mechanism being a predominant excitation mechanism in a tube array was reported as early as 1962 by Roberts [33]. He proposed a "jet switching" mechanism which is synchronized with adjacent tube motions. This synchronization can extract energy from the flow in excess of the system's dissipative potential resulting in large amplitude oscillations. In a recent paper Paidoussis [2] compares the results obtained by Roberts for a single row of cylinders and more contemporary experimental data from several other sources (figure (2.9)). Based on Roberts' assumption that his "jet switching" mechanism will occur if $U/f_n D > 60$, since some time is needed for the switching of the jet to take place, the comparison of the theory with the experimental data seems to be in good agreement. His theory fails to explain the phenomena at low values of the reduced velocity parameter ($U/f_n D$) which corresponds to two-phase and liquid flows.

The research of Connors [34] is considered to be the first to establish the nature of the fluidelastic mechanism. In his model, which is independent of any "jet switching" mechanism, Connors showed that, for a single row of tubes in

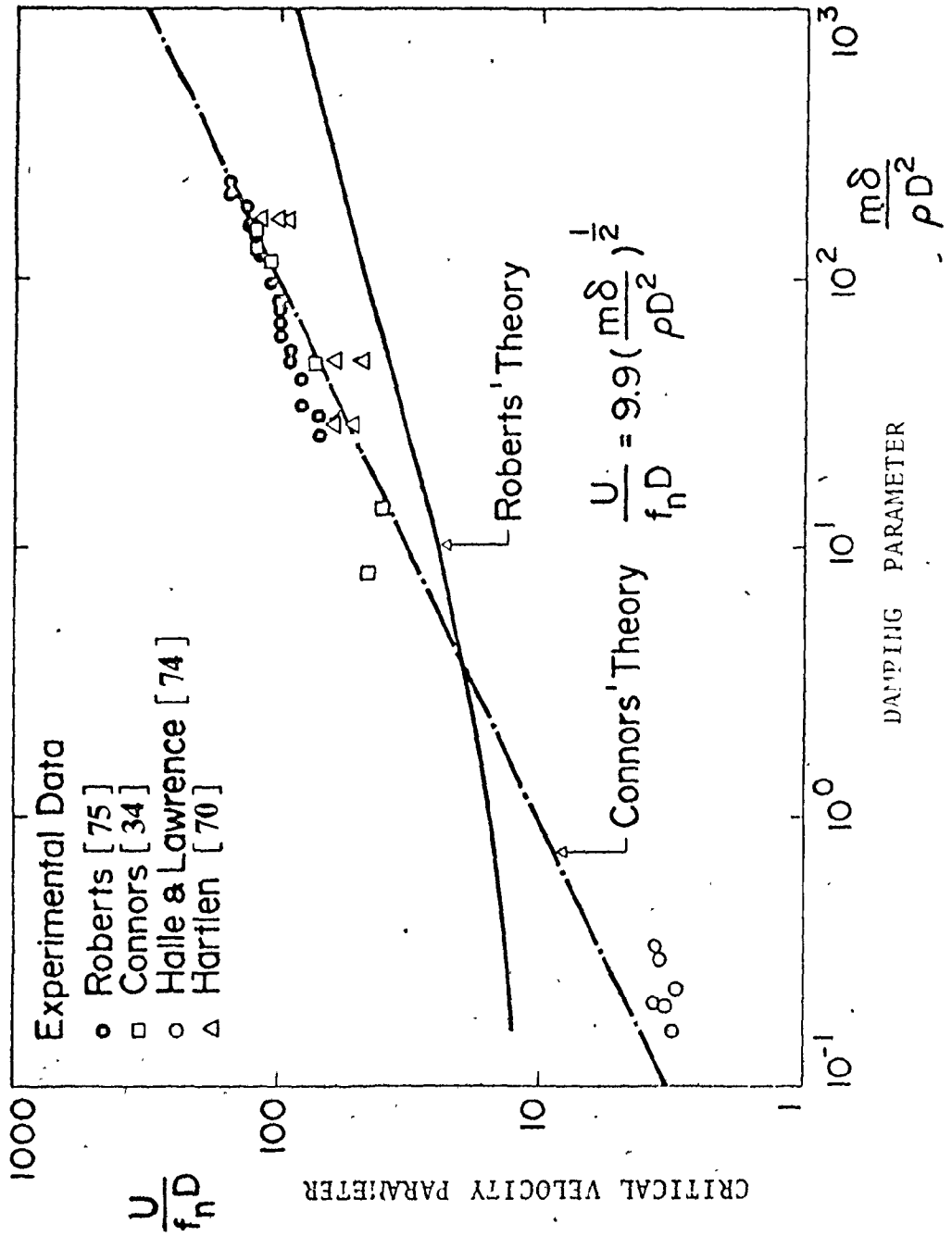

Figure 2.9: Comparison of Robert's results with contemporary experimental data.

cross-flow, the tube extracted energy from the fluid as it moved through a given cycle relative to its neighbours. By equating this quasi-statically measured work to the theoretical energy dissipated by damping for the same cycle, a stability threshold between the reduced velocity and reduced mass parameters was established in the form:

$$U/f_n D = \kappa (m\delta/\rho D^2)^{1/2} \qquad (2.1)$$

where

- U: flow velocity,
- f_n: tube natural frequency,
- D: tube diameter,
- m: total tube mass (including added mass) per unit length,
- δ: the logarithmic decrement of damping of the tube in the fluid,
- ρ: shell side fluid density,
- κ: a constant.

The value κ was determined from Connors experiments for a tube row to be 9.9. It is now accepted that the value of this constant is considerably less for tube banks.

Connors' relationship became accepted as a design tool but unfortunately has been misused, since it was used to predict stability thresholds for tube arrays. This resulted in a number of non-conservative predictions for a number of designs, as it can be seen from the stability diagram presented in figure (2.9). Connors' work was generalized later by Blevins [35] who developed

a two-dimensional analytical model for the fluidelastic whirling of a tube row in cross-flow.

Considerable work was done on obtaining additional experimental data ([36], [37], [38]) to refine this model and improve the applicability of Connors' relationship for different geometries and flowing fluids of tube arrays. The general approach was to retain Connors' stability criterion and refine further the values of κ. With a few exceptions, e.g., [32], [38], little effort was devoted to the physical understanding of the physical phenomena involved.

Some of the key features of the theoretical model developed by Blevins [35] indicated that:

(a) A certain pattern of tube motion is required before an instability can occur.

(b) The critical flow velocity is expected to increase sharply when the natural frequency of neighbouring tubes is altered.

(c) The fluid-dynamic component of damping is expected to increase with the flow velocity.

(d) The critical flow velocity increases as the number of the tubes in a row decreases.

Connors' theory also fails to explain why the frequency of oscillation of the fluid-elastic region coincides with the tube natural frequency. It also implies that the tube damping (δ) and the mass ratio ($m/\rho D^2$) are linearly dependent.

However, recent results published in the literature indicate that these features are doubtful. Weaver and Grover [39]

have shown that even when all tubes but one become immobile in a tube array, that flexible one can become unstable at the same critical velocity at which the flexible array becomes unstable. Also Weaver and Lever [32] observed that the detuning of neighbouring tubes has no effect on the instability of the array.

In another paper Weaver and El Kashlan [40] have studied the effects of flow velocity on the aerodynamic tube damping. Their results indicate that the aerodynamic damping increases with the flow velocity until it reaches about 50% of the stability threshold. It then decreases, contrary to the prediction made by Blevins' model, and appears that as the velocity approaches the threshold, the value of damping appears to approach the value of damping found in quiescent fluid, as shown in figure (2.10).

In another publication Weaver and Grover [38] reported results when the tube damping alone was varied. The results indicated that the reduced velocity parameter, $(U/f_n D)$, depended on damping to the power 0.21 rather than to the power 0.5. They suggested that the stability threshold should rather be in the following form:

$$(U/f_n D)_c = \kappa (m/\rho D^2)^{0.5} (\delta)^{0.21} \qquad (2.2)$$

In the same paper they suggested that damping and mass ratio, the product of which forms the damping parameter in Connors' model may be independent parameters.

A similar result was reported from Nicolet et al. [31]. They suggested that the reduced velocity depends on damping

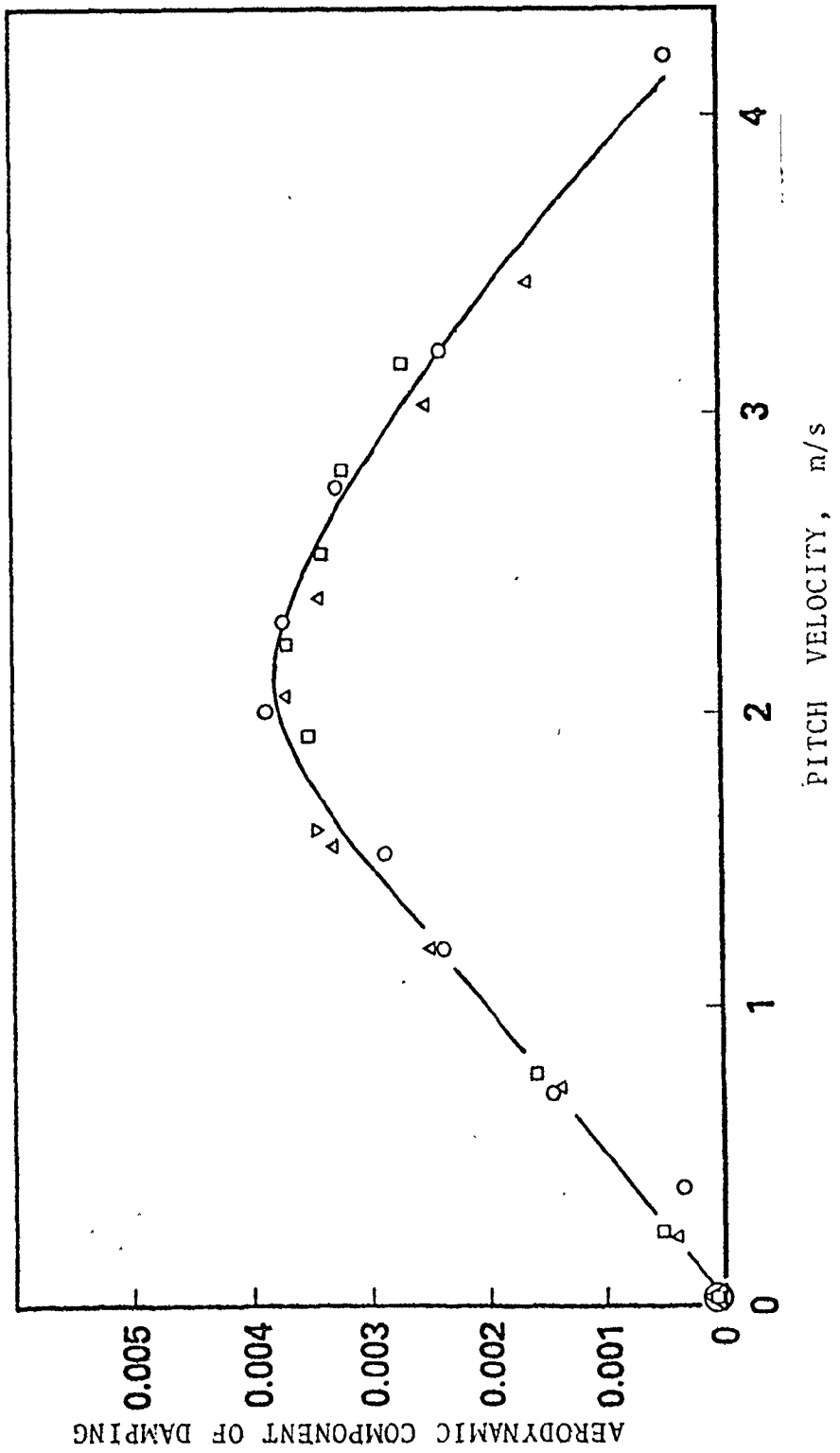

Figure 2.10: Variation of Damping with Pitch Velocity for an in-line array. (from ref. 40)

to the range of powers between 0.1 and 0.3. The same authors, as a result of their experiments, varying the mass ratio $(m/\rho D^2)$, by pressurizing the working fluid and therefore varying the fluid density, reported that the reduced velocity depended on the mass ratio to the power 0.3.

Recent results reported by Weaver and El Kashlan [40] indicate that the mass ratio and the damping are independent parameters. In their experimental work they varied the mass ratio by using tubes of different material and keeping damping the same. The dependence of the reduced velocity to the mass ratio was found to be proportional to the power of 0.29. Their results are shown in figure (2.11). They also suggested an improved stability equation in the form:

$$(U/f_n D) = \kappa \, (m/\rho D^2)^{0.29} \, (\delta)^{0.21} \qquad (2.3)$$

The form of this equation, contrary to Connors' theory, indicates that the critical reduced velocity is less dependent on mass and damping ratios than it was originally assumed to be. The above mentioned examples strongly indicate our lack of understanding of the real phenomena occurring during fluid-elastic excitation of tube arrays. Although these results represent valid information and help us understand part of the phenomena, they unfortunately cannot be generalized since they are results obtained for one specific set of parameters.

The geometry of the tube array should be included as part of the parameters affecting the phenomena. Paidoussis in a

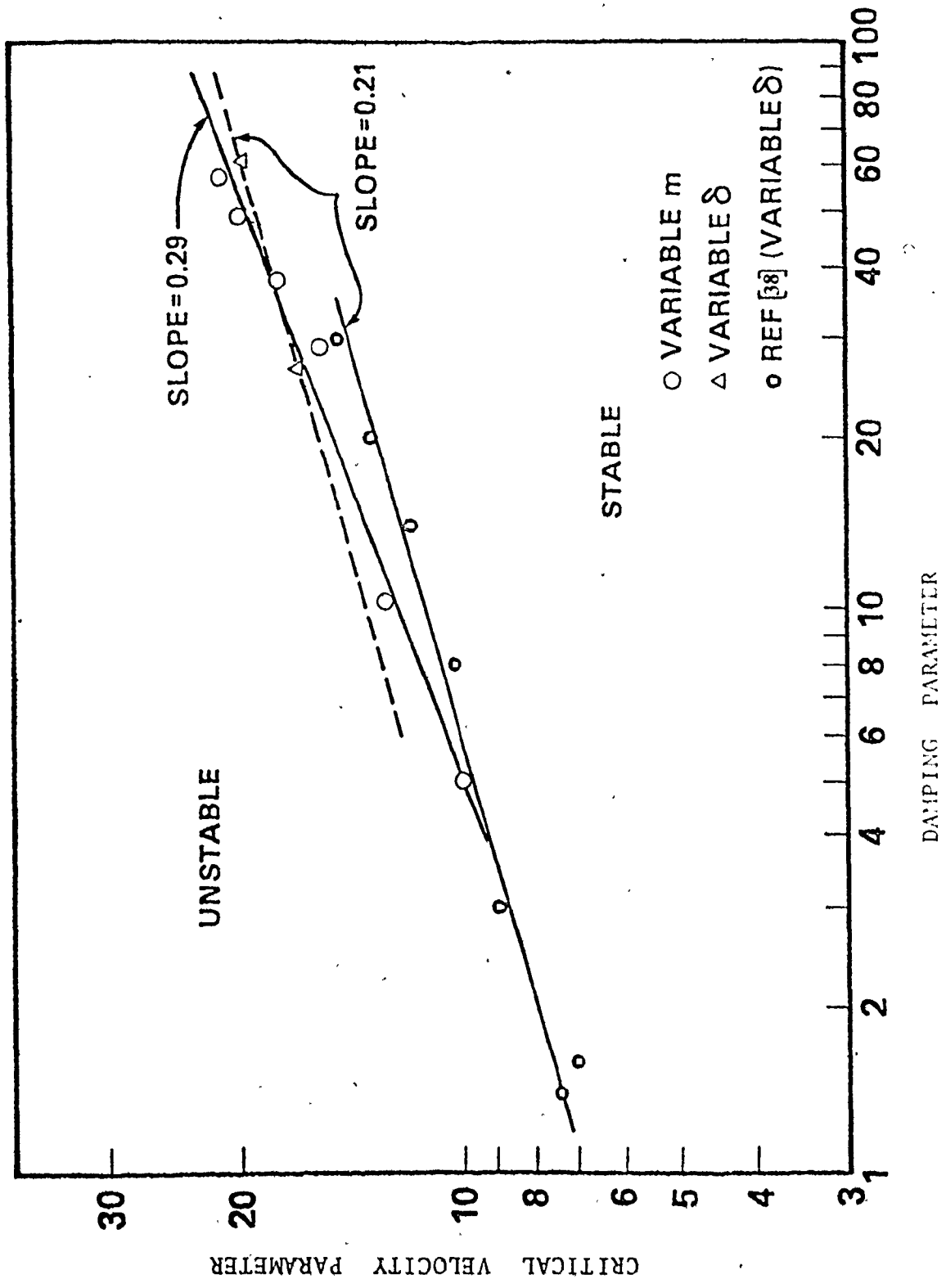

Figure 2.11: Dependence of the velocity parameter to the mass ratio.

recent paper [2] suggests, as a first attempt to explain the existing discrepancies in published data and in view of the supporting evidence presented earlier, that the stability equation of tube arrays should be of the form:

$$(U/f_n D) = \kappa \, (m/\rho D^2)^a \, (\delta)^b \, ((P/D)-1)^c \qquad (2.4)$$

He also clearly suggested that further experimental evidence is needed in order to be able to determine the values of the variables with some confidence.

Finally in an attempt to explain the scatter of the experimental results in the literature, Weaver [40] indicates that even for a given geometry, equation (2.4) represents a three-dimensional surface. When one attempts to present the results in the conventional way, using for example equation (2.1) which assumes that the mass ratio and damping are linearly dependent, then the stability boundary becomes the projection of this three-dimensional surface on the reduced velocity and damping parameter plane. As an example, figure (2.12) is presented from ref. [14]. It is also suggested that it would be very useful if a conventional definition to determine the stability threshold was adopted, since in many cases the way the critical velocity is obtained experimentally is doubtful.

In conclusion, it can be said that there are four possible mechanisms causing flow-induced vibrations in tube arrays; flow periodicity phenomena, acoustic resonance, turbulent buffeting and fluidelastic excitation. The principle mechanism

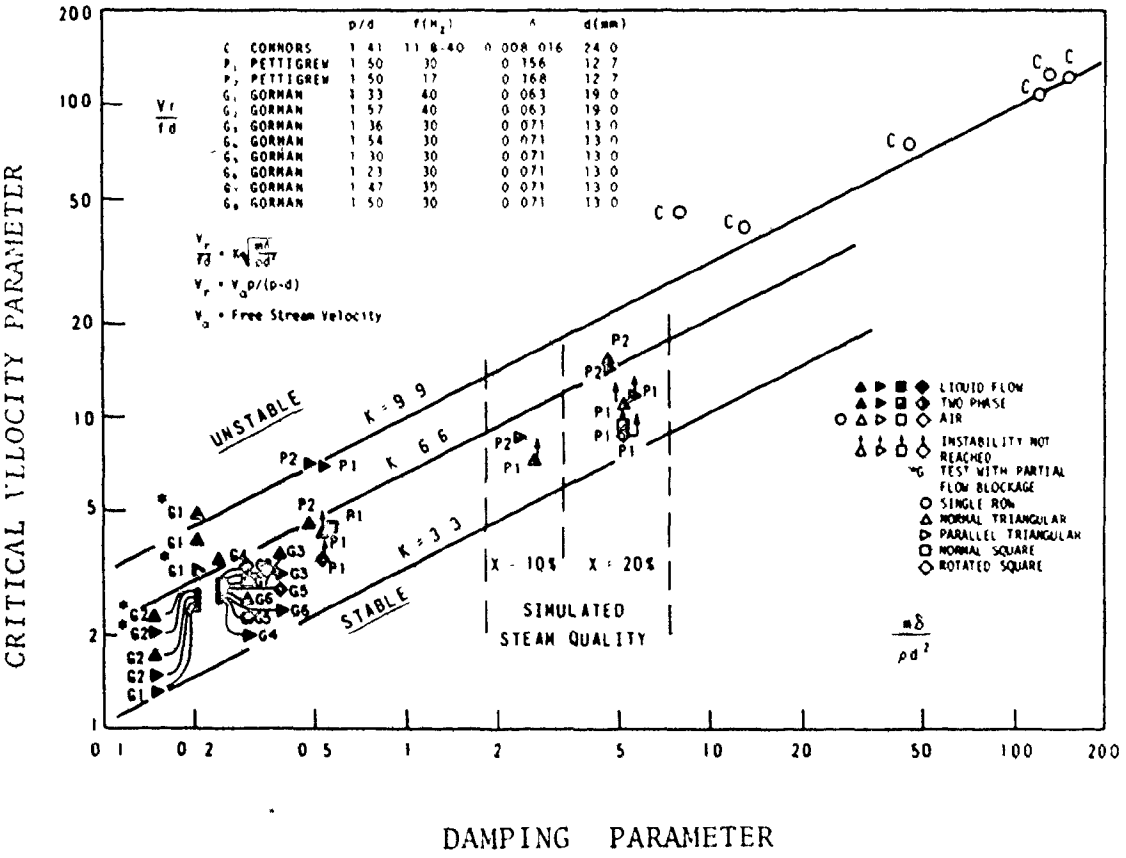

Figure2.12: Non-dimensional presentation of experimental data on fluidelastic instabilities in cross-flow.(from ref. 14)

that in general is accepted as causing major vibration problems in cross-flow of tube arrays is the fluidelastic excitation. Ironically this is the least understood mechanism of all possible excitation mechanisms, which clearly indicates that more research and development is required, for the understanding of the fluidelastic instability mechanism.

CHAPTER 3

EXPERIMENTAL EQUIPMENT

A water/wind tunnel is a device designed for passing a stream of fluid with prescribed spatial and temporal variations over a model or full-size structure which is placed in its working section. The rest of the components are used to generate this stream. Tunnels are conventionally divided into low-speed and high-speed tunnels. In low-speed tunnels the predominant factors are inertia and viscosity while the influence of compressibility is negligible. This type of tunnel provides usually good Reynolds number similarity. In high-speed tunnels the forces due to inertia and compressibility are of major importance and usually provide good Mach number similarity. Two different types of tunnels are generally used:

(a) the closed-circuit tunnel, in which the same fluid is recirculated and,

(b) the open-circuit tunnel in which all the working fluid is discharged to the atmosphere at the one end, while fresh fluid is drawn in at the other end.

Since it was desired to design a general purpose, low-speed tunnel using water as the working fluid the first approach was selected. The design principles, limitations and description of the present facility are given below.

3.1 Water Tunnel Design

(a) Design Limitations

The major design limitations for the water tunnel were (a) space availability and (b) a limited budget available for the project. The modification of an existing water loop shown in Fig. (3.1.1) was suggested in order to serve both the above limitations. It was decided to remove the sections between points (A) and (B), (Fig. 3.1.1), where victaulic fittings were fitted, and design the active components and working section to fit in this space.

This idea although economically sound imposed further space restraints on the design. The existing pump and power unit, flow control valve, piping and existing 90^{o} elbows were used in the present design.

(b) The By-pass Line Design

Accurate control, and measurement of the flow velocity well over a range of flow velocities in the working section of the tunnel is one of the major requirements of the design. It was apparent that the existing 0.304 m. in diameter (12") gate valve would not provide adequate control of the flow, especially at small flow velocities. It was obvious that there was a need for a parallel by-pass line of a smaller diameter. Fig. (3.1.2) shows a schematic of the present design of the by-pass line. The line consists of a 0.152 m (6") schedule 40 pipe and a gate valve, to provide flow control over a range of 0.07 m/s to a maximum of 0.8 m/s mean flow velocities

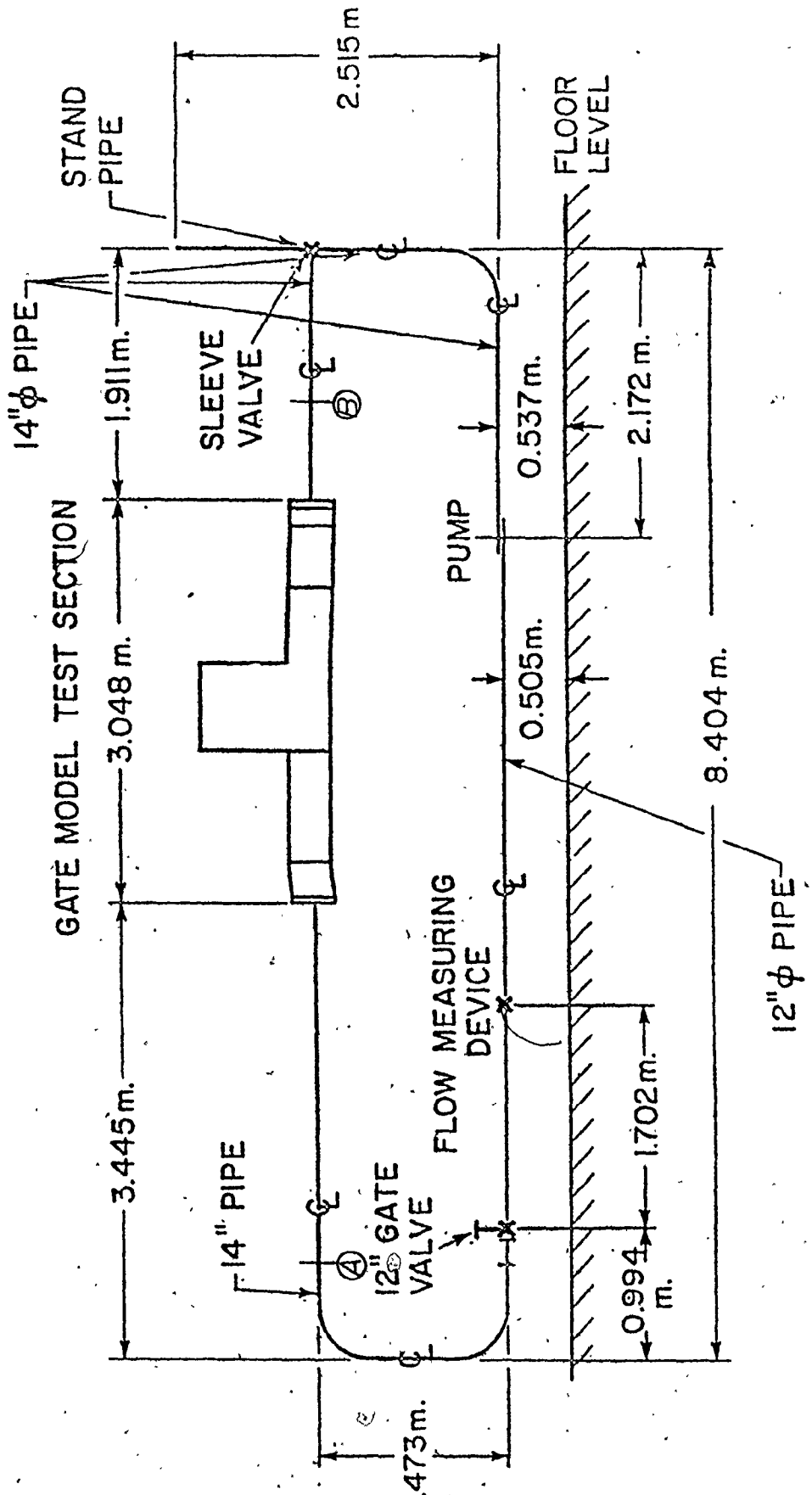

Figure 3.1.1 Initial water loop

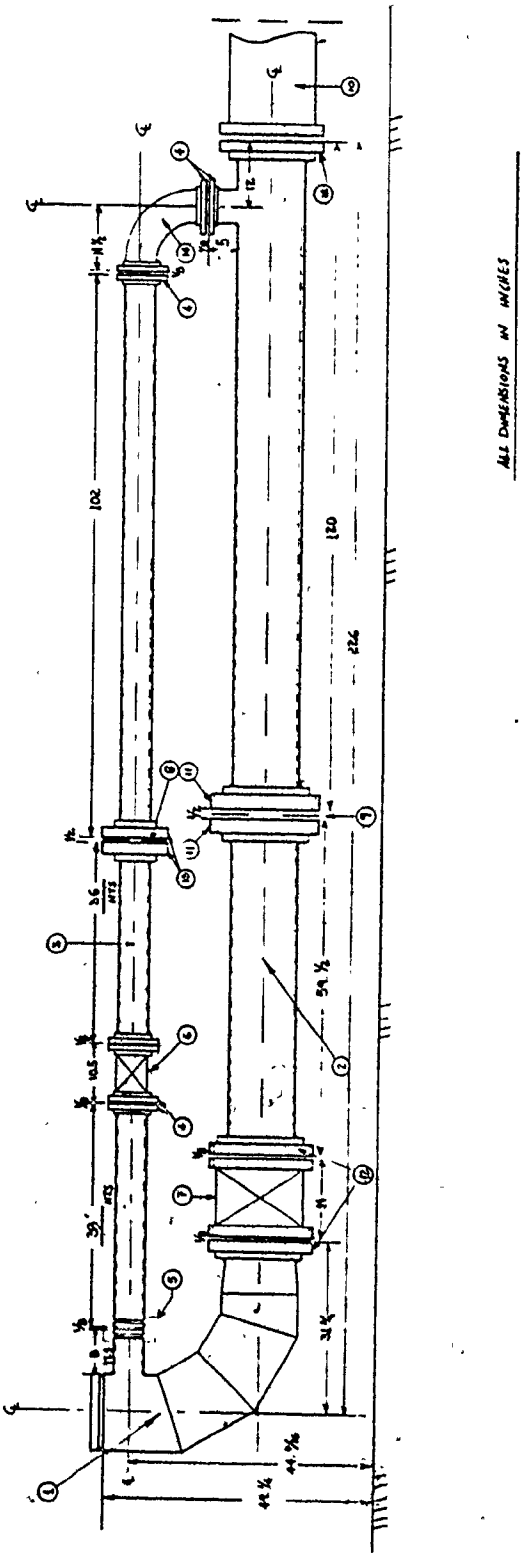

Figure 3.1.2: Schematic of the by-pass loop

based on a 0.305 m x 0.305 m working section.

The size of the line was determined from the facts that (a) six inches piping was available at no cost and (b) a large beta ratio (orifice diameter to pipe diameter) orifice plate could be used, introducing minimum flow disturbance, while it provided the required pressure differential for the working range of the by-pass rotameter.

The main line could provide control over a range of flow velocities of 0.4 m/s to 4 m/s, which indicated that there was enough overlap between the two lines, for accurate control of the flow in the working section. The measurement of the flow for both lines is achieved by means of two restriction orifice plates and the use of by-pass full-view rotameters. The main line orifice (01 Fig. 3.1.2) is positioned a distance of 3.05 m (10 diameters) downstream from the pump and 1.51 m (5 diameters) upstream from the control gate valve V1. Both dimensions satisfy the minimum free undisturbed length of piping that should be allowed upstream and downstream of an orifice as specified by the Institute of Hydraulics Handbook [41].

The by-pass orifice (02 Fig. 3.1.2) is positioned 2.59 m (17 diameters) downstream from the short elbow and 0.9 m (6 diameters) upstream from the control valve V2, both dimensions satisfying the minimum undisturbed pipe length requirements.

Both orifice plates have an orifice bore to pipe diameter ratio of 0.75. Since accuracy of the flow rate measurement depends also upon proper installation of the orifice and tap

locations for the by-pass connections, orifice flanges are used.

The length of the rotameter piping is kept to a minimum by installing the rotameters as close to the orifices as possible, satisfying the manufacturer's requirements for the maximum allowable length of rotameter piping.

The rotameters used are Brooks full-view rotameters, type 1110-08-2-C1A. The rotameter for orifice 02 has a range of 100 USGPM to 1700 USGPM and for orifice 01 the rotameter range is 500 USGPM to 6,500 USGPM.

The by-pass rotameter is usually calibrated as a differential unit so that the overall accuracy is dependent on both design and installation of the primary element. In general if proper installation is established then these rotameters will indicate rates of flow that are correct within 2% of maximum flow over the range of flows for which they are designed.

To ensure that the velocity in the test section is accurately known both orifice-rotameter assemblies were calibrated against the flow velocity in the test section. The calibration curves are shown in Appendix A.

(c) The Water Tunnel

The low-speed water tunnel schematic is shown in Fig.(3.1.3.) A description of the tunnel and the design principles of each component is presented below. The pump (P) used is a double suction Babcox and Wilcox centrifugal pump rated at 22.7 m^3 per minute for 33.5 m of head, which is assumed

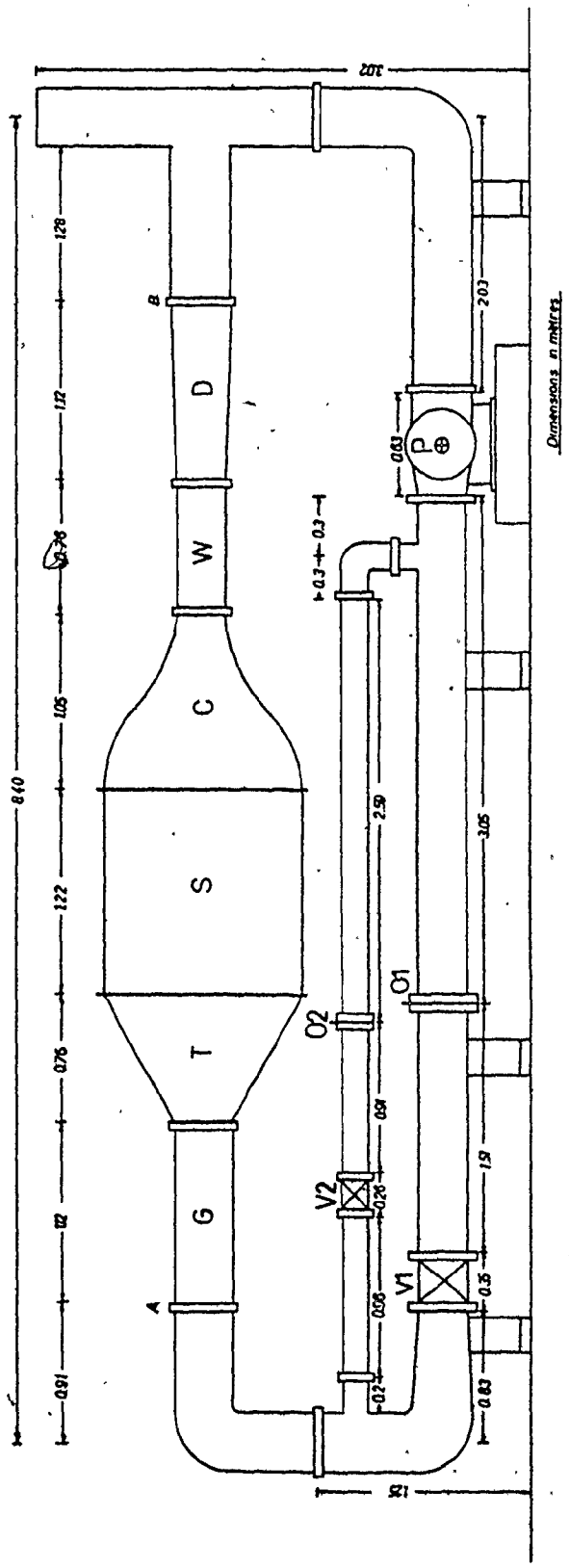

Figure 3.1.3: Schematic of the water tunnel

to provide adequate power for the working range of the tunnel. Power for the pump is provided from a V8, 6.5 liters Chrysler internal combustion engine rated at 190 HP and fitted with an automatic transmission. The exhaust manifolds are replaced with marine manifolds and the engine's operating temperature is controlled using an external heat exchanger system.

The fluid leaving the pump is driven either through the main line or the by-pass line, as described in the previous section, towards the first corner of the loop. All four corners, which existed from the previous loop, were designed and equipped with turning vanes so that minimum losses and disturbances of the flow occur in these regions. After the fluid passes the second corner it is driven through a connecting straight piece of pipe (G, Fig. 3.1.3) towards a wide angle transition piece (T) to the settling chamber (S) where the flow is conditioned. The fluid then enters the contraction (C) where it is accelerated before it enters the working section (W). Leaving the working section, the fluid passes through a square to circular transition piece (D) before it is directed towards the third turn. Through the third and fourth turns, the fluid is driven back to the pump.

During the preliminary design a number of important parameters, such as for example, the geometry and dimensions of the working area cross-section, size and type of contraction to be used must be defined. It was desirable that the working section be of a minimum of 0.305 m square cross-sectional area so that it would be similar to the working section of the existing

wind-tunnel facility. This would allow for interchange of working sections between the two facilities at a minimum cost.

After the dimensions of the working section were defined, it was decided, as is explained below, to use a two-dimensional contraction having a 4:1 contraction ratio.

(i) Contraction Design

The existence of a contraction upstream of the test section in most flow facilities causes the acceleration of the fluid before it enters the working section. The acceleration of the flow results in considerable reduction of mean-flow nonuniformities, producing a uniform velocity profile at the test section entrance.

In fact, Bradsaw [42] by applying Bernoulli's equation to an incompressible flow, has shown that an irregularity of the axial velocity, which is expressed as a fraction of the mean velocity across the section, is reduced to the square of the contraction ratio. The contraction also causes a reduction of the relative turbulence level at the working section.

The contraction design is basically the search for the optimum wall shape, which leads to the required flow conditions in the working section, having a minimum length.

Parameters such as the contraction ratio, wall shape, and nozzle length are critical for the contraction performance. If we assume that the flow is incompressible and no separation of the boundary layers occur, then the flow in the contraction may be

described by invicid flow equations, reducing the design to the analytical or numerical solution of Laplace's equation for the stream function or for the velocity potential. This approach is very attractive and a number of investigators [43-55] to date have published analytical solutions for flows in axisymmetric [43-46], two-dimensional [47-52] and three-dimensional [45] contraction designs.

For the two-dimensional cases, which are of interest in our design, Lighthill [49] and Goldstein [50] use the methods of conformal transformation to obtain the wall contour. Another approach is the use of the hodograph (velocity) plane. This technique is demonstrated by Whitehead et al. [47] and Libby [51]. Choosing a path in the hodograph plane, the velocity along the wall of a contraction can be described. The wall contour which corresponds to the chosen velocity distribution is then obtained by transformation into the physical plane. Both of these methods allow the theoretical design of any arbitrary contraction shape. However, from the practical point of view, it should be realized that these methods are mathematical solutions for the analysis of the flow and offer little design information concerning the optimum shape and contraction length.

An alternative approach to the solution would be the use of design charts (Rouse and Hassan [56], Morel [48]) to simplify the task of the designer.

The experimental work of Rouse and Hassan using an electrolytic bath as an electrical analogy to the potential flow, provides a design chart which is intended mainly as a criterion

for avoidance of liquid cavitation near the exit of the nozzle, while the possibility of separation near the inlet have not been considered and therefore their chart should not be used as the only design criterion.

A numerical solution approach is adopted by Morel [48] in which contrary to the analytical studies, a wall shape is first defined and then the solution for the velocities within it is obtained. The advantage of the numerical solutions compared to the analytical ones is that any wall shape of a finite-length contraction can be studied. Morel provides the designer with simple to use design charts and procedures that were constructed by compilation of results from a systematic series of calculations of 120 different nozzles, that lead to the optimum contraction shape for a given application.

Morel has considered only one family of wall shapes in his studies. The wall shapes used is a family of two matched cubic arcs, each having its apex at the end of the nozzle while their slopes are matched in the interior (Fig. 3.1.4).

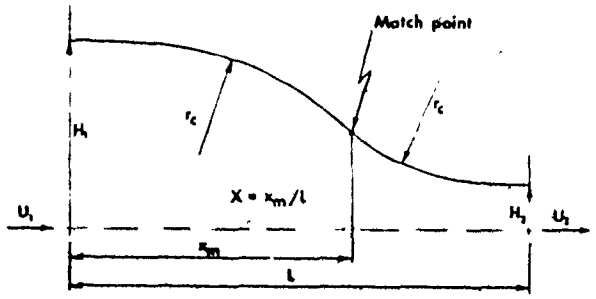

Figure 3.1.4 Wall shape made of two cubic arcs

The cubic was judged to be a good choice for a simple one parameter family and was found to be near optimum for axisymmetric contraction designs and sufficiently close to the optimum for two-dimensional designs. This is supported by the experimental results reported by Rousse and Hassan [56].

Results reported by Hussain and Ramjee [57] also indicated that nozzles having matched cubic arcs as wall contours can be regarded as having the best performance between the four different types of nozzles that they tested. Their results indicated that the cubic arc nozzles yielded the mildest inlet adverse pressure gradient due to their smallest inlet curvature, the smallest boundary layer thickness and the smallest turbulence in the exit plane. In view of the simple design procedure and the performance of the matched cubic arc family of wall contours, it was decided to follow this design procedure as outlined by Morel [48] for the design of our contraction.

Given the size of the working section and the available space it was determined that the maximum contraction ratio that could be achieved would be a ratio of 4:1 for a two-dimensional contraction and 16:1 for a three-dimensional contraction. At this point no decision between the use of a two-dimensional and a three-dimensional contraction was made. Although a three-dimensional contraction was expected to have better performance characteristics than a two-dimensional one, the ratio of performance to cost had yet to be determined.

To compare the performance between the two configurations, we should be able to predict the contraction performance at the design stage. For this, a three-dimensional, finite element potential flow computer program, developed by El Shammaa [58] was employed.

A total of four different 3-D contractions with contraction ratio of 16:1 were designed and their velocity profiles at the exit plane of the nozzle were obtained using the computer program. The velocity was set to be uniform, at a length equal to the major dimension of the contraction cross-section, upstream of the inlet and downstream of the nozzle exit, in order to satisfy the assumed uniformity of the boundary conditions. The velocity profile could then be obtained at the exit of the contraction. Similarly three different two-dimensional designs were simulated, using the same boundary conditions as in the three-dimensional case, using the computer program.

The design procedure to obtain the wall contour is described in Appendix B.

The three-dimensional results indicated that the velocity nonuniformities at the exit varied from 0.9% of the mean velocity to 2.5% of the mean, between the four different designs. The two-dimensional results indicated nonuniformities from 0.8% to 2.8% of the mean velocities. It should be noted that the nonuniformities mentioned and predicted here are referred to the axial streamwise velocity.

In view of the very similar performance predicted

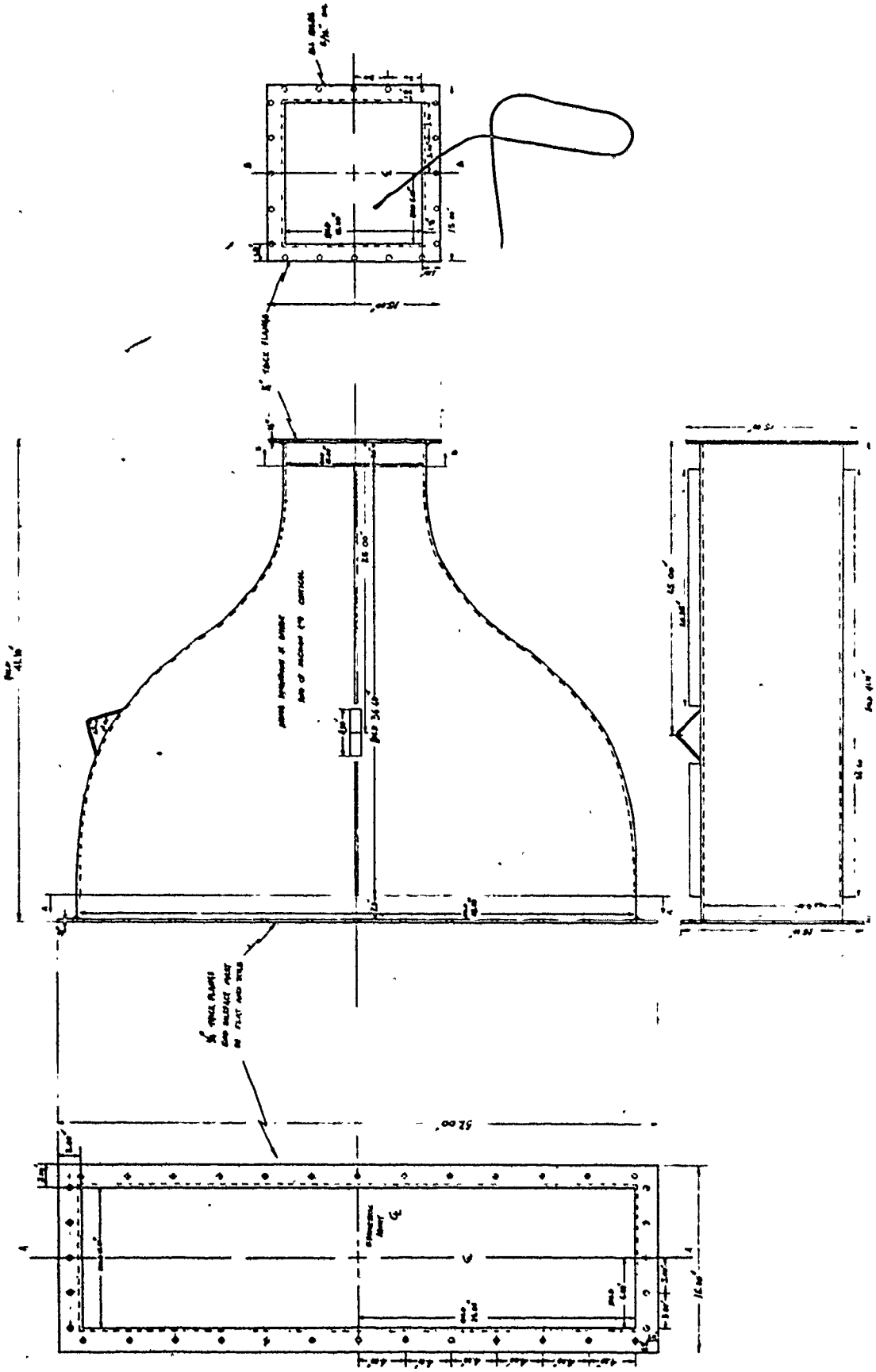

Figure 3.1.5 Schematic of the contraction

between the two configurations and the considerable difference in the construction costs, the use of a two-dimensional contraction was decided. Fig. (3.1.5) shows the contraction, made of 3 mm thick stainless steel used in this design. Its active length is 0.93 m (36.6") while its total length is 1.04 m (41.1") allowing two straight pieces of duct, 0.05 m (2") long, upstream and downstream of the nozzle.

The equations of the contour are given by (see Appendix B).

$$H = 2 - 0.147\, x^3 \quad \text{for } 0 < x \leq 1.83$$

and

$$H = 9.375\, (1 - \frac{x}{3.05})^3 + 0.5 \quad \text{for } 1.83 \leq x < 3.05$$

where H is the distance of the wall from the centerline and x is the length of the contraction in feet.

(ii) Settling Chamber

Fig. (3.1.6) shows the settling chamber schematic positioned upstream of the contraction. The role of the settling chamber is in the conditioning of the flow upstream of the contraction by means of screens, honeycombs, straightening tubes, etc. The dimensions of the settling chamber used are, 1.22 m long by 1.22 m high and 0.305 m wide and is made of a 3.2 mm thick, galvanized carbon steel. An observation acrylic "window" is positioned at 0.20 m distance from the chamber exit and is designed to be flush with the inside surface of the chamber so that the flow is not disturbed. A 60% open

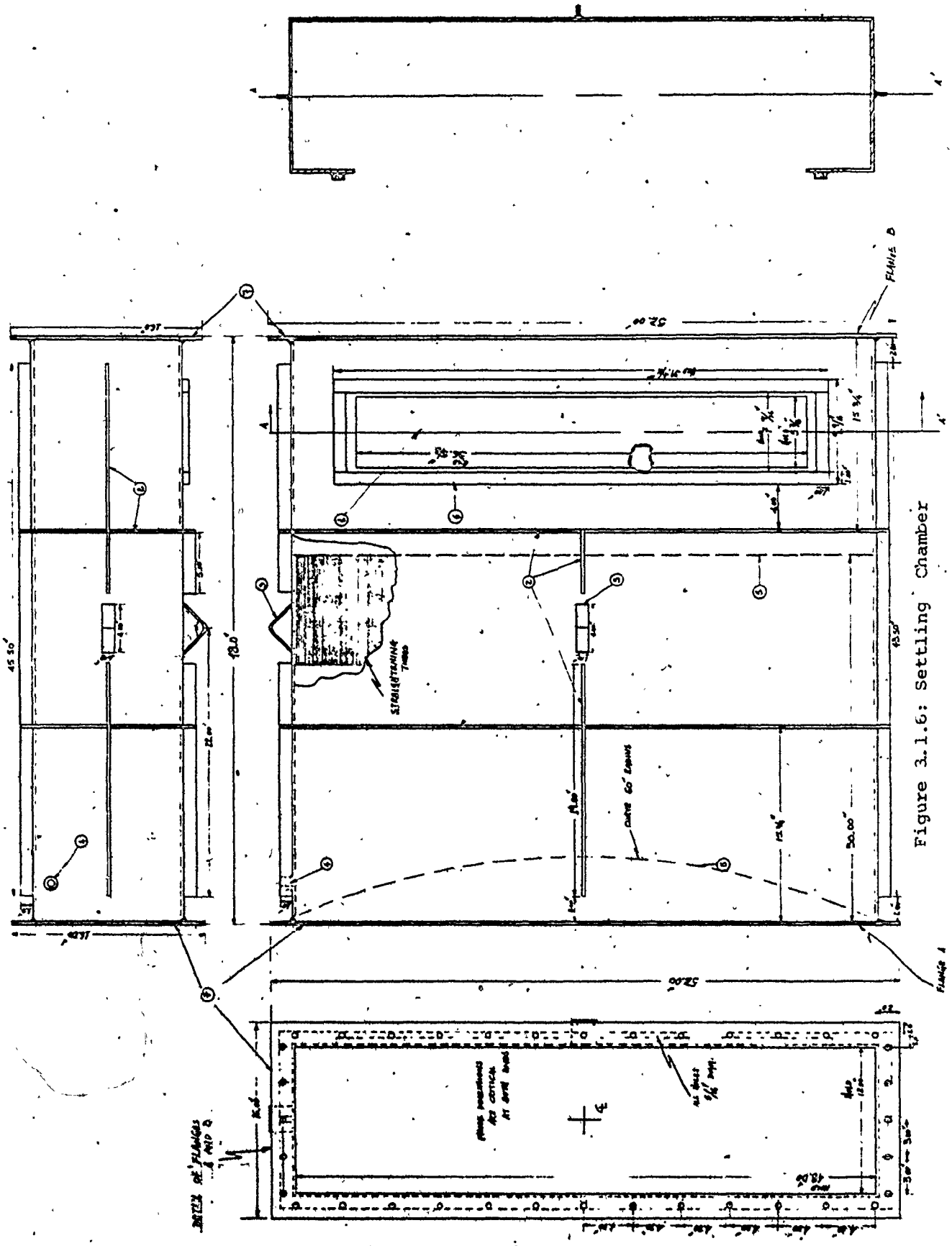

Figure 3.1.6: Settling Chamber

screen is positioned at a distance of 0.76 m from the chamber inlet. The role of the screens, when placed at a greater distance from the working section, in the low speed region upstream from the contraction, is that they can reduce the free stream turbulence. The physical explanation is that a screen will remove large scale eddies at the expense of introducing a large number of small scale eddies (maximum size is of the dimension of the mesh size) which in turn are found to decay rapidly.

The scale of the eddies that are introduced by a screen depends on the Reynolds number based on the diameter of the screen wires. If the Reynolds number is less than 40 then no eddies are shed and therefore no turbulence is introduced by the screen. In order to secure the low Reynolds numbers required, the screens are located in the low-speed area of the settling chamber. The maximum Reynolds number for the set of screens used, at maximum flow velocities is calculated to be 100. This indicates that at high flow velocities, small scale of turbulence is expected to be induced by the screens, but is expected to decay rapidly.

Upstream of the 60% screen a set of straightening aluminum tubes, 6.4 mm in diameter and 0.23 m long, are positioned, so that they cover all the flow area. Their act is similar to that of honeycombs. The existence of the straightening tubes will result in the breakdown of possible large scale vorticity in the flow and will reduce large lateral flow nonuniformities by forcing the flow to pass through the

tubes. The resulting lateral nonuniformities will be of the order of the tube diameter that can be further reduced by the action of the screens.

Finally, another screen with an initial radius of curvature of 1.52 m and 40% open is positioned at the inlet of the chamber as shown in Fig. (3.1.6.) Provisions were taken, during the design stage, to allow enough space in the chamber to permit us to install more screens in the event that further improvements of the flow, upstream from the working section would be required.

(iii) Wide Angle Transition

Upstream from the settling chamber, a wide angle transition piece is installed as shown in Fig. 3.1.7. The principle action of this component is to decelerate the flow before it enters the settling chamber. The main design criterion is the efficient conversion of kinetic energy to pressure energy. The usual rule of thumb for the design of diffusers is to use an expansion of 5 degrees included angle, in order to avoid separation. Since the small expansion angle required would result in an unacceptably long and costly structure, it was decided to design a wide (30^{o} half angle) angle transition. The total length of the transition is 0.76 m and is made of 3.2 mm thick galvanized carbon steel.

Due to the rapid expansion, separation of the flow from the walls will occur, but it can be limited by the positioning of the screens. The screens at this section play

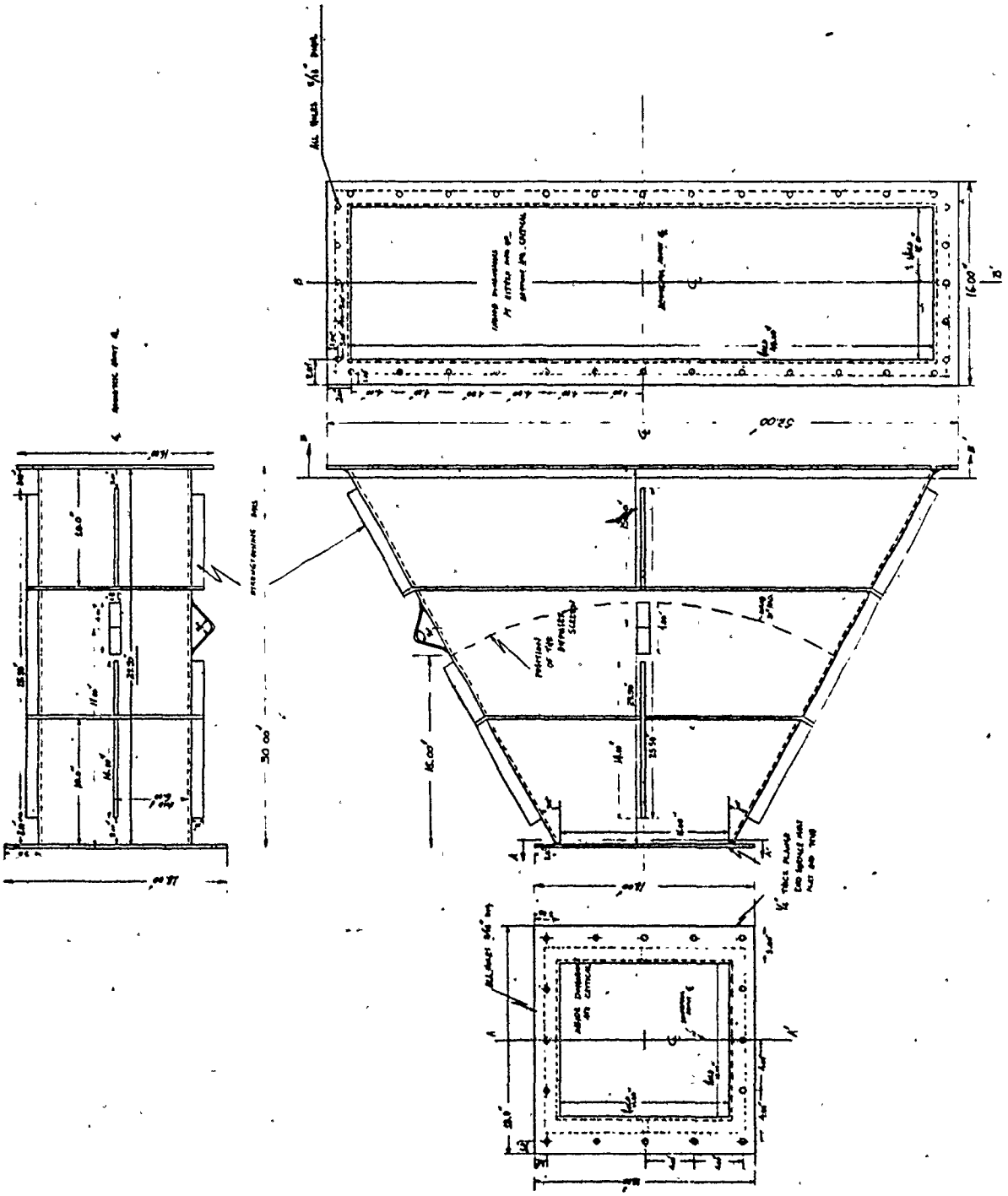

Figure 3.1.7 Wide angle transition

a dual role. Firstly, they will smooth out velocity variations at the expense of static pressure drop and secondly, their existence will cause reattachment of the flow on the walls. Two curved screens, both 40% open, were installed. The first screen is positioned at a distance of 0.38 m from the inlet and has a radius of curvature of 0.79 m. The screen is curved in order to improve its strength to resist the hydrodynamic loading. The second screen is positioned similarly at the outlet of the transition and is the same screen that is described at the inlet of the settling chamber. Here again enough space is allowed to position additional screens if needed.

All three components described previously, as it can be seen on the corresponding figures, are equipped on their outside surfaces with stiffening bars to reinforce their structural rigidity.

Finally the wide angle transition is connected to the tunnel piping through a straight connecting pipe, 1.12 m long and 0.36 m in diameter, as shown in Fig. (3.1.8)

The test section is connected to the tunnel piping downstream through a square to circular transition piece, 1.12 m long, as shown in Fig. (3.1.9.) The nominal dimension of the square end is that of the test section, i.e., 0.305 m square and the circular end has a diameter of 0.36 m in diameter. An overall view of the tunnel is shown in the photographs of figures (3.1.11) and (3.1.12).

(iv) Water Tunnel Performance

After the test section was positioned in the tunnel,

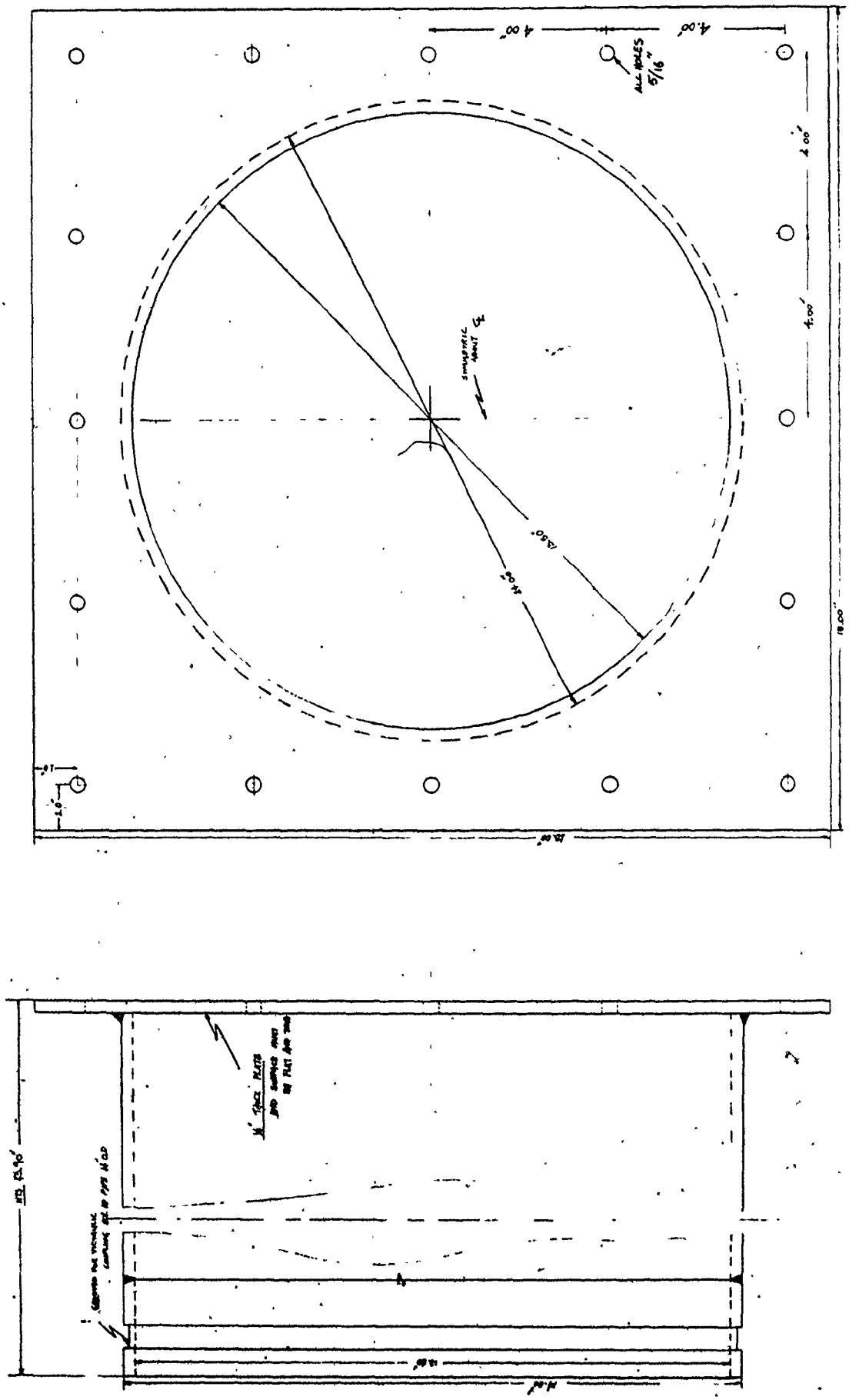

Figure 3.1.8 Connecting Pipe

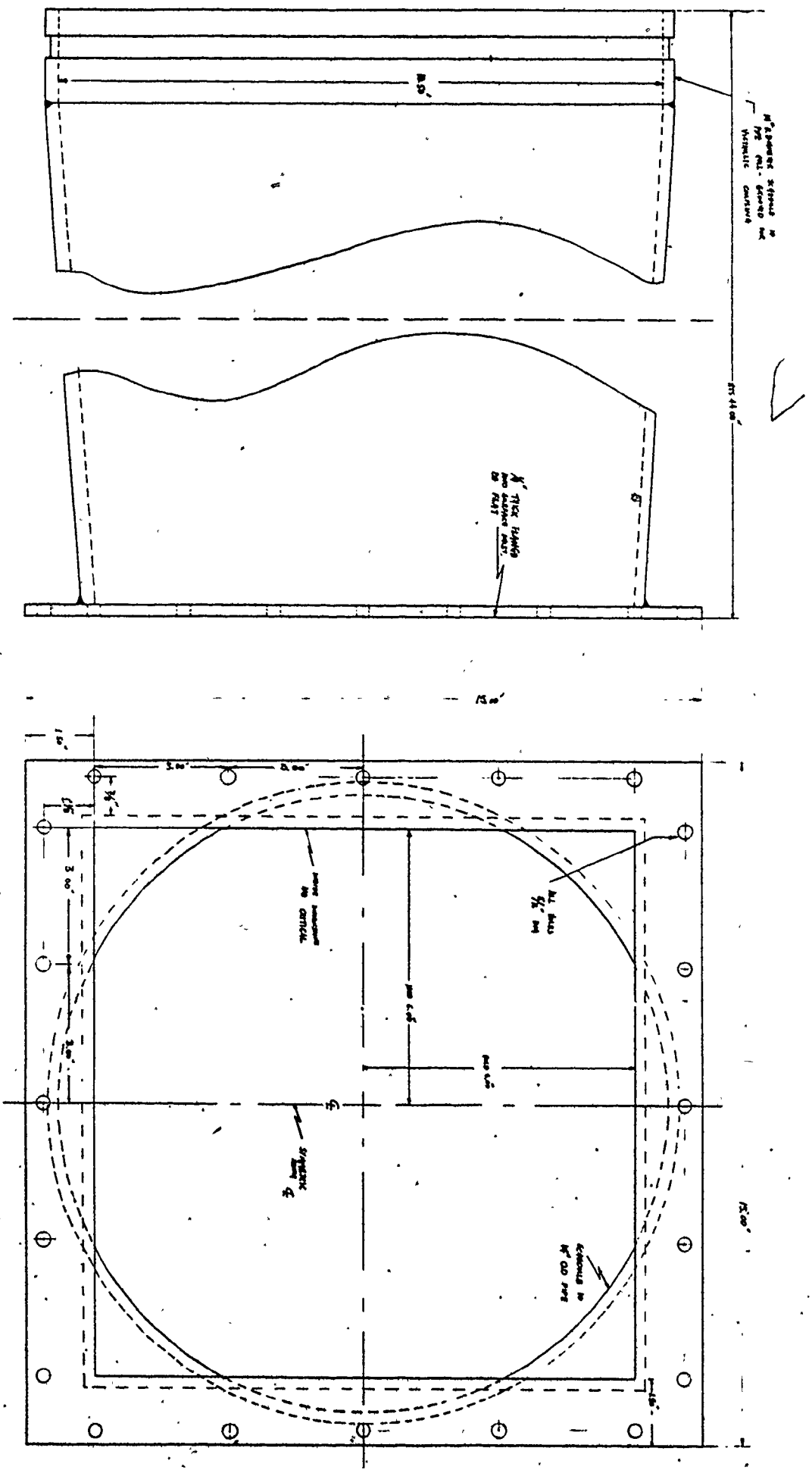

Figure 3.1.9 Square to circular transition

measurements to evaluate the overall performance of the tunnel were conducted. The local velocity was measured at a distance of 0.20 m downstream from the contraction exit, using a pitot-static probe. The normalized velocity distribution is shown in Fig.(3.1.10.) It can be seen that the velocity distribution is uniform within 1%, outside the boundary layer at an upstream velocity of 1.15 m/s.

The maximum upstream turbulence intensity recorded over the operating range of speeds, was only about 0.5%. Since the tunnel would be employed to study vibrations in tube bundles, the noise in the flow and vibration levels were also investigated. Power spectrum analysis of the signal obtained from a hot-film anemometer in the flow over a wide range of frequencies indicated that no predominant frequencies occurred in the flow except from the expected turbulent power spectrum of the flow. Using a three-dimensional accelerometer mounted on the structure of the working section, a structural vibration study was conducted.

The structural vibration levels in all three axes, at the lower frequency range (0-100 Hz) were negligible. Very small vibration levels were observed at high frequency ranges (150-500 Hz) which are not expected to contribute to the excitation of the tube bundle under study, due to the adequate frequency separation. The overall performance of the tunnel was considered satisfactory and no improvements to the original design were necessary.

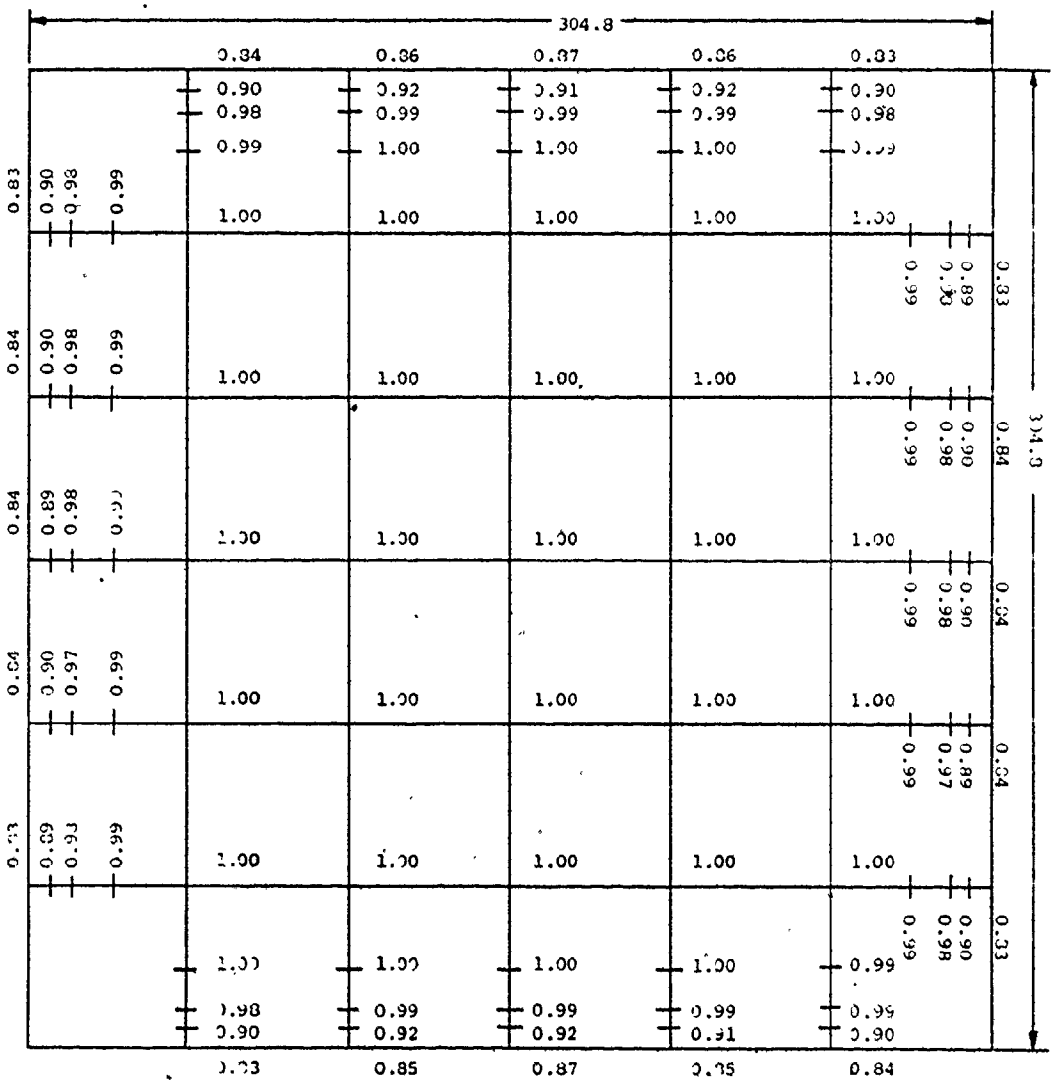

Figure 3.1.10 Normalized velocity distribution

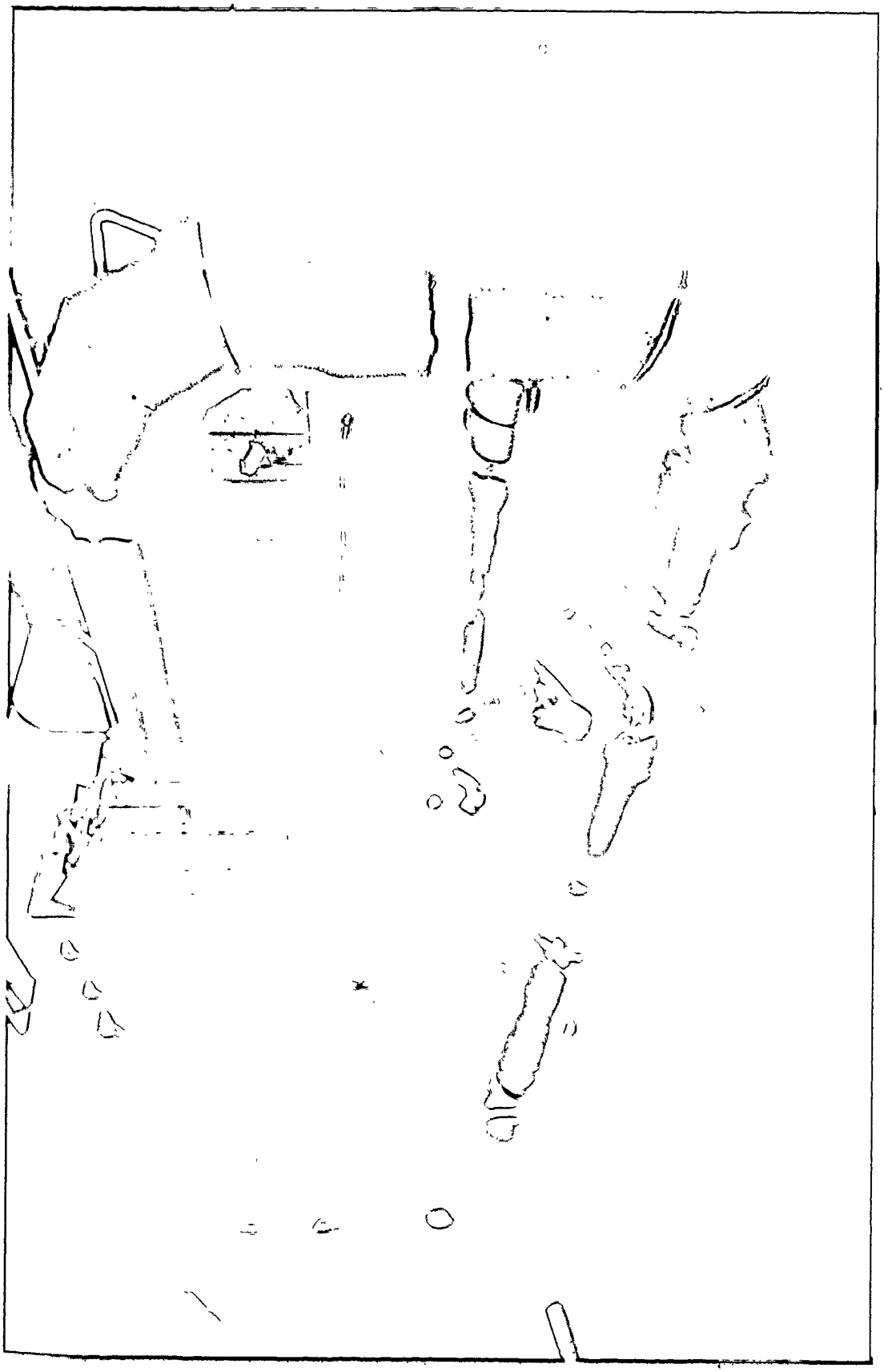

Figure 3.1.11 Overall View of the Water Tunnel

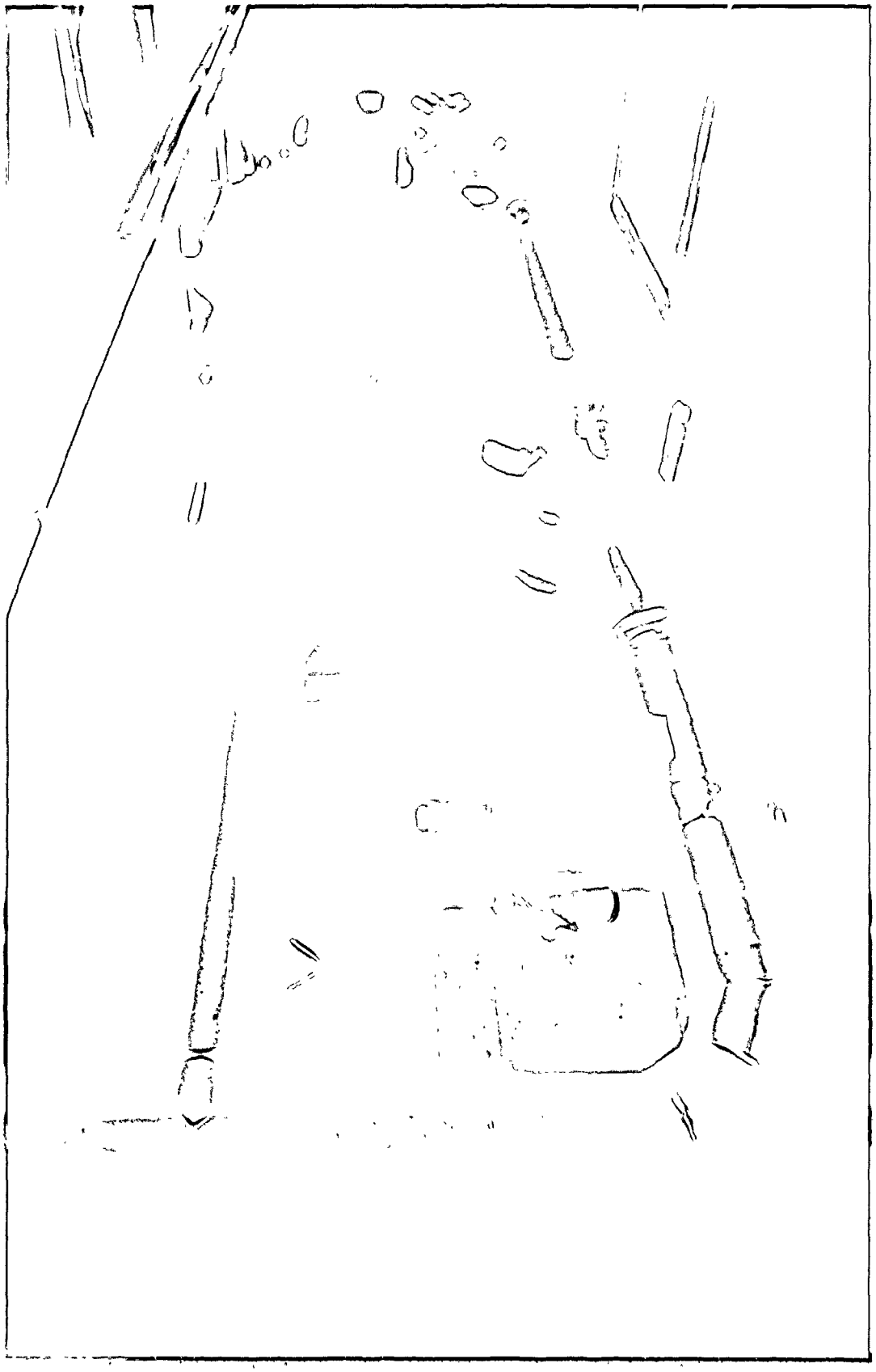

Figure 3.1.12 Overall View of the Water Tunnel

3.2 Test Section

(a) Test Section Design Principles

As it is desired to design and develop an experimental facility to study excitation phenomena associated with the liquid cross-flow induced vibrations in heat exchanger tube bundles, the design of a test section to model the behaviour of such equipment in liquid cross-flow becomes necessary. A justification of the present design is attempted below.

The type of array used for the present work is a parallel-triangular tube-array with pitch to diameter ratio of 1.375. One reason for the use of such an array is that it is a popular array, widely used in the contemporary design of heat transfer equipment. Another reason is that we also wanted to compare the present results with those obtained from the wind tunnel studies using this array pattern and pitch. The width and the depth of the array are important for the correct simulation of excitation phenomena such as vorticity, response to turbulence and fluidelastic response. Experimental results reported in the literature [59, 60] indicate that this phenomena can be effectively simulated using models only a few rows deep. El Kashlan [59] reports that the minimum critical velocity for fluidelastic instability occurs in the third and fourth row of the array and is estimated to be about 20% lower than the critical velocity deep inside the bundle as shown in Fig. (3.2.1.)

It is also known that the fluid motion associated with the vibration of a structure has an important effect on its dynamical behaviour, particularly on its natural frequencies.

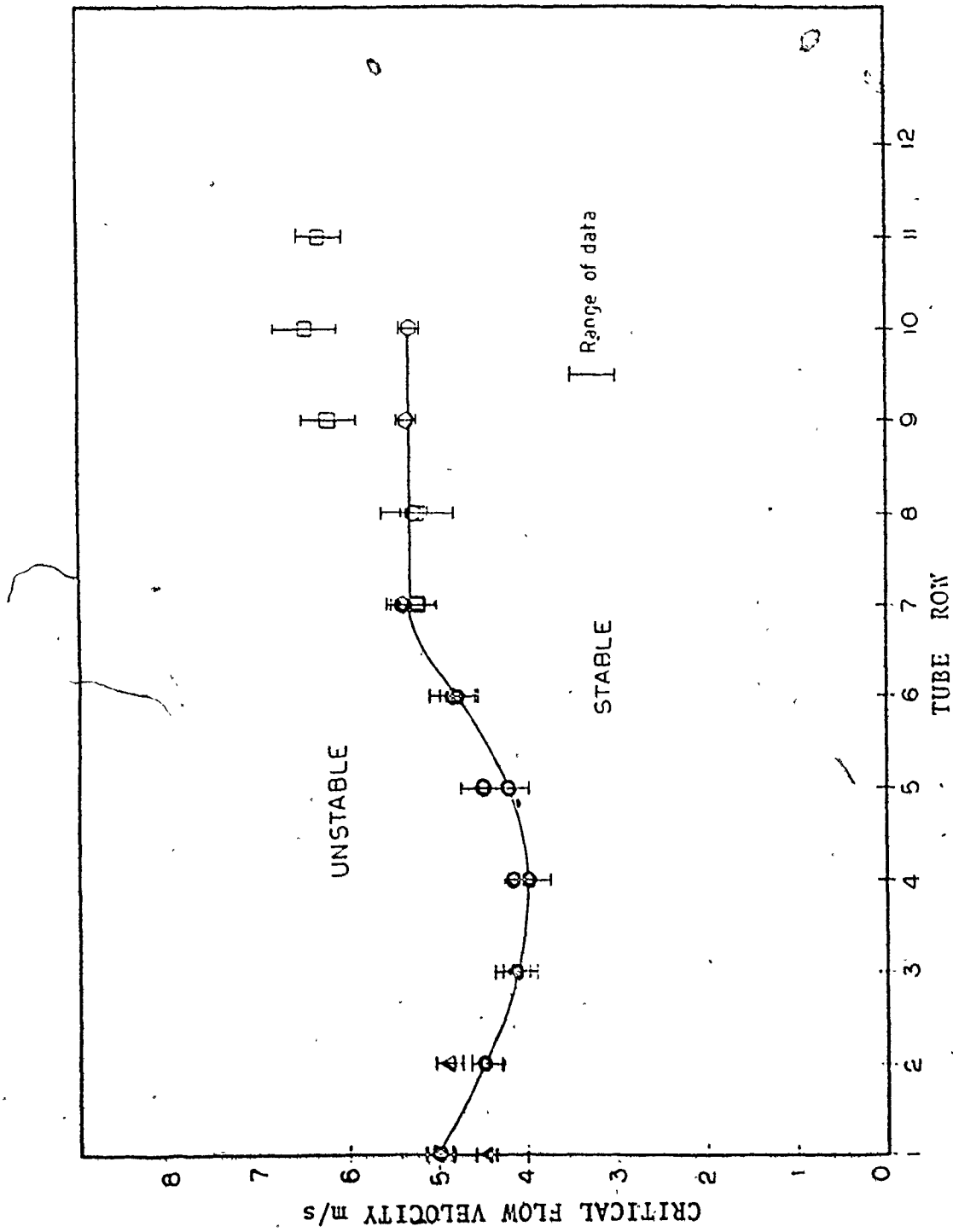

Figure 3.2.1: Diagram of critical velocity v's tube row.

While this effect is usually negligible for bodies vibrating in air, it can be very important for structures vibrating in water. This effect can be accounted for by an addition to the mass of the body which is referred to as "added" or "hydrodynamic" mass. Parameters such as amplitude and frequency of the structure's motion, shape, submergence, and confinement can affect the added mass term. In the case of a staggered tube array in liquid flows, an energy transfer between neighbouring tubes, through the fluid, known as fluid coupling is also present.

If proper dynamic simulation is to be achieved these parameters should be adequately modelled. In the literature, Chen [61, 62] has shown that the coupling between a cylinder and other cylinders which are not immediately surrounding it is negligible. This indicates that phenomena associated with the added mass effects in a tube bundle can be properly simulated with models that are only a few rows deep as long as the tubes surrounding the tube under study are flexible too.

Vorticity is not expected to be a predominant excitation mechanism. If it occurs it is expected to affect only the first few rows of the tube bundle. This is also confirmed from the observations reported in the literature by Gorman [37]. He observed that only the inlet tubes of certain arrays passed through well defined amplitude peaks before the onset of the fluidelastic instability. These peaks are considered to be the result of resonant interaction between vorticity forces and the inlet tubes. Turbulence of the free stream is expected to

increase inside the tube bundle with the number of rows up to about the fifth row. No need for simulation of the internal axial flow exists in the present study since the axial flow effects will be negligible. The reason is that in order for the axial flow to create instabilities, the flow velocity in the tubes should reach velocities that are far in excess from the axial velocities encountered in the present design of heat exchangers. Finally since we attempt to simulate the dynamic behaviour of the centre portion of a tube, for which we assume that both its ends are rigidly fixed, our model flexible tubes should be effectively rigid but elastically mounted. The restoring forces should be linearly proportional to tube displacement for small displacements and good frequency control is required. The damping of the model tubes should also be viscous and if possible controlled. The length of the model tube can be sufficiently small as long as the boundary layer effects of the flow at both its ends compared to its total length exposed to the flow can be considered to be negligible.

In view of the information presented we can conclude that a model a few rows deep can adequately simulate a tube bank. This results in a dramatic reduction of the model costs and set up time.

The description of the test section used for the present study is presented below.

(b) The Acrylic Working Section

The acrylic section is positioned between the contraction and the square to circular transition in the tunnel. The total

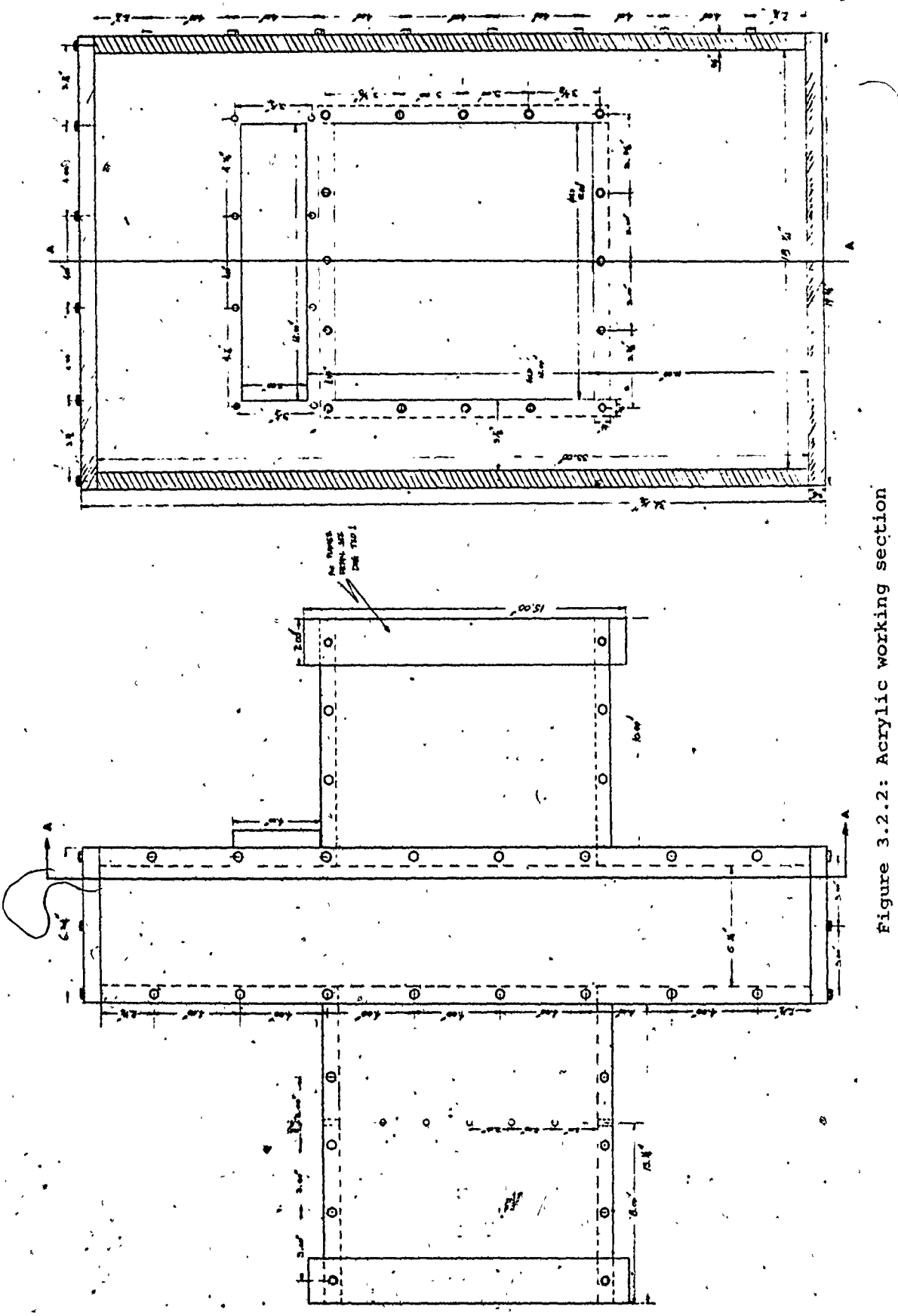

Figure 3.2.2: Acrylic working section

length is 0.76 m and is constructed out of 19 mm thick acrylic plate as shown in Fig.(3.2.2.) Its major function is that it provides a leak proof enclosure for the tube bundle. Its top is removable for easy access to the test section.

(c) The Tube Bundle

(i) Piano-wire tubes

The type of flexible model tube used for this study is a piano-wire suspended light aluminum tube, as shown in Fig.(3.2.3.) This type of tube-model has been used by previous investigators [59, 60] and has demonstrated excellent performance characteristics.

The aluminum tubes were 298.5 mm long, had a 25.4 m O.D. and a 1.02 mm wall thickness. They were mounted on a 1 mm diameter piano wire, allowing 305 mm of free wire length at both ends. The piano-wire tube assembly was then mounted on a steel frame, in the following way. The wire passed through the two 9.5 mm thick steel plates of the steel frame. A 6.4 mm brass screw with a concentric hole was passed at the ends of the wire half way through the outer steel plates of the steel frame. The wire was bent and held by a nut and bolt assembly at the ends of the brass screw. A wing nut was then attached at the bottom brass screw. At the top brass screw, a compression coil spring was installed concentrically, and a washer wing nut was installed on the brass screw on top of the compression spring. Adjusting the bottom wing nut allowed the correct positioning of the model tube in the test section. The compression of the coil-

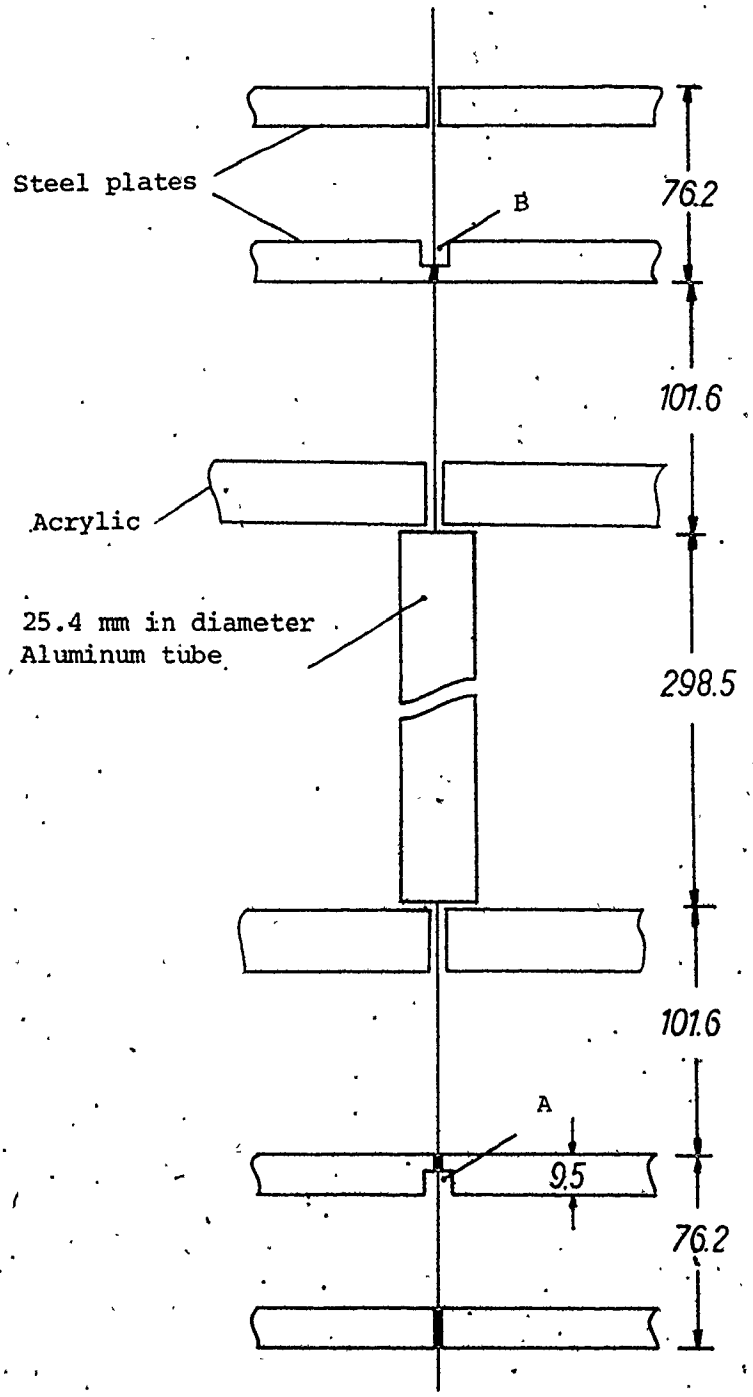

Aluminum filler was poured in grooves A and B

Figure 3.2.3 Piano-wire model tube

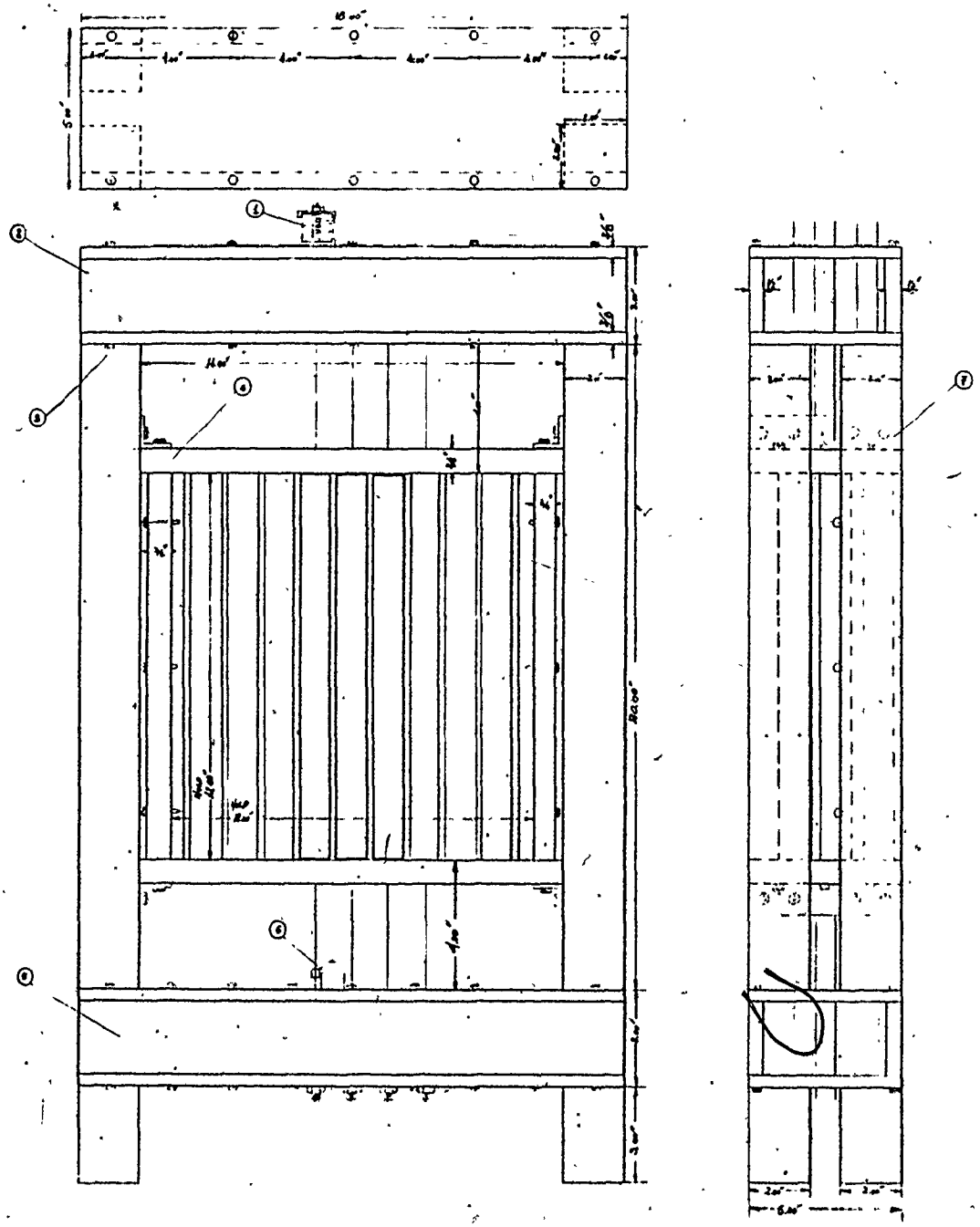

Figure 3.2.4: Test section assembly

spring allowed fine control of the translational natural frequencies of the tubes.

The steel frame used to mount the 10 flexible model tubes is shown in Fig. (3.2.4) The frame consisted of two hollow box type components held 508 mm apart with four 51 x 51 x 6.4 mm square steel tubing bolted at the four corners of the hollow-type boxes. The hollow boxes consisted of two horizontally positioned 457 x 127 x 9.5 mm thick steel plates, held 57.2 mm apart by two 457 x 57.2 x 12.7 mm thick vertically positioned steel plates, and bolted together.

The maximum deflection at the middle of the box due to the maximum tension of all the piano-wires was estimated to be less than 0.013 mm. The structure should be very rigid so that no change in the tuned natural frequencies of the tubes would result from the tuning of subsequent tubes.

(ii) The test array

A parallel-triangular array having a pitch to diameter ratio of 1.375 was used as shown in Fig. (3.2.5.) The array was 9 rows wide by 6 rows deep. Half tubes were installed at the section side walls to reduce water tunnel wall effects. Only the ten numbered tubes shown in Fig. (3.2.5) were mounted flexibly. The design of each of the flexible tubes was the same as described in the previous section. Only tubes numbered 3 and 4 were studied in this work. Hereafter, these tubes will be referred to as tube number 3 and tube number 4 respectively. These two tubes were instrumented with two accelerometers each.

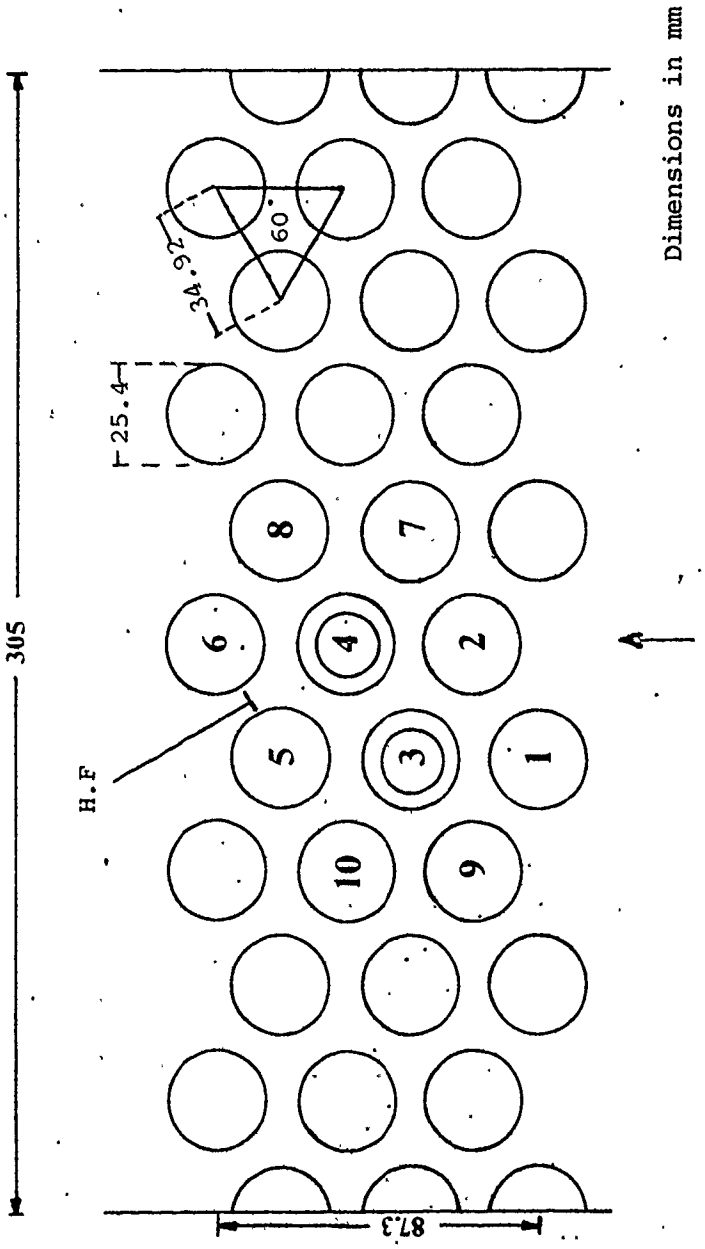

Figure 3.2.5 The tube array

The accelerometers were mounted on a fixture at right angles to each other, with their sensitive axes at the same horizontal plane. The fixture was then inserted into the tube and was positioned rigidly at a distance of 99.5 mm from the top of the tube. A counter-balance weight of 19 grams was inserted from the bottom of the tube and fixed rigidly into position in order to balance the tube with respect to its centre. The location of the sensitive axis of each accelerometer was marked on the outside of the tube for easy alignment of the tubes when positioned in the test section. The reason that the accelerometers are not positioned at the centre of the tube is that we wish to detect "rocking" frequencies as well as translational frequencies of the tube. The end cover plates of the tube were then installed and water leakage inside the tubes was prevented using a silicone sealant. A schematic of the instrumented tube is shown in Fig. (3.2.6.)

The non-flexible tubes are made of clear acrylic rod and are mounted on an acrylic sub-frame shown in Fig. (3.2.7), which in turn is mounted on the steel frame of the test section. Ten holes are drilled at the top and bottom of the acrylic sub-frame, corresponding at the centres of the flexible tubes to allow the wires of these tubes to pass through and be attached to the steel frame.

The role of the acrylic sub-frame is that it provides support for the fixed tubes and when the test section is inserted in the working section, the walls of the sub-frame are aligned with the walls of the working section. It also provides a

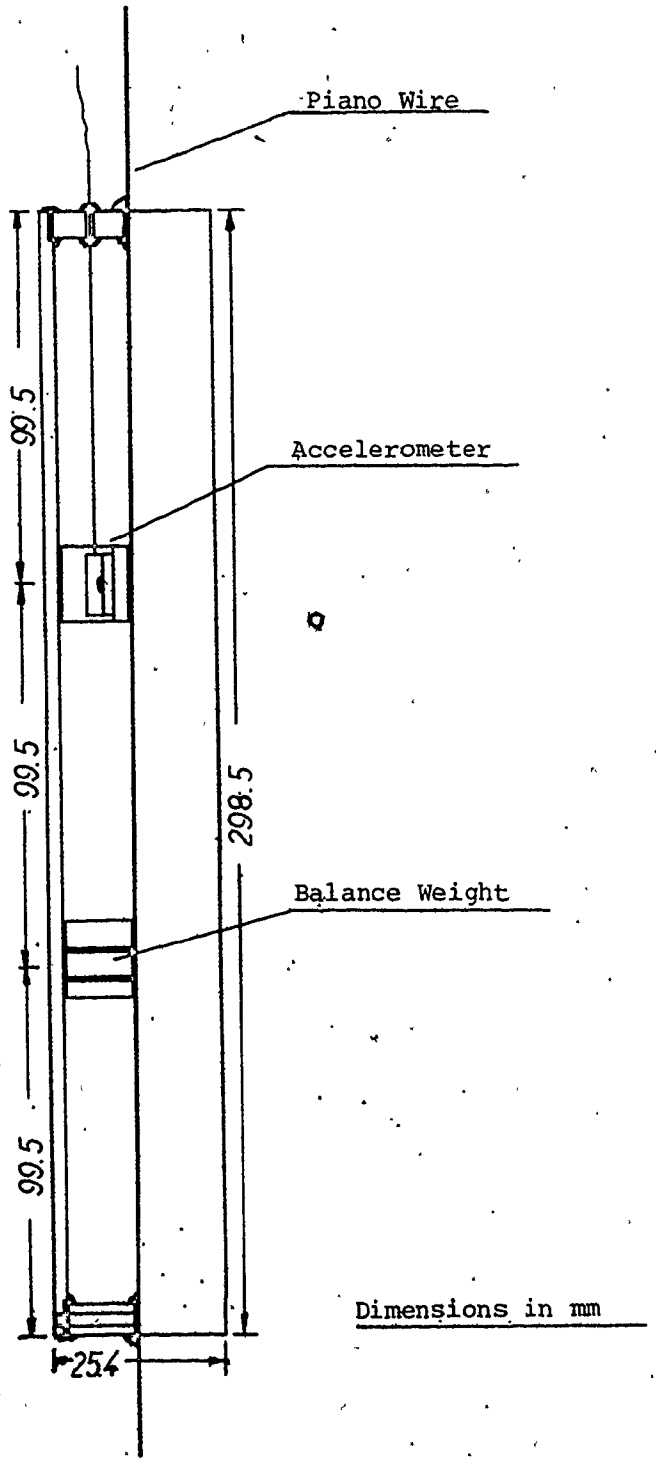

Figure 3.2.6: Instrumented model tube

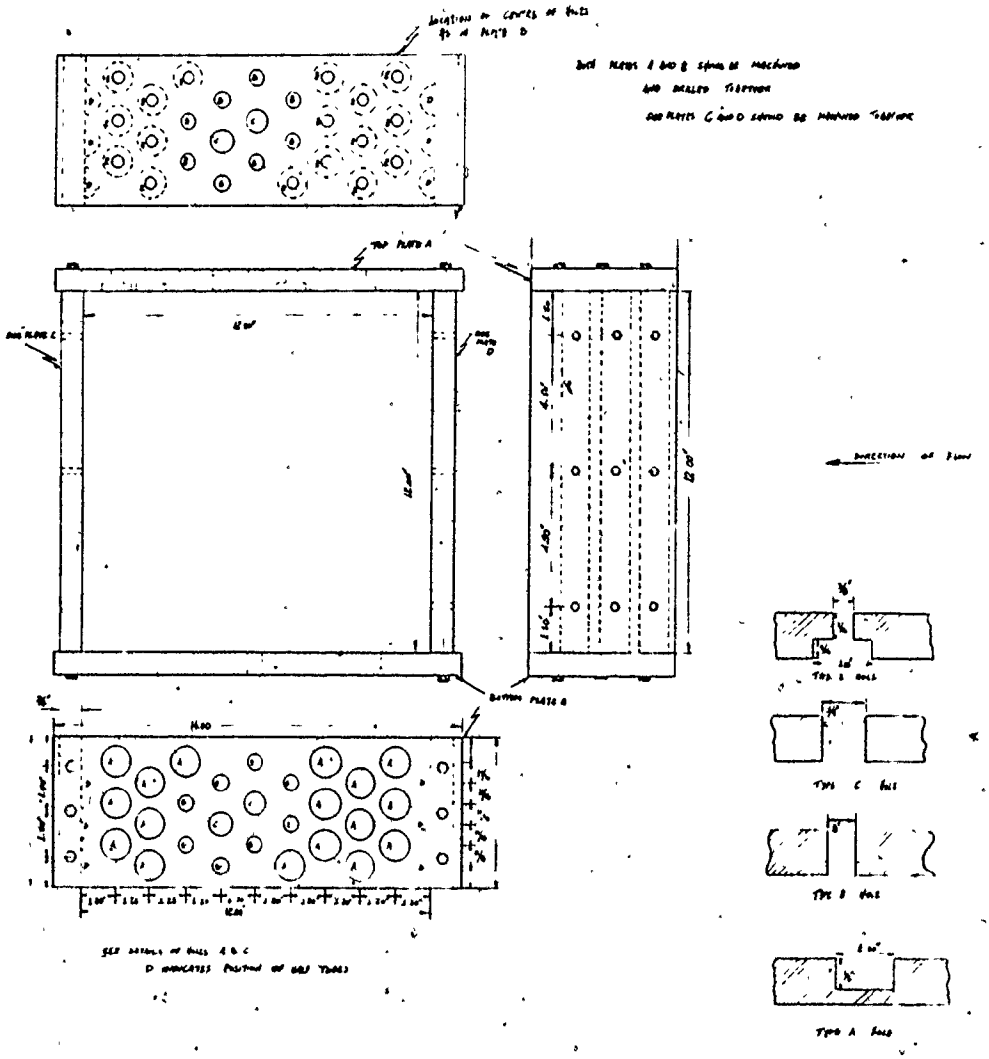

Figure 3.2.7: Acrylic subframe

continuous enclosure around the tube array so that only the assembly of fixed and flexible tubes are exposed in the flow.

The overall assembly of the test section is shown in the photograph of Fig.(3.2.8). A view of the working section is shown in Fig.(3.2.9) while a view of the assembly of the working section with the test section in position is shown in Fig.(3.2.10) where the flow is from right to left.

The upstream velocity in the tunnel was measured using the calibrated flowmeters installed in the main and by-pass lines. The transitional natural frequency of the flexible tubes was measured by releasing the tube after displacement from its static equilibrium position and viewing its frequency on an electronic frequency analyzer. For the non-instrumented flexible tubes, a capacitive probe was employed to obtain the displacement signal. For the instrumented tubes the output signals from the accelerometers were used. The tension in the piano-wire was adjusted in order to obtain the desired frequency for each tube. The procedure was repeated for all flexible tubes, until all were tuned to a natural frequency of 40 ± 0.2 Hz in air. No relaxation or creep was noticed to occur in the wires, i.e., the tubes maintained their tuned natural frequencies throughout the tests. The natural frequencies of the tubes were checked periodically to ensure that no detuning occurred.

The logarithmic decrement of free vibrations of the two instrumented flexible tubes (tube number 3 and tube number 4) was measured by releasing the tube after it was displaced from its static equilibrium position and recording the subsequent

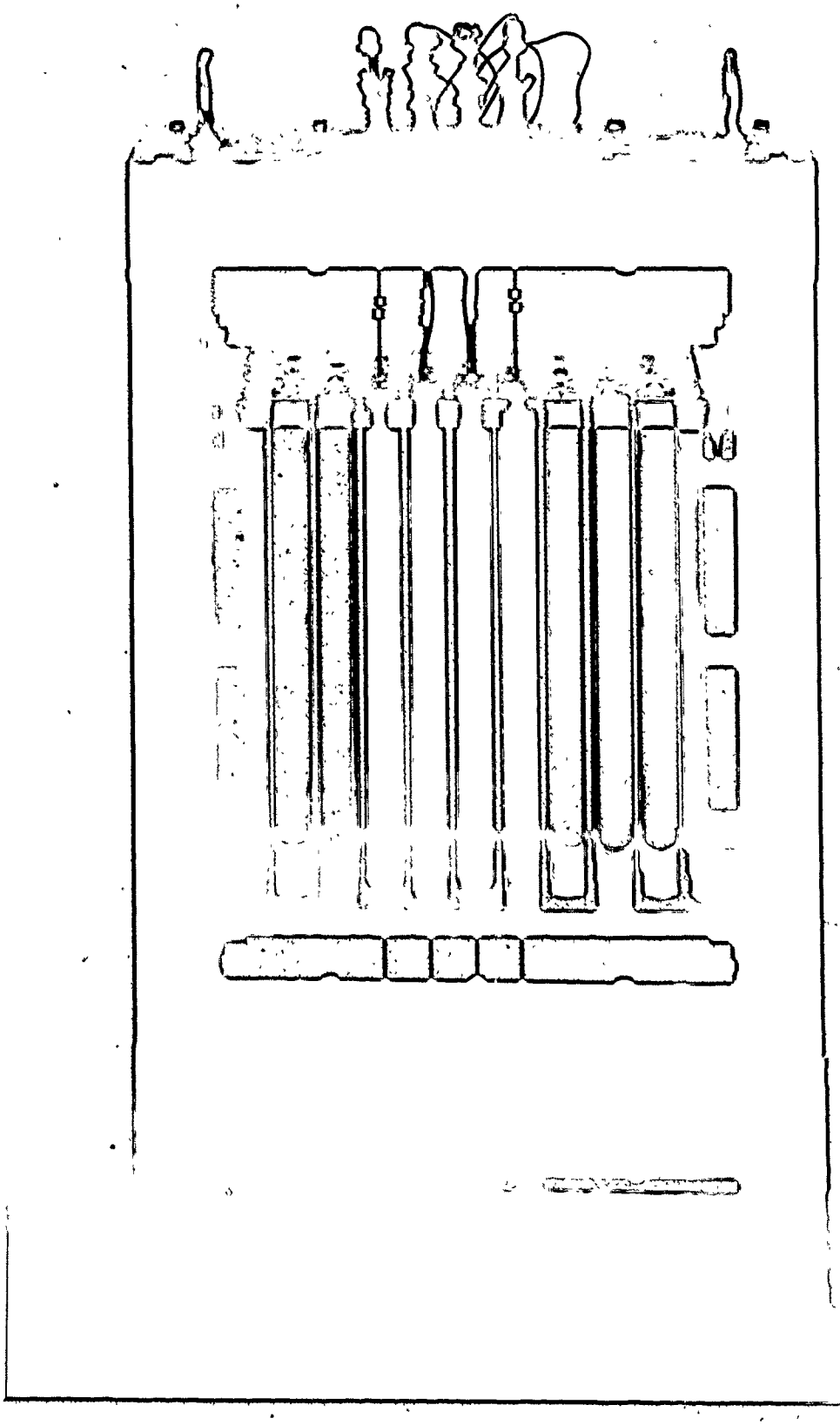

Figure 3.2.8 Overall View of the Test Section

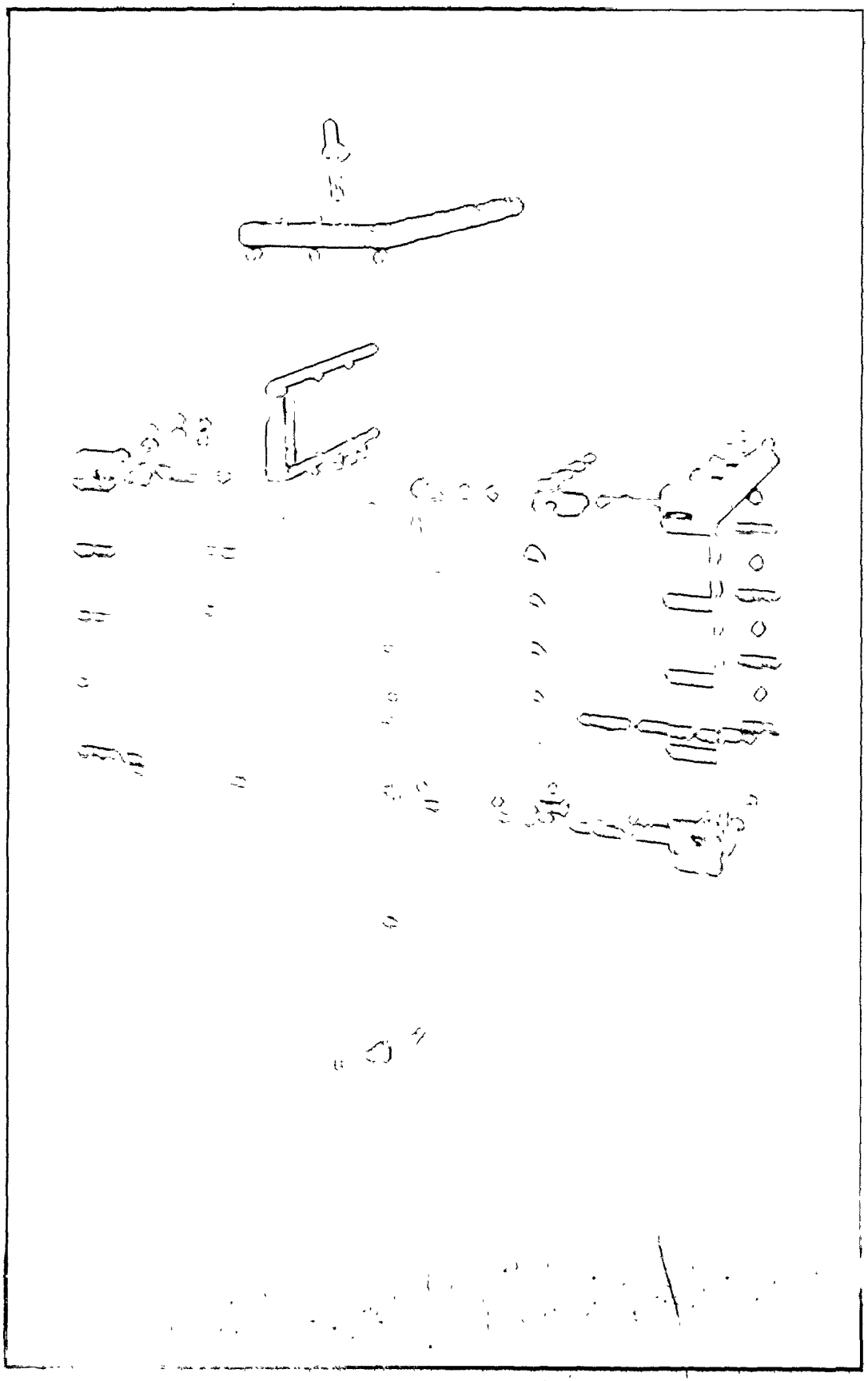

Figure 3.2.9 . A View of the Working Section

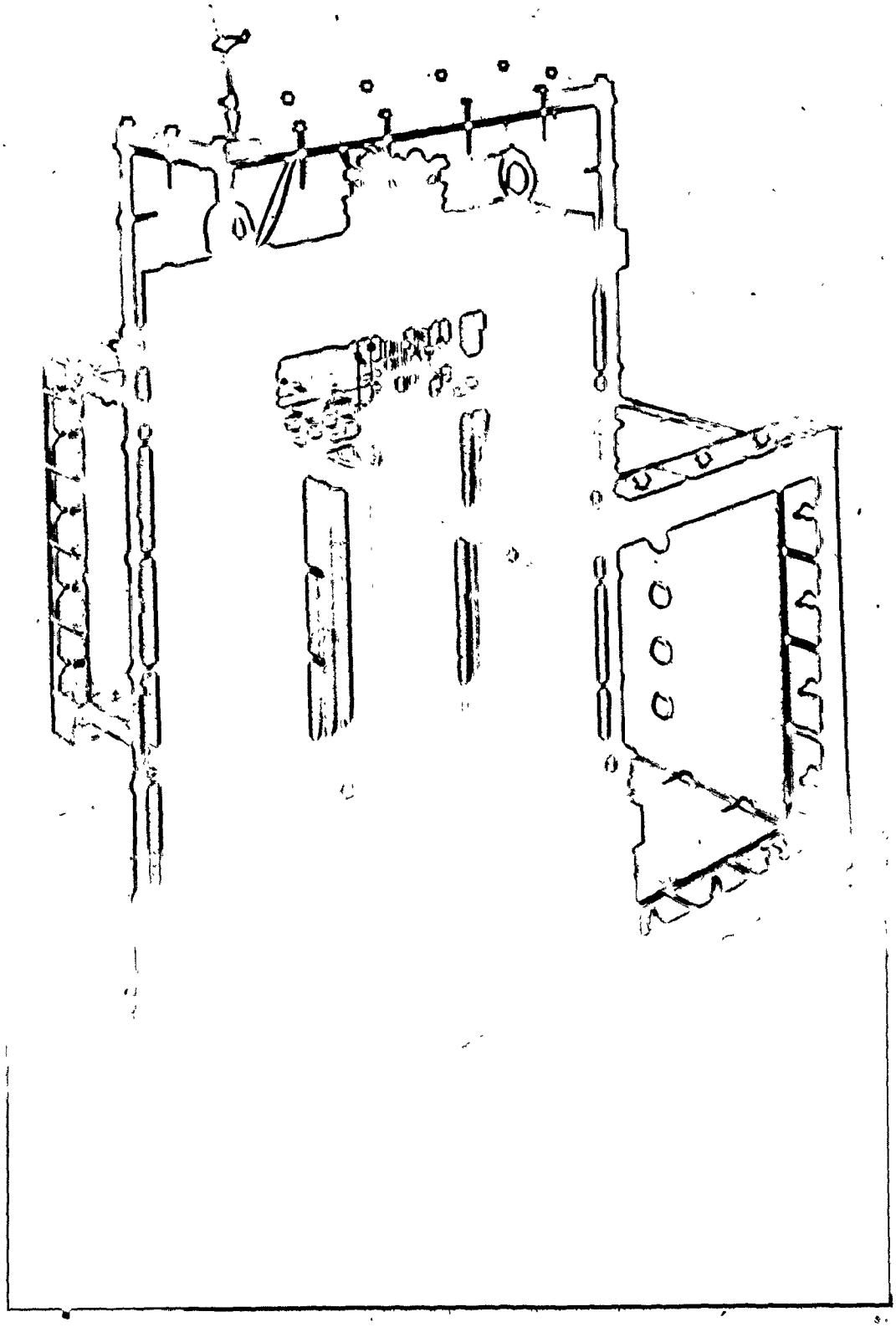

Figure 3.2.10 A View of the Working Section with Test
in

amplitude decay trace on a U.V. recorder. The number of free vibration cycles required for the amplitude to decrease from a particular amplitude to a selected lower amplitude were counted and the value of the logarithmic decrement was derived. To avoid the amount of impact damping that would be present due to the inevitable manufacturing tolerances between the drilled holes in the steel plates of the steel frame and the piano-wire of the tubes, aluminum filler was poured around the wires in specially provided grooves as shown in Fig.(3.2.3.)

3.3 Instrumentation

The upstream flow velocity was measured using a pitot-static probe and a micro-manometer using carbon tetrachloride as the working fluid. The flowmeters that were installed at the main and by-pass lines were calibrated using the pitot static probe. The flowmeters used were Brooks full-view rotameters type 1110-08-2 C1A with ranges from 100 to 1700 USGPM and 500 to 6500 USGPM for the by-pass and main line respectively.

The restriction orifice plates used were made out of 304 grade stainless steel with bores of 115.6 mm for the 152.4 mm (6") schedule 40 by-pass line and 230.25 mm for the 304.8 mm (12") schedule 10 main line.

The tube motion of the instrumented tubes was monitored using two Entran EGAL-125F-10DY miniature accelerometers located in such a way that the streamwise and transverse response could be obtained independently.

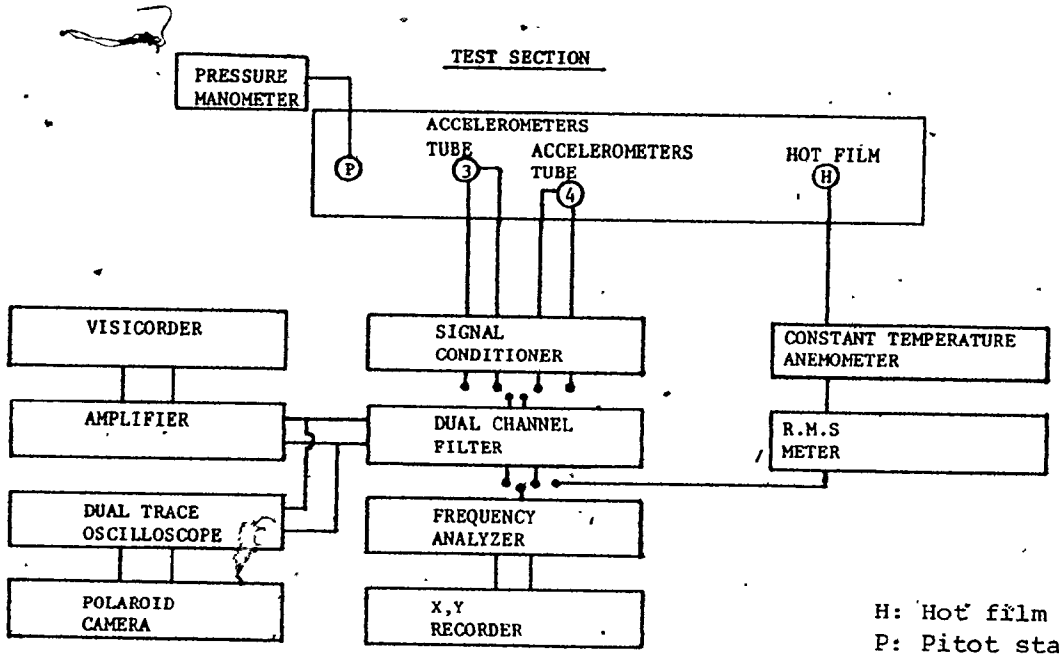

Figure 3.3.1: Instrumentation layout

Non-instrumented tube frequency tuning was accomplished using a Mechanical Technology Inc. non-contacting capacitance displacement probe type ASP 10 and a MTI Accumeasure 1000 Bridge, feeding the output signal to the frequency analyzer. The frequency spectra were obtained using a Spectral Dynamics SD 335 real time frequency analyzer and plotted using a Hewlett-Packard 7004B X-Y recorder.

The accelerometer output was amplified using a four channel Vishay 2310 signal conditioning amplifier. It was then filtered using a Rockland 432 two channel low pass filter. Tube mode shapes were recorded using a Polaroid type G12 Tektronix Oscilloscope camera mounted on a type 564 B Tektronix dual trace storage oscilloscope.

The damping records were obtained using the traces of a Honeywell 2106 Visicorder and a Honeywell accudata 6-channel amplifier.

Finally, the frequency spectrum of the flow was determined using a T.S.I. type 1230 W hot film conical probe and a T.S.I. model 1051-2 monitor and power supply with a T.S.I. model 1053B constant temperature anemometer and a T.S.I. model 1056 variable decade resistance.

An overall layout of the instrumentation is shown in Fig. (3.3.1) The photograph of Fig. (3.3.2) shows the instrumentation used.

Figure 3.3.2 Overall View of the Instrumentation

CHAPTER 4

EXPERIMENTAL RESULTS

The experimental facility described in the previous chapter was used to conduct the present experiments. As shown in figure (3.2.5) the parallel triangular array used was six rows deep with five tubes in each row and had a pitch ratio of 1.375. Ten tubes were flexible (numbered 1 to 10 in figure (3.2.5)) and two of them (tube numbers 3 and 4) were instrumented with two accelerometers each.

The presentation of the results in this chapter is divided into four parts:

(1) Amplitude response and stability threshold of the tubes.

(2) Tube frequency response and flow periodicity measurements.

(3) The effect of detuning all adjacent tubes on the stability threshold of tube no. 3.

(4) Comparison of present results with those previously published.

The experimental procedure will be described first followed by the presentation of the results obtained.

4.1 Amplitude Response and Stability Threshold of Tube No. 3 and Tube No. 4

The set-up procedure for the testing to establish the

stability threshold of both tubes was the same. All the flexible tubes were tuned to a frequency of 40 $\pm$ 0.2 Hz in air as described in Section (3.2). The tube frequency spectrum in still air is shown in figure (4.1.1). The top figure shows the tube response for an off-centre excitation which in addition to the 40 Hz fundamental frequency shows that the "rocking" mode frequency is 84 Hz. When the tube is excited centrally the lower figure is obtained, indicating absence of the rocking motion. A record of damping in still air of tubes no. 3 and no. 4 was also obtained as shown in figure (4.1.2).

The value of damping for each tube in air was calculated for an average of ten records of measurements for both the streamwise and transverse directions separately. The standard deviation in these measurements was found to be less than 10% of the average value used in the calculations to follow. The tuned bundle assembly was then immersed in water. As expected, the fluid coupling in water was quite significant. It was found that more consistent data could be obtained if all the flexible tubes but the one being monitored were held fixed. To "freeze" the motion of adjacent tubes special wooden blocks were attached to the top and bottom of the tube suspension wires. The natural frequency in quiscent water for both directions were then recorded as shown in figure (4.1.3), and found to be 22.5 $\pm$ 0.2 Hz for both tubes in both directions.

The damping value of each tube was obtained for each tube holding the adjacent tubes fixed. When all tubes in the bundle

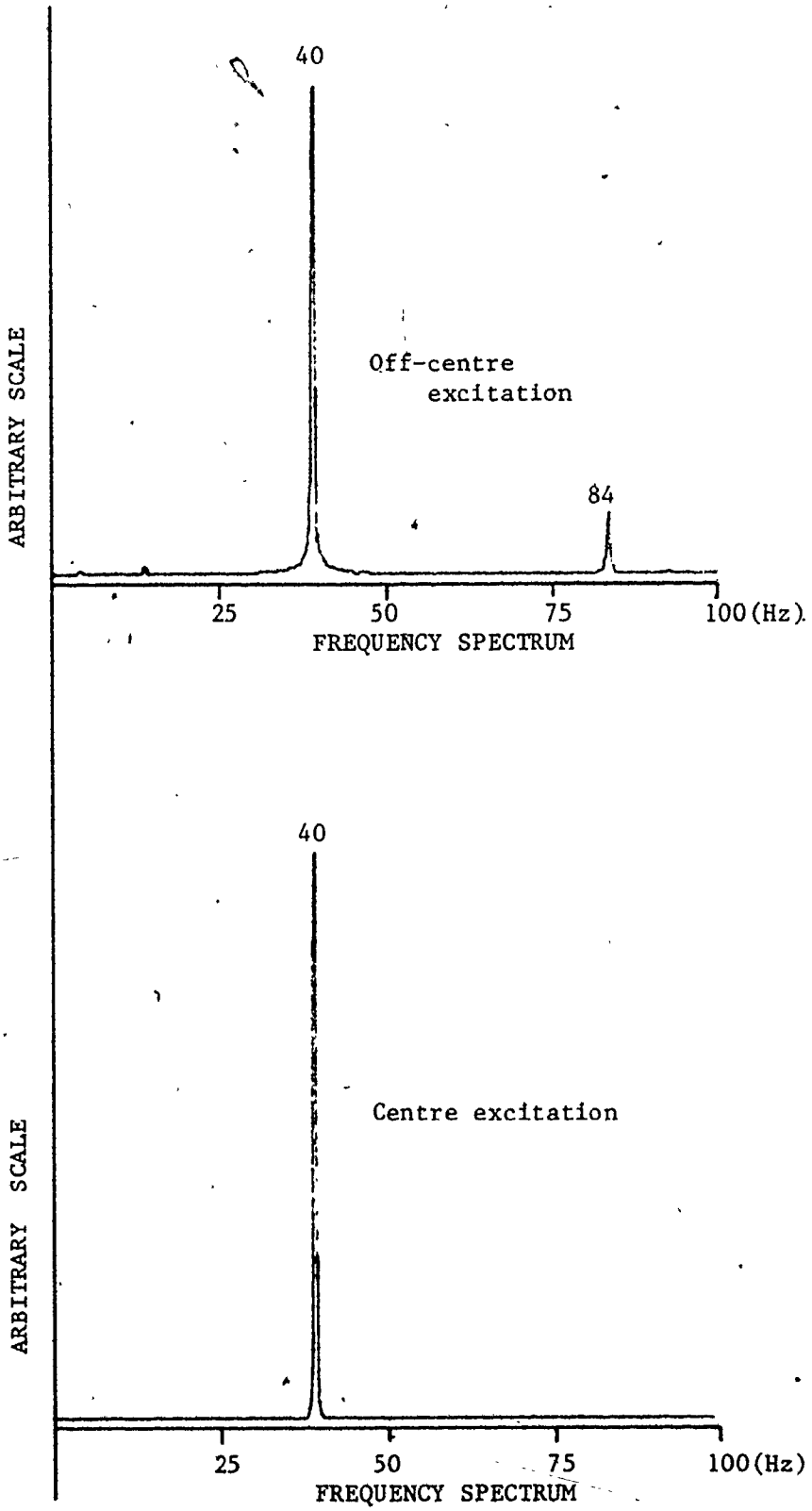

Figure 4.1.1: Natural frequency power spectrum of tube no. 3 vibrating in air.

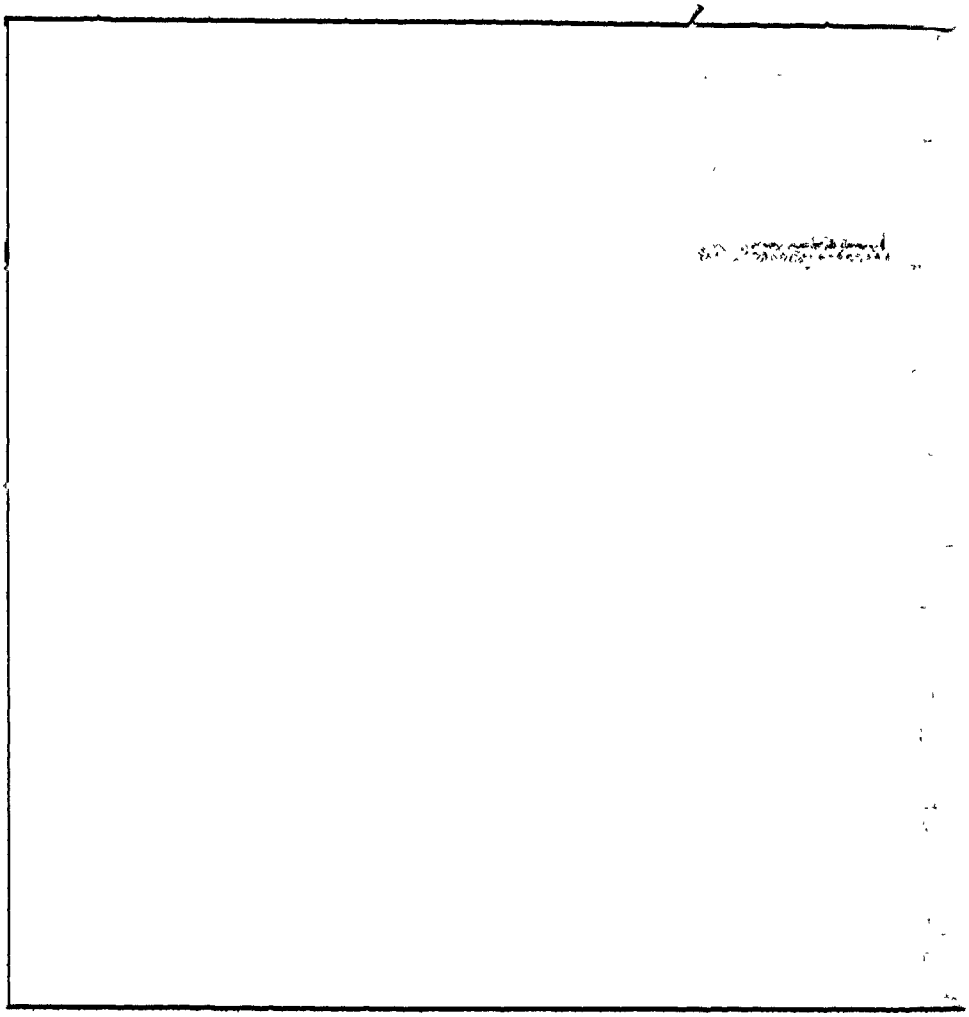

Figure 4.1.2: Air damping record for tube no. 3.

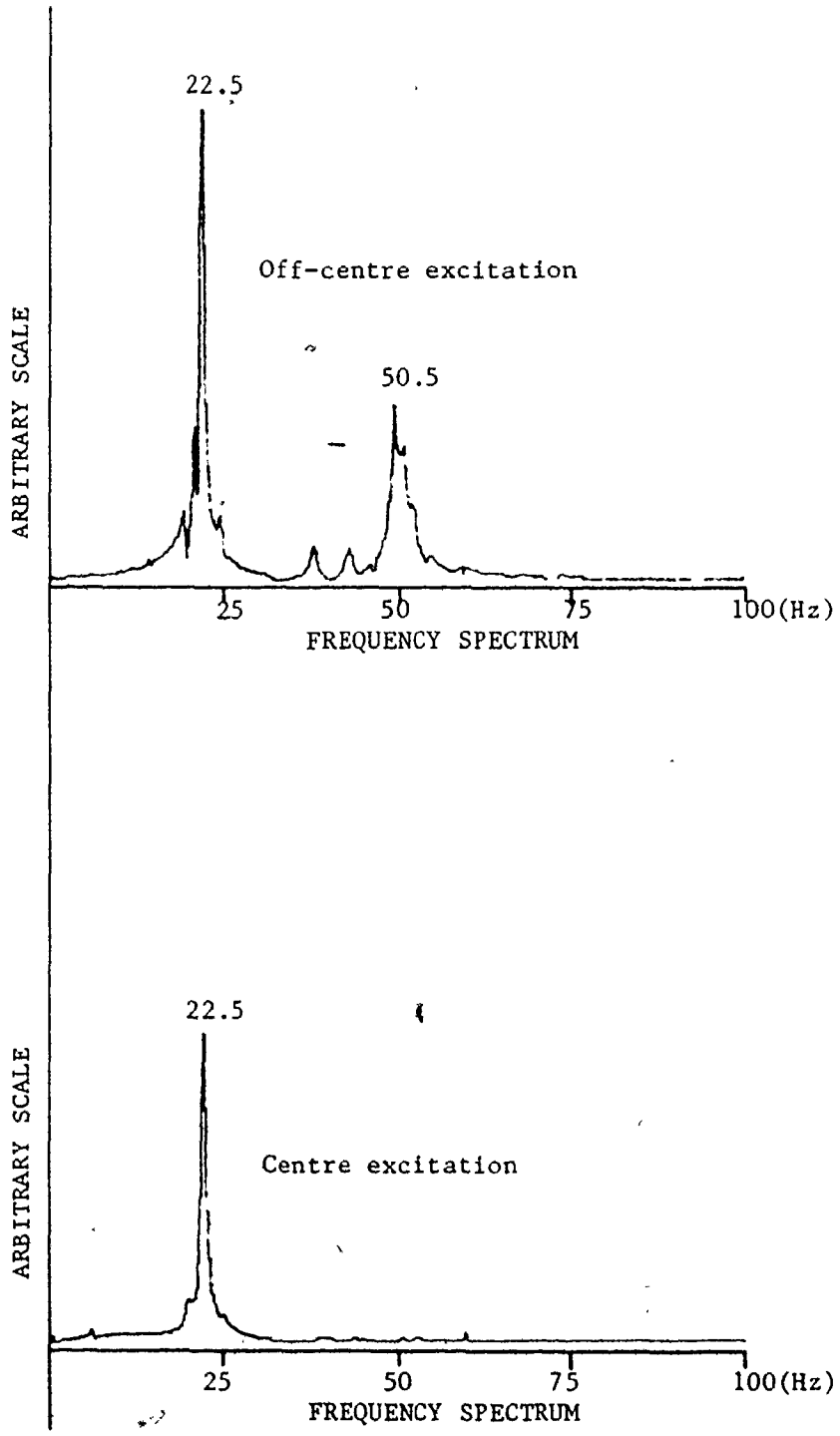

Figure 4.1.3: Natural frequency power spectrum of tube no.3 vibrating in quiescent water.

were flexible, the amplitude decay traces indicated significant modulations as energy was transferred back and forth between tubes yielding meaningless results. Similarly to the air damping, the water damping value used is the average of ten measurements per tube in each direction. A typical damping record obtained in quiscent water is shown in figure (4.1.4).

When the tuning of the tubes and measurements of frequency and damping were completed, the tube bundle assembly was inserted into the test section. The first test consisted of a record of the tube response with increasing flow velocity. At a given flow velocity, the response of the tube in both the streamwise and transverse directions and the corresponding frequency spectra were obtained. The frequency spectrum of the flow was also recorded. The mode shape appearing on the oscilloscope screen was photographed whenever considered appropriate, and the trace of tube motion in both streamwise and transverse directions was recorded on the visicorder.

The amplitude of the oscillation was computed as the square root of the sum of squares of the overall R.M.S. streamwise and transverse response measurements from the Fourier analyzer. In all measurements, frequency spectra and tube response data are the result of 32 sample averages. This was found to be sufficient to ensure excellent repeatability of the results.

The flow velocity upstream of the test bundle was adjusted and its value obtained from the calibrated rotameter in the water tunnel. The flow velocity was then incremented

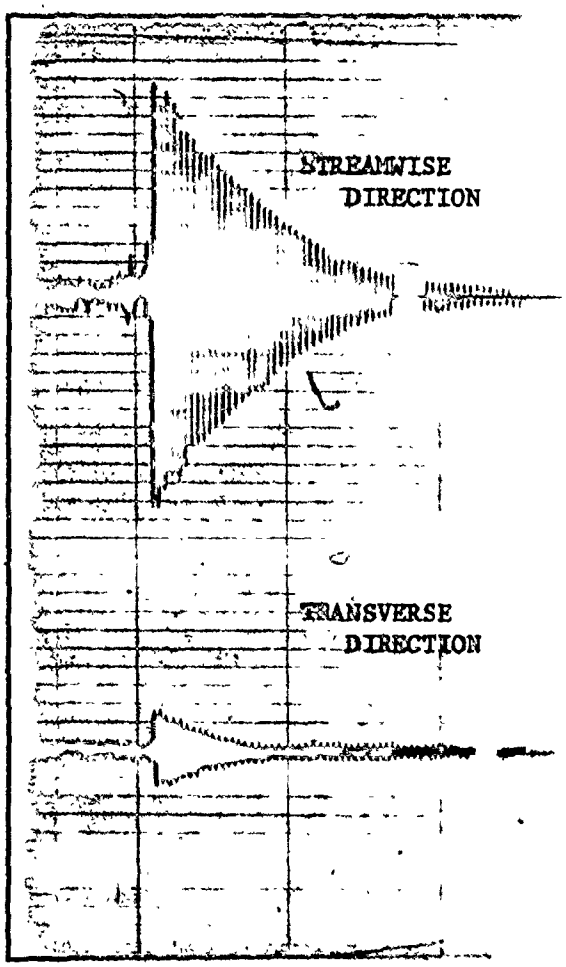

Figure 4.1.4: Water damping record for tube no. 4.

and after steady state operating conditions had been established the same procedure was repeated. This process was continued until danger of tube-to-tube clashing occurred due to large amplitude tube oscillations. Each test was conducted twice. The first time, monitoring tube no. 3 and the second monitoring tube no. 4. The results of these tests are presented below:

(a) Effect of Flow Velocity on the Response of Tube No. 3

The response curve of tube no. 3 with increasing flow velocity is shown in figure (4.1.5). The flow velocity used in this plot is the "pitch" velocity defined as:

$U_p = U_u \ (P/(P-D))$ where

U_u: upstream undisturbed flow velocity m/s

P: pitch of the present array: 34.9 mm

D: tube diameter: 25.4 mm

which yields $U_p = 3.67\ U_u$.

The first part of the response curve, OA, figure (4.1.5) indicates the random response of the tube due to turbulent buffeting. Figures (4.1.6) (a) and (b) show a very small amplitude random tube response. The flow direction in the oscilloscope traces of figure (4.1.6) is from the bottom to the top of the picture. The frequency spectra of the tube response in this range of velocities, as shown in figures (4.1.7), (4.1.8) and (4.1.9) clearly indicate that the tube

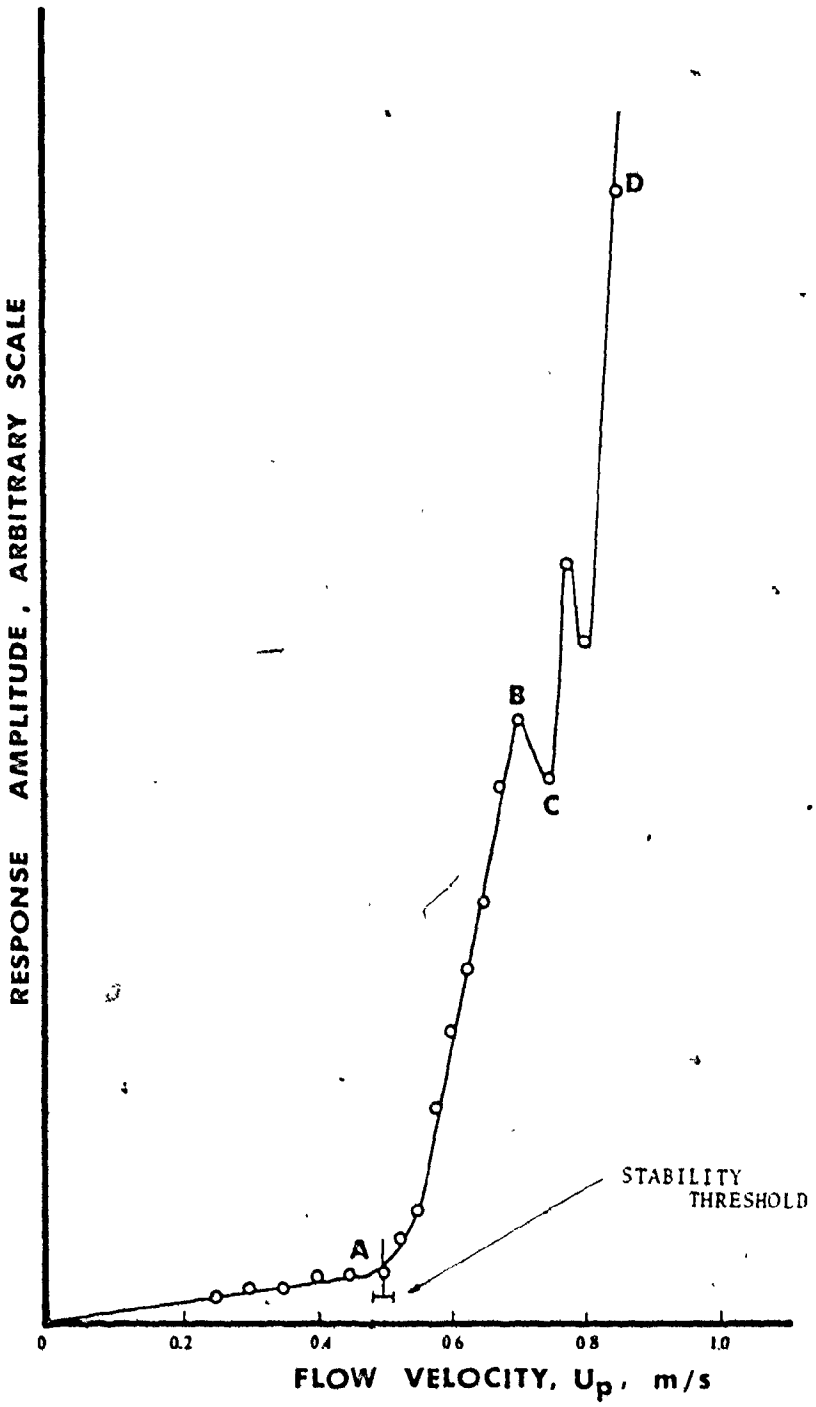

Figure 4.1.5: Amplitude response of tube no. 3 with increasing flow velocity.

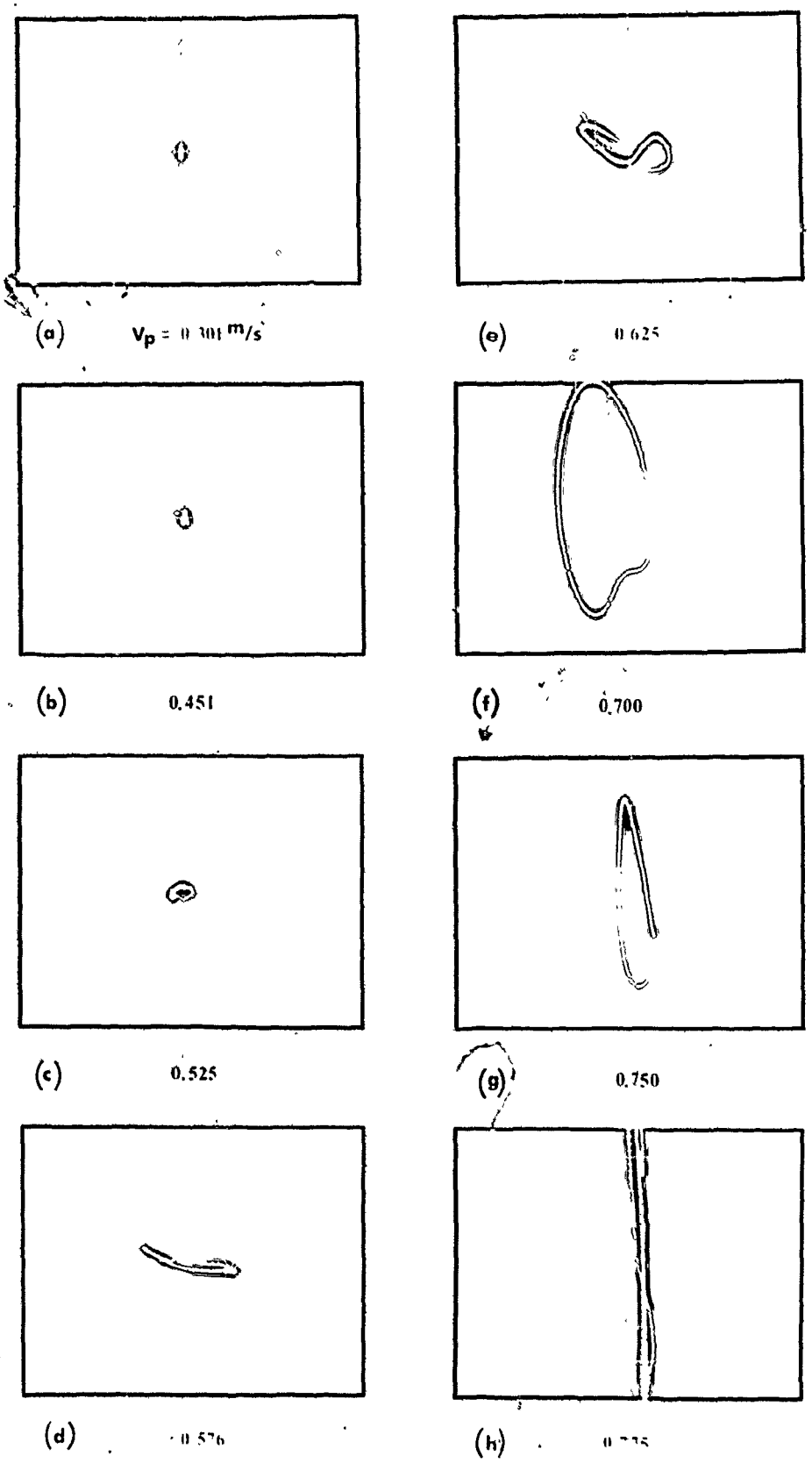

Figure 4.1.6 Oscilloscope mode shapes of tube no. 3

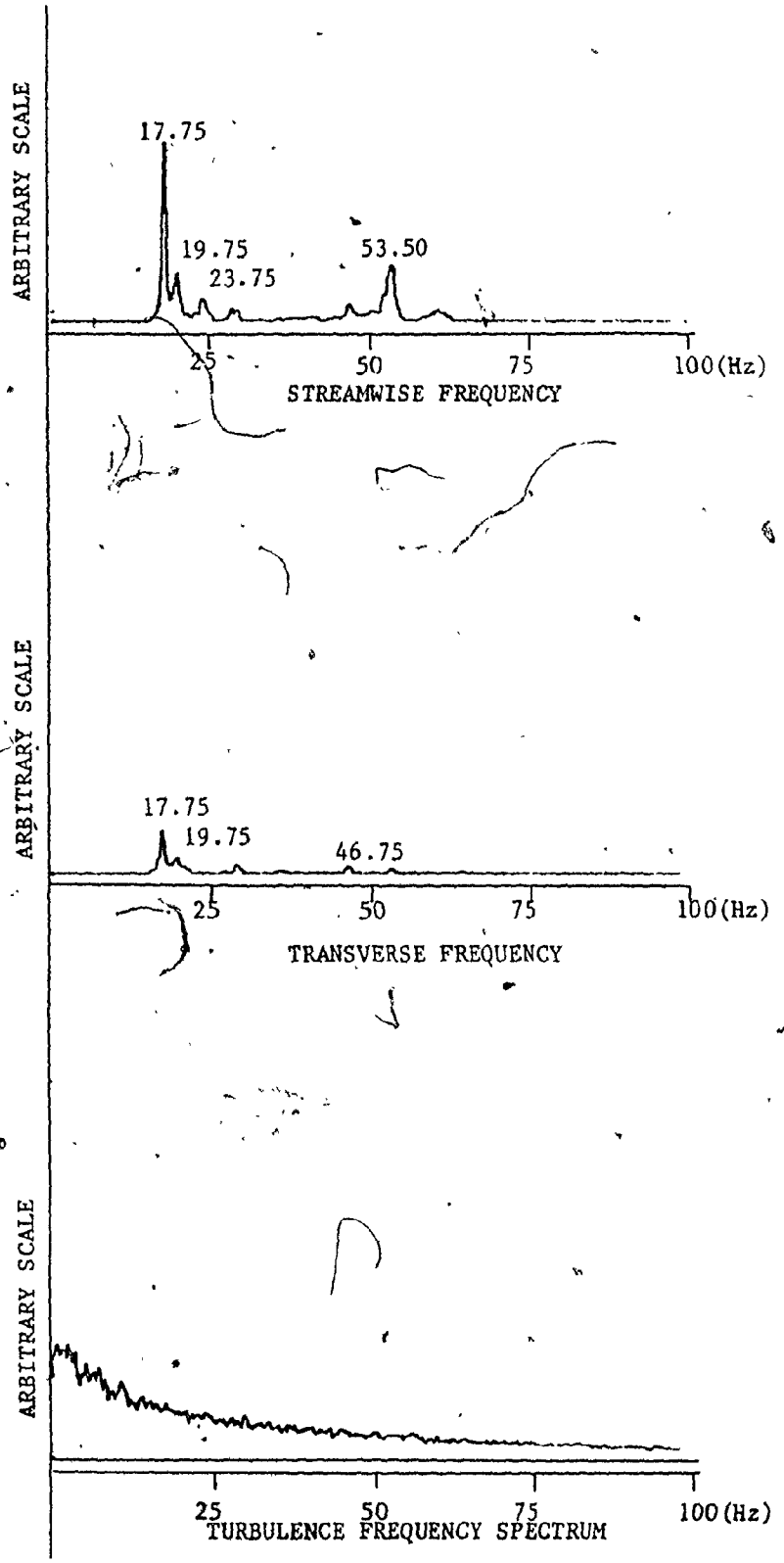

Figure 4.1.7: Amplitude and turbulence power spectra of tube no.3 at Up=0.301 m/s

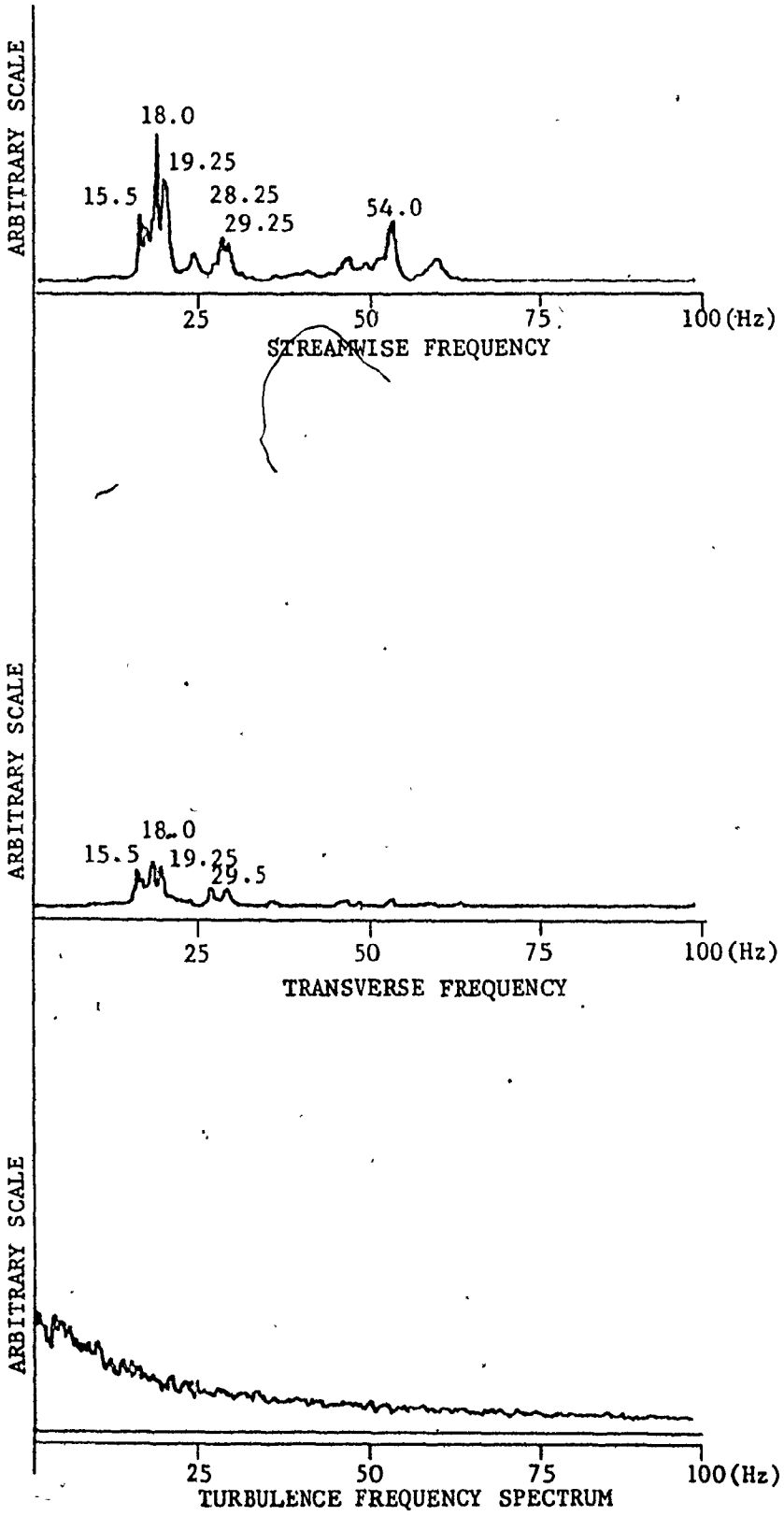

Figure 4.1.8: Amplitude and turbulence power spectra of tube no.3 at Up=0.451 m/s

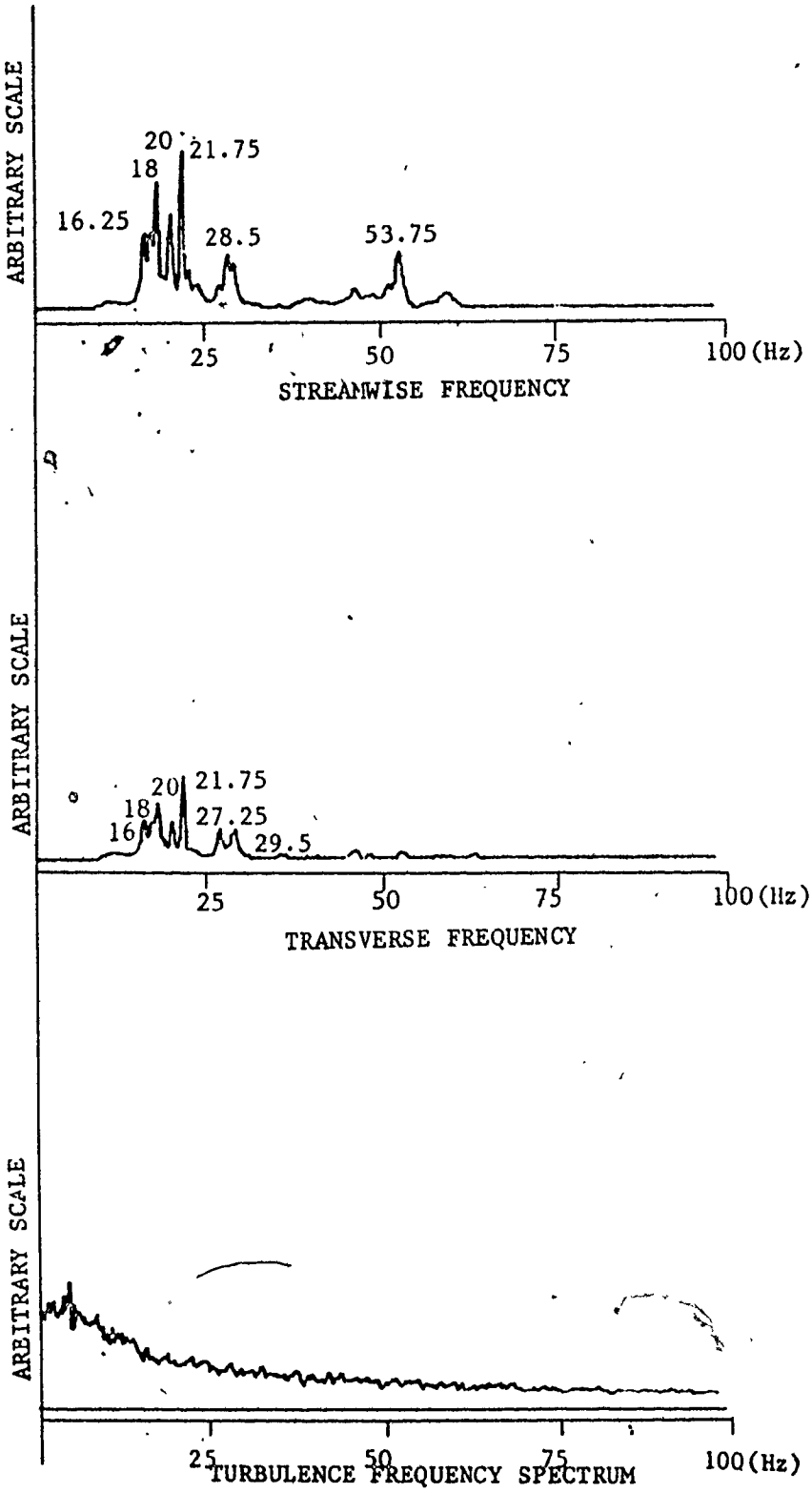

Figure 4.1.9: Amplitude and turbulence power spectra of tube no.3 at Up=0.500 m/s

response is random in nature.

However as the flow velocity exceeds 0.50 m/s the tube amplitude response becomes more regular, increasing considerably in both the streamwise and transverse directions as shown in figure (4.1.6) (c). This marks the stability threshold for the tube. It is very important to notice that the tube motion frequency is not at the 22.5 Hz natural frequency determined above but at a considerable lower frequency of 16.25 Hz as shown in figure (4.1.10). It is also important to note the flow periodicity of 16.25 Hz which is detected in the turbulence frequency spectrum obtained downstream from the array as illustrated in figure (4.1.10).

A further increase of the velocity at 0.576 m/s resulted in a sharp increase of the amplitude of the whirling tube motion as shown in figures (4.1.6) (d) and (4.1.11) in a direction transverse to the flow. As the flow approaches 0.70 m/s the tube motion appears to be organized in both streamwise and transverse directions as shown in figure (4.1.6) (f), with very large amplitudes. The frequency spectrum in the streamwise direction indicates the presence of a second frequency at 17.25 Hz, while in the turbulence frequency spectrum a low frequency (7.75 Hz) component is observed. As the velocity is further increased at 0.750 m/s the tube response tends to become more random in the streamwise direction. Its motion appeared to be modulated and consisted of a number of frequencies as shown in figure (4.1.13), resulting in a small overall amplitude reduction, as can be seen in figure (4.1.5).

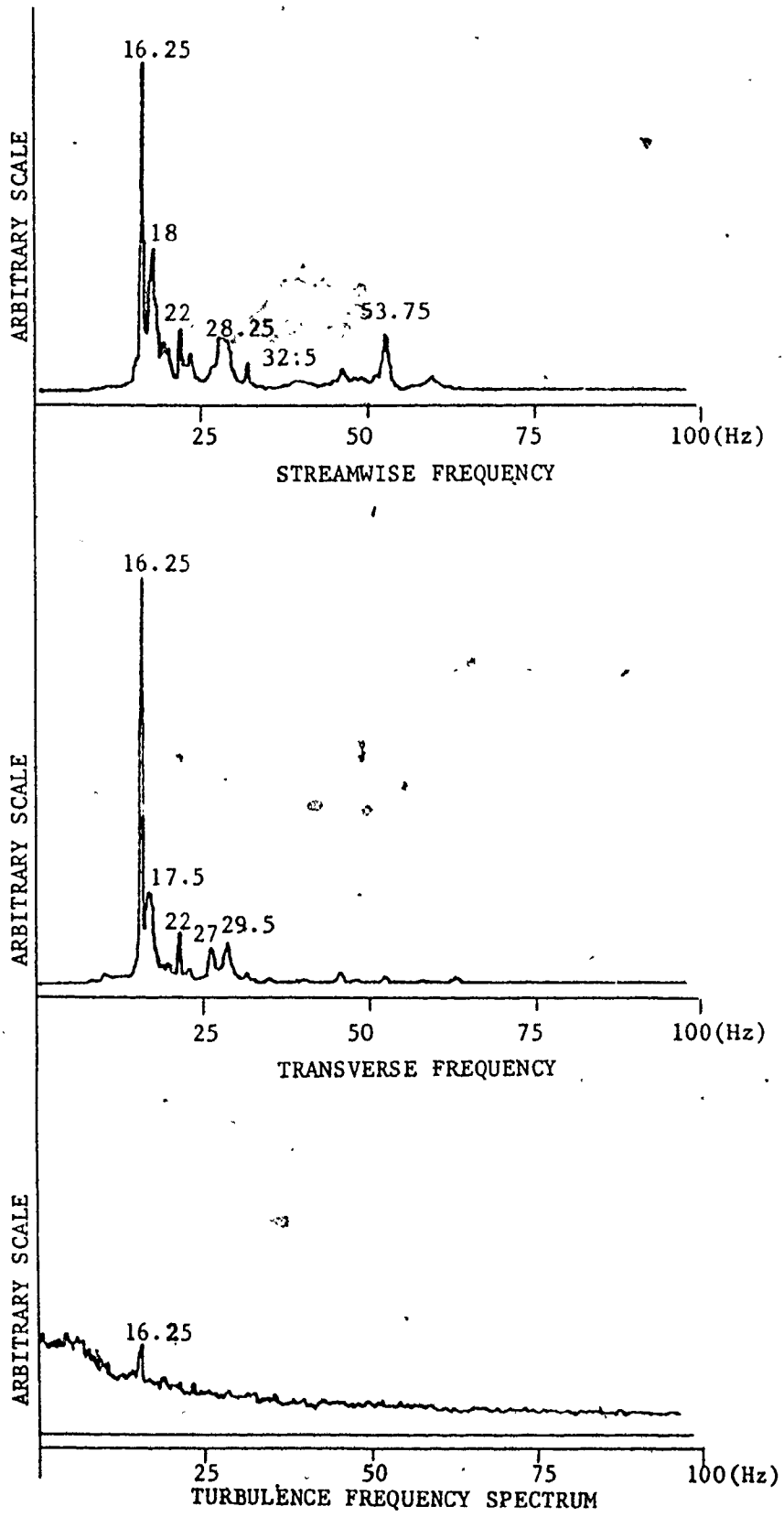

Figure 4.1.10: Amplitude and turbulence power spectra of tube no.3 at Up=0.525 m/s

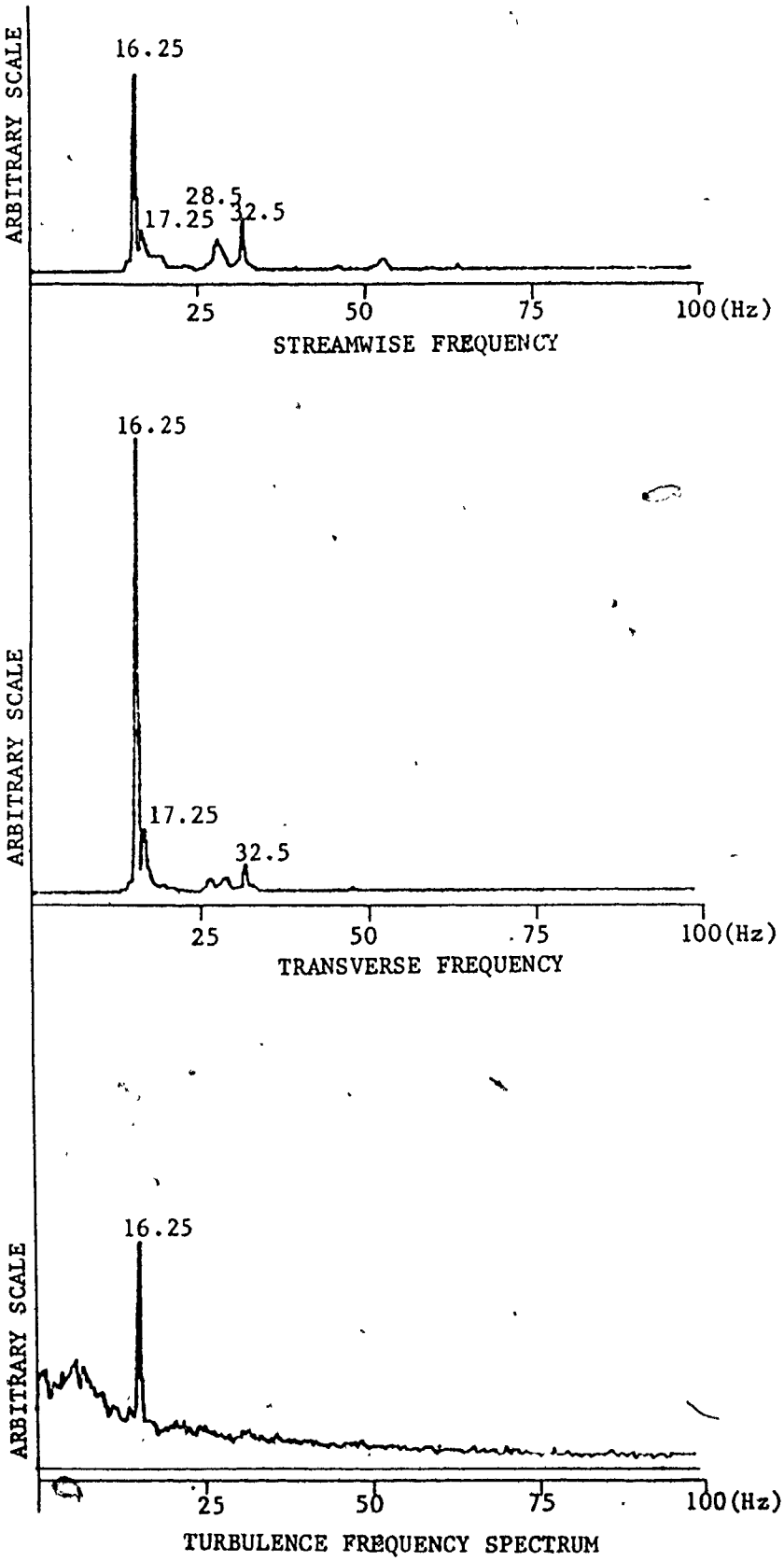

Figure 4.1.11: Amplitude and turbulence power spectra of tube no.3 at Up=0.576 m/s

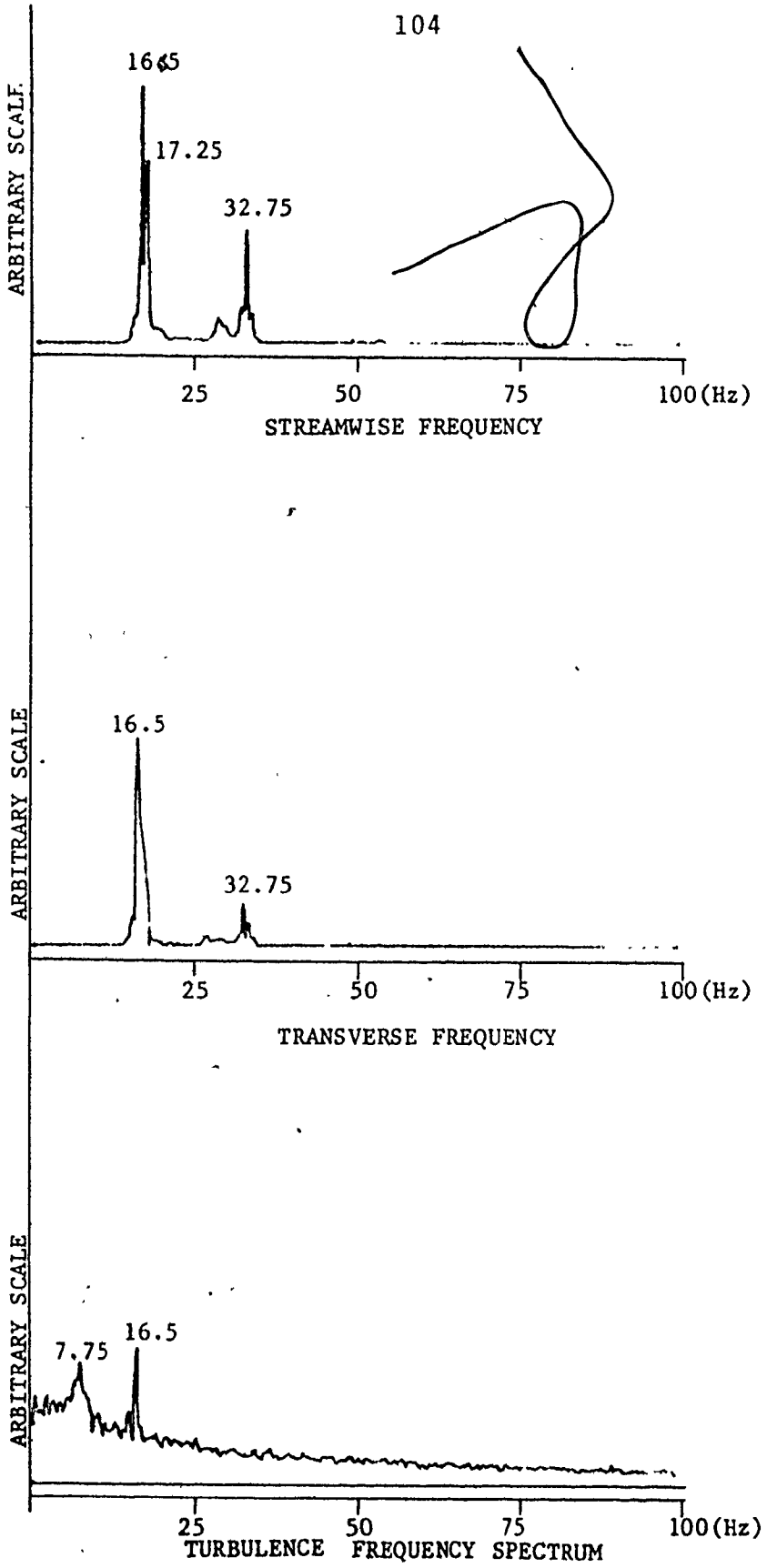

Figure 4.1.12: Amplitude and turbulence power spectra of tube no.3 at Up=0.700 m/s

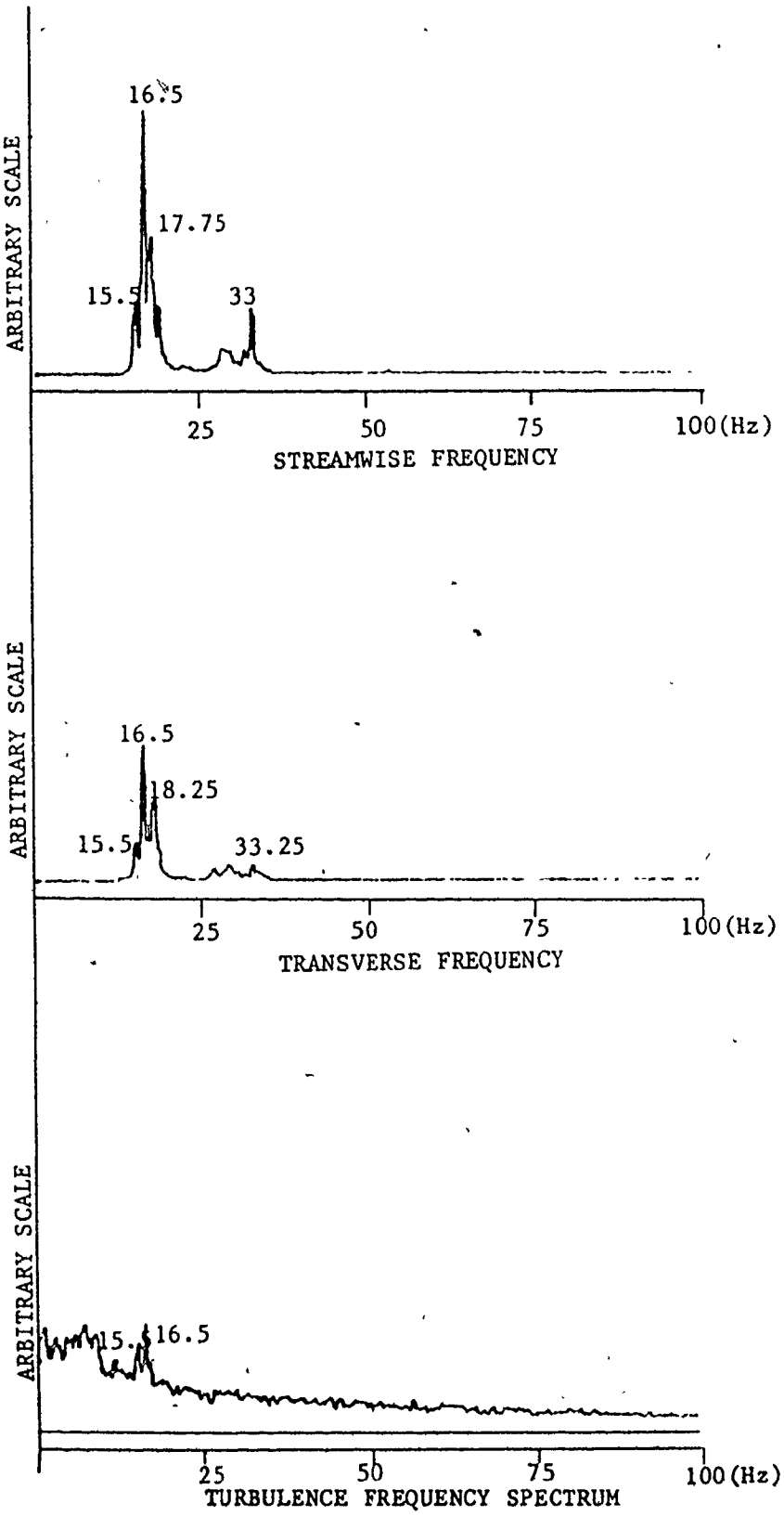

Figure 4.1.13: Amplitude and turbulence power spectra of tube no.3 at Up=0.750 m/s

A small increase in the flow velocity, at 0.775 m/s, resulted in a clear streamwise tube oscillation with very large amplitude at a new higher frequency of 19 Hz as shown in figures (4.1.6) (h), (4.1.5) and (4.1.14). We also note that the 19 Hz frequency component in the turbulence spectrum is quite small despite the large streamwise tube motion.

A further increase of the flow velocity of 0.80 m/s resulted in the reoccurrence of randomly modulated, streamwise in direction, tube motion as shown in figure (4.1.15) at two predominant frequencies of 15.5 Hz and 19.25 Hz while in the transverse direction the major frequency appears to be at 18.25 Hz. As shown in figure (4.1.5) the overall amplitude is reduced and the turbulence frequency spectrum indicates a flow periodicity at 15.5 Hz. Finally at a flow velocity of 0.825 m/s the tube motion amplitude is almost doubled, the motion being in the streamwise direction at a frequency of 15.5 Hz as shown in figure (4.1.16).

The stability threshold for tube no. 3 can be easily defined from figure (4.1.5). It is important to note that there is no widely accepted definition of the stability threshold of arrays in the literature. A number of different methods have been employed by different investigators and the consistency of these methods is rather poor. Our inability to apply a consistent method in determining the stability threshold, has contributed to the observed scatter in the published experimental data. In the present study the stability threshold

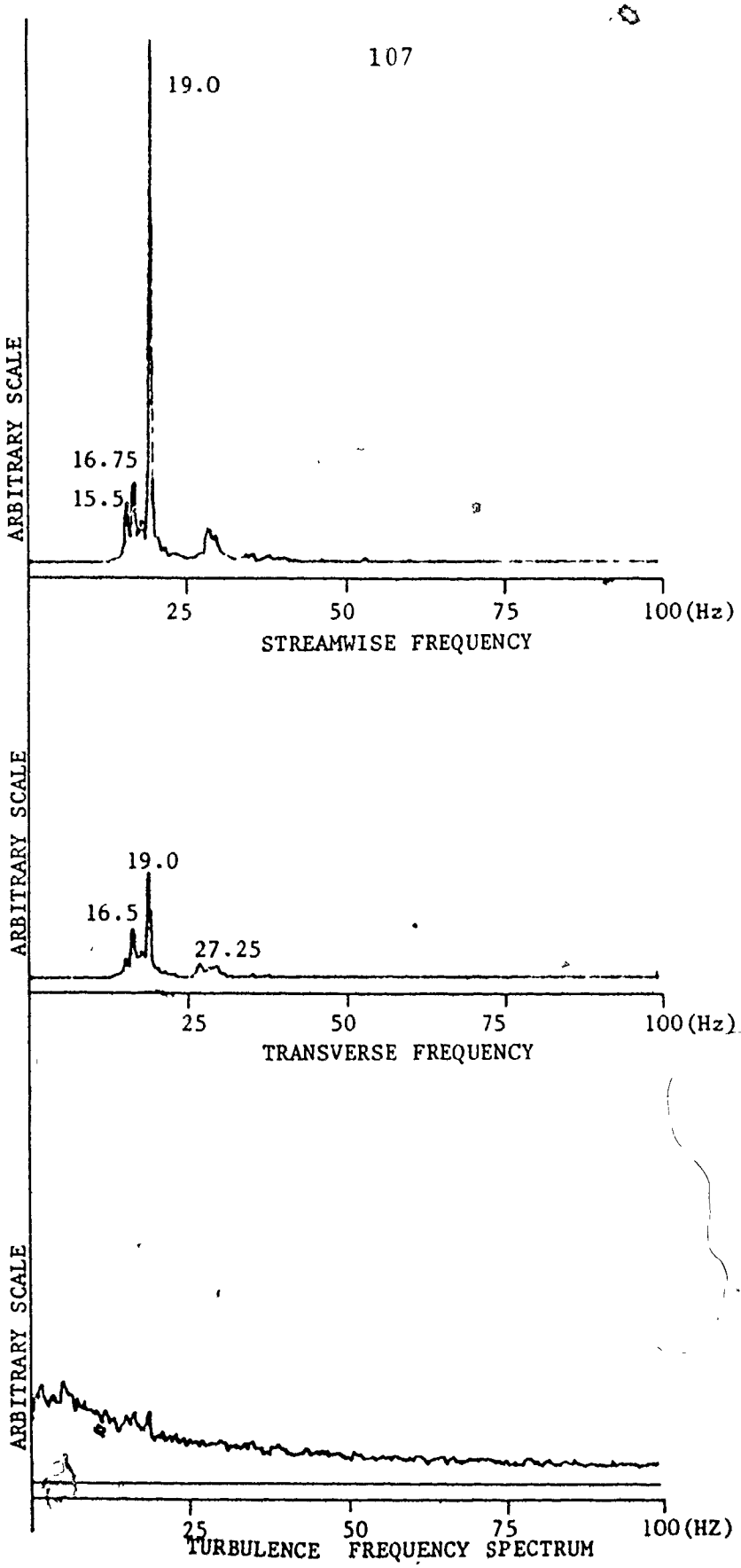

Figure 4.1.14: Amplitude and turbulence power spectra of tube no.3 at Up=0.775 m/s

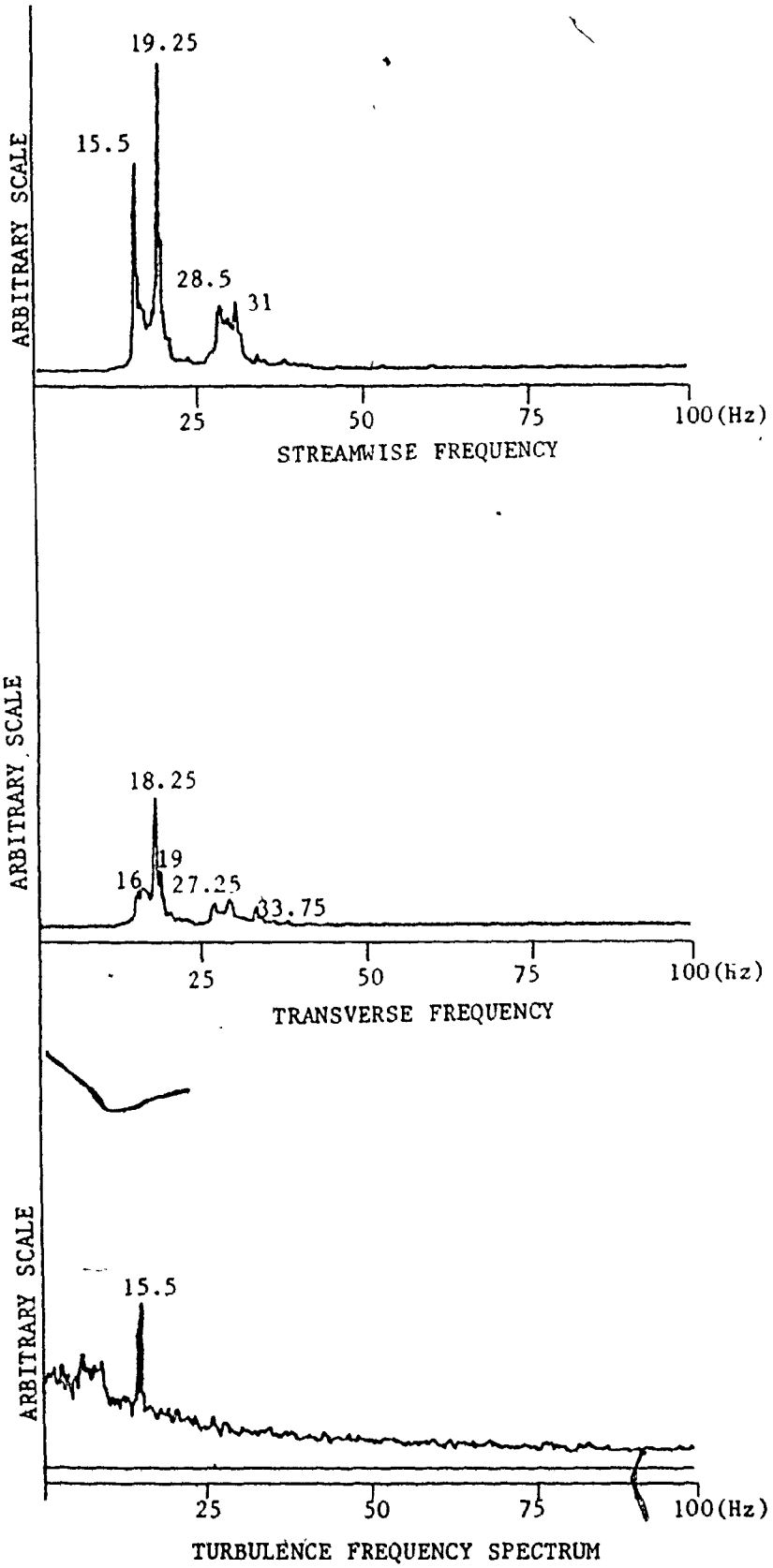

Figure 4.1.15: Amplitude and turbulence power spectra of tube no.3 at Up=0.800 m/s

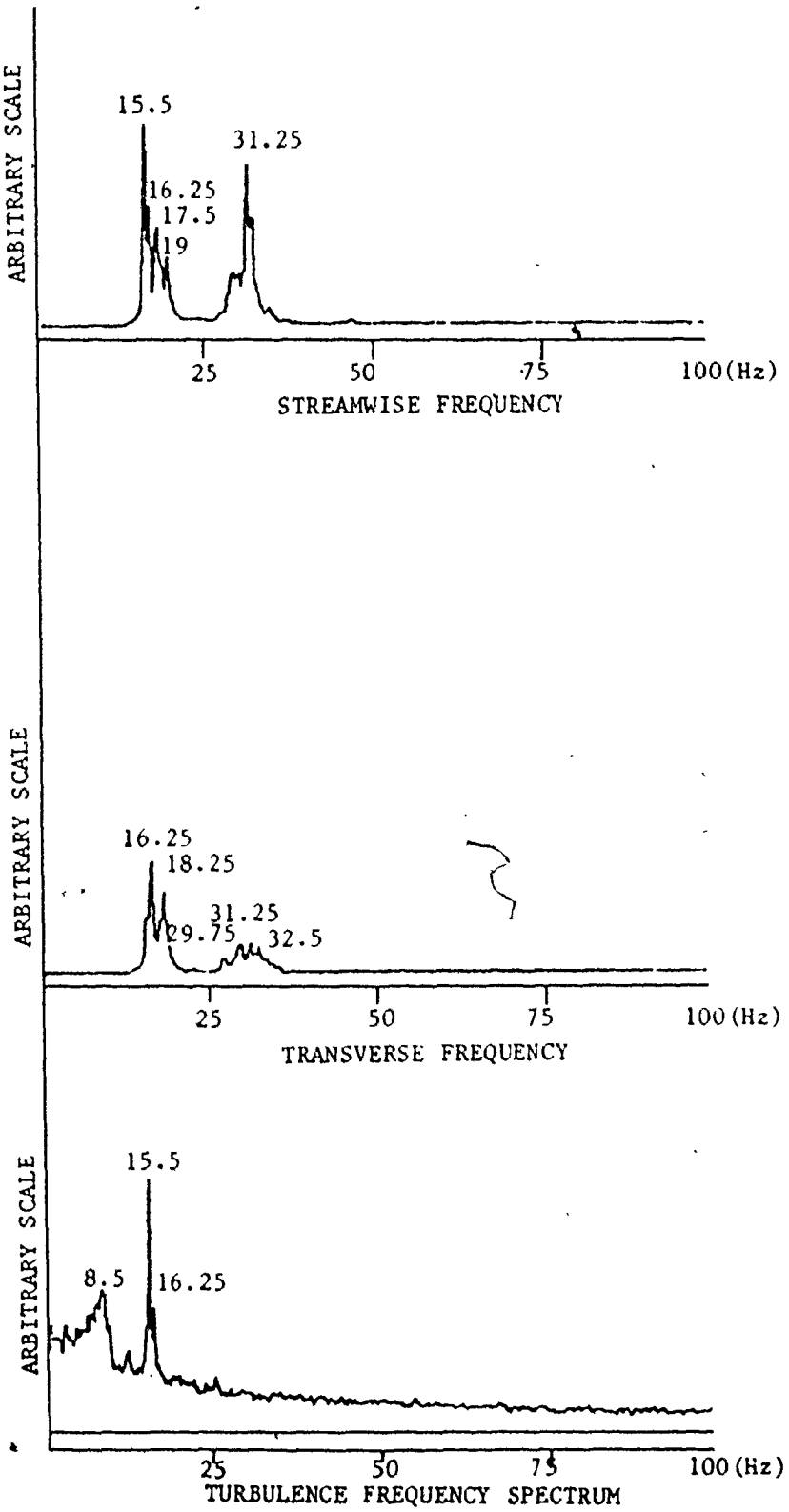

Figure 4.1.16: Amplitude and turbulence power spectra of tube no.3 at Up=0.850 m/s

is defined as that flow velocity at which the random response due to turbulent buffeting gives way to a more periodic response at the tubes' natural frequency.

For tube no. 3 this critical flow velocity appears to be at approximately 0.5 m/s (point A) as can be seen from figure (4.1.5). The slope of the response curve at this point changes abruptly and the rate of amplitude increase with flow velocity becomes much larger (part AB of the response curve). At this point we should also note, that the periodic motion of the tubes whirling in an organized fashion, due to the presence of fluidelastic excitation, (part AB of the response curve), occurs at a frequency approximately 30% lower than their monitored natural frequency in quiescent water (16.25 Hz instead of 22.5 Hz). This can be explained by the effect of increased added mass in the fluid coupled modes of the flexible tube bundle.

The tube response at flow velocities between 0.70 m/s and 0.80 m/s (part BC of the response curve) appears to demonstrate some disorder in the whirling tube motion. It is possible that there is some vorticity response superimposed on the fluidelastic instability. The Strouhal number based on the pitch velocity and the observed frequency at the stability threshold is about 0.79. This is of the same order as found previously for this type of array. Vorticity and fluidelastic responses cannot be separated in these experiments.

The bumps in the response curve (part BC), are

associated with shifts in relative mode shape. At each relative mode shape, the added mass is significantly different and hence the dominant frequency of the response changes. The peaks in the response curve are associated with well defined motion in two different natural frequencies corresponding to 16.5 Hz and 19 Hz as can be seen in figures (4.1.12) and (4.1.14). The points between the peaks show a less well defined behaviour at several frequencies, as shown in figures (4.1.13) and (4.1.15) and apparently correspond to transition from one mode to another.

(b) Tube No. 4 Response with Flow Velocity

The test procedure for this test was exactly the same as for the test of tube no. 3. The response of tube no. 4 with increasing flow velocity is essentially the same as tube no. 3 and is shown in figure (4.1.17). The random response to turbulent buffeting (part OA of the response curve) is shown in figures (4.1.18) (a), (4.1.19) and (4.1.20). The onset of fluidelastic instability, point A, occurs at the same flow velocity of approximately 0.50 m/s, as for tube no. 3. Between points A and B on the response curve, the motion of the tube builds in amplitude in the direction transverse to the flow, as shown in figures (4.1.18) (b) to (f) and (4.1.21), (4.1.22). At a flow velocity of approximately 0.75 m/s a similar disorganisation of the flow, as was observed for tube no. 3, is noticed. There is an overall amplitude reduction,

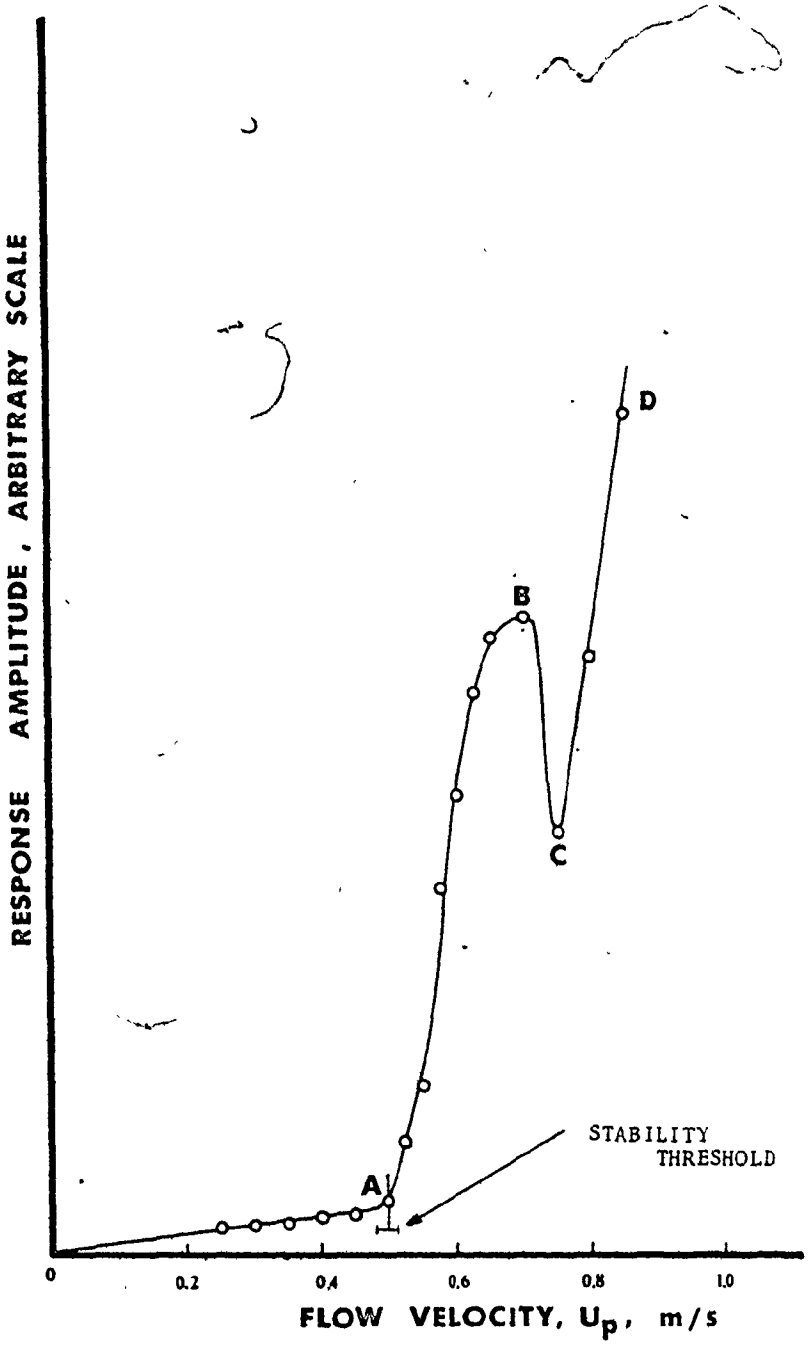

Figure 4.1.17: Amplitude response of tube no. 4 with increasing flow velocity.

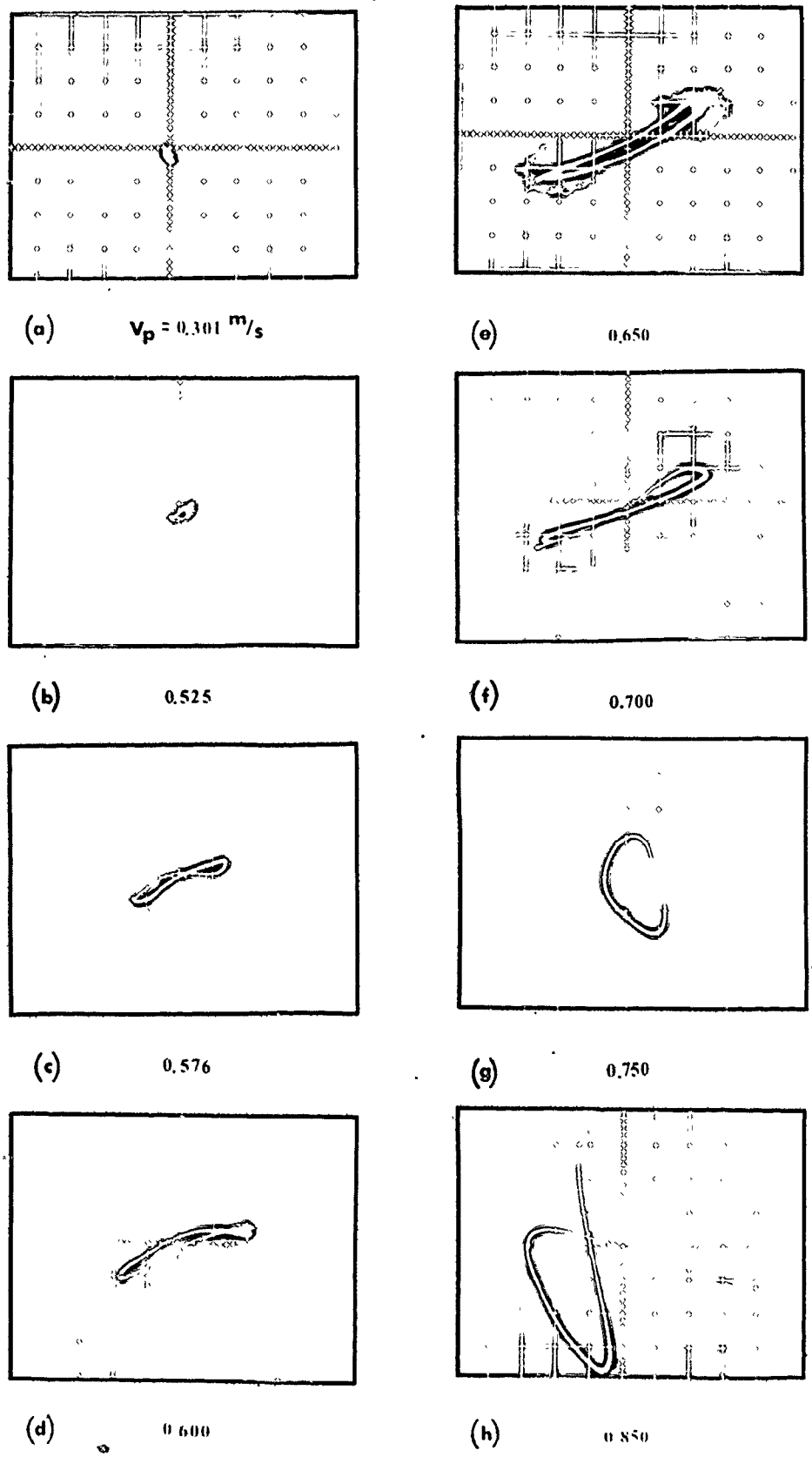

Figure 4.1.18 Oscilloscope mode shapes of tube no. 4

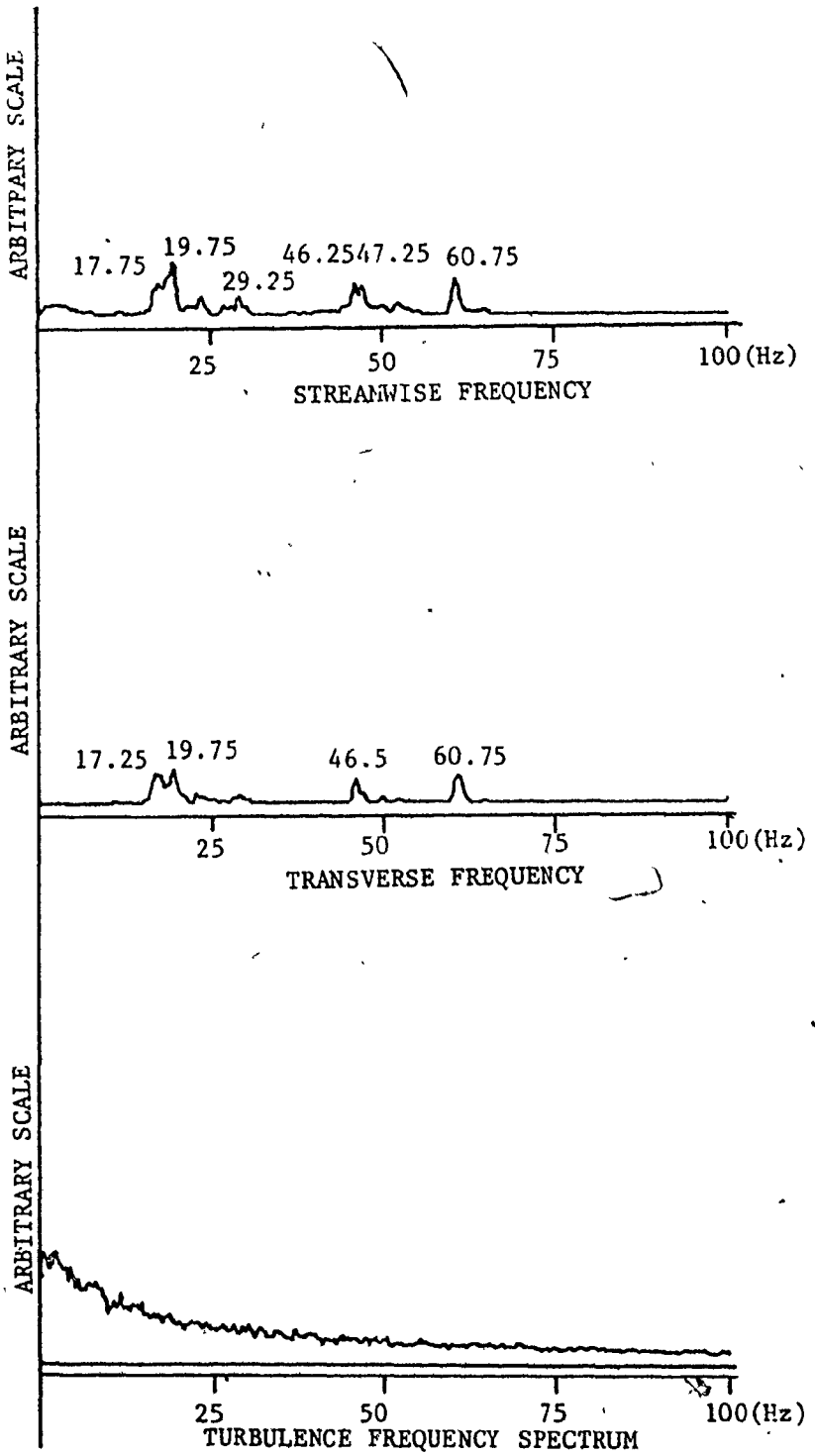

Figure 4.1.19: Amplitude and turbulence power spectra of tube no.4 at Up=0.301 m/s

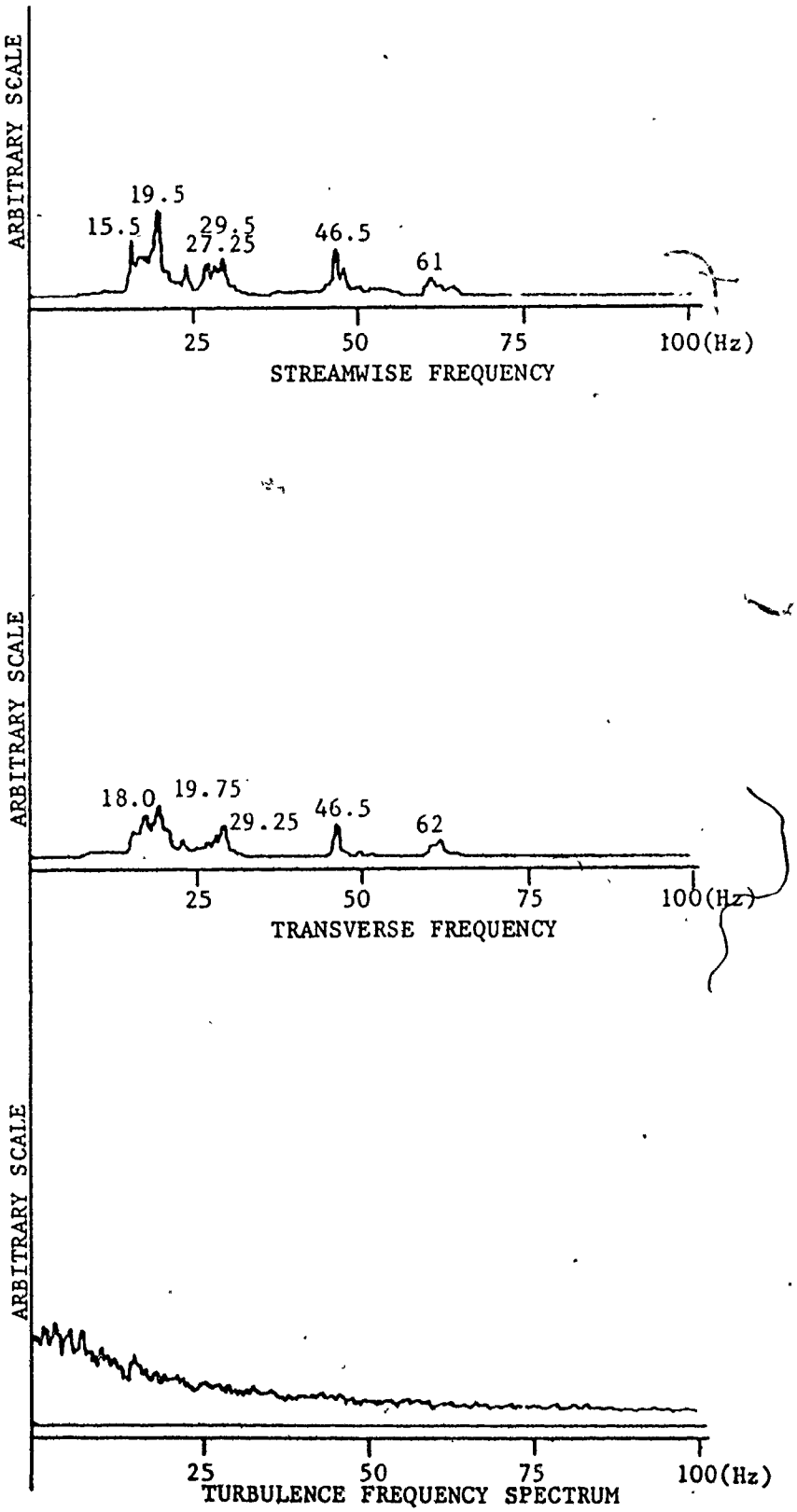

Figure 4.1.20: Amplitude and turbulence power spectra of tube no.4 at Up=0.451 m/s

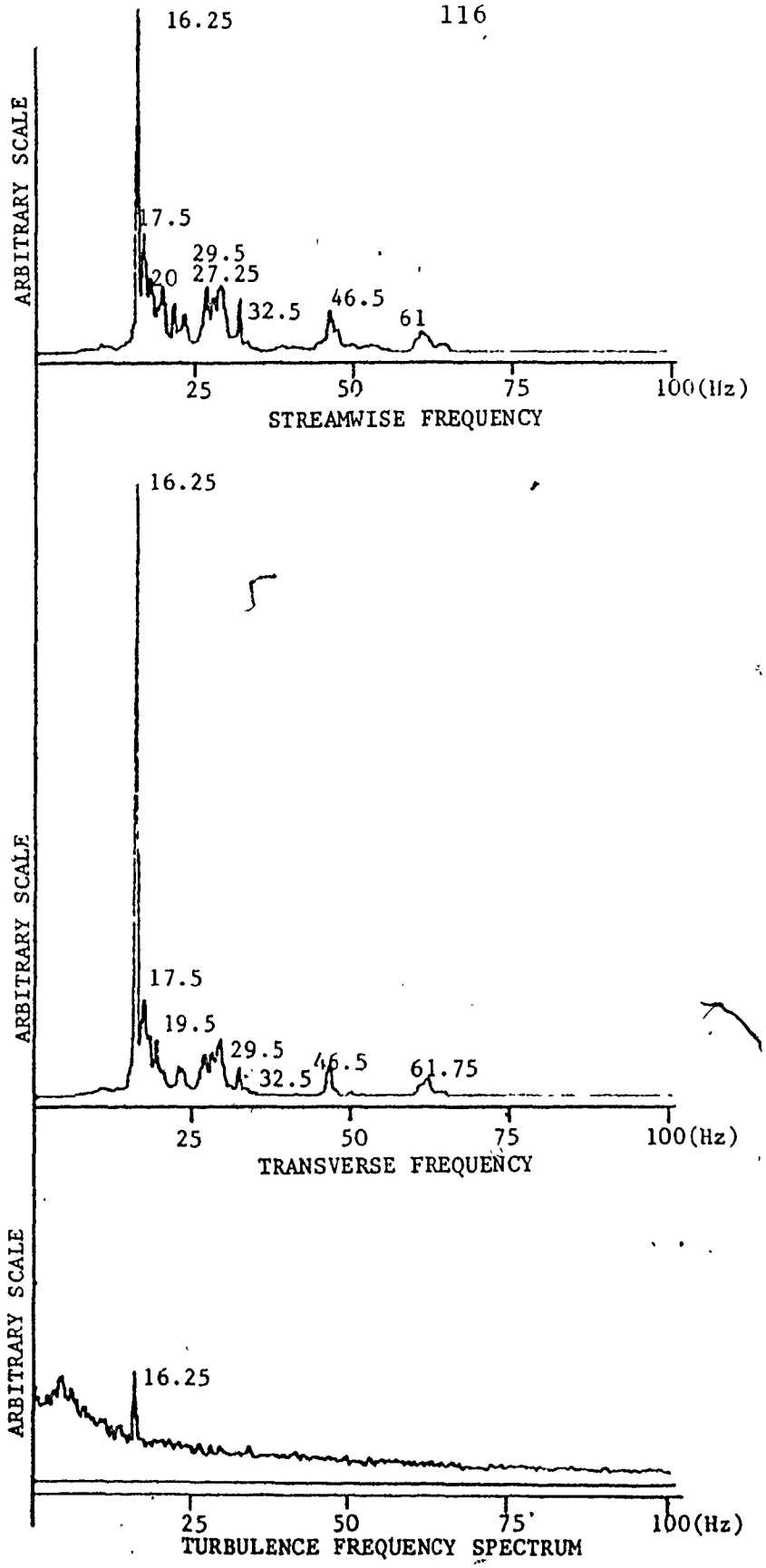

Figure 4.1.21: Amplitude and turbulence power spectra of tube no.4 at Up=0.525 m/s

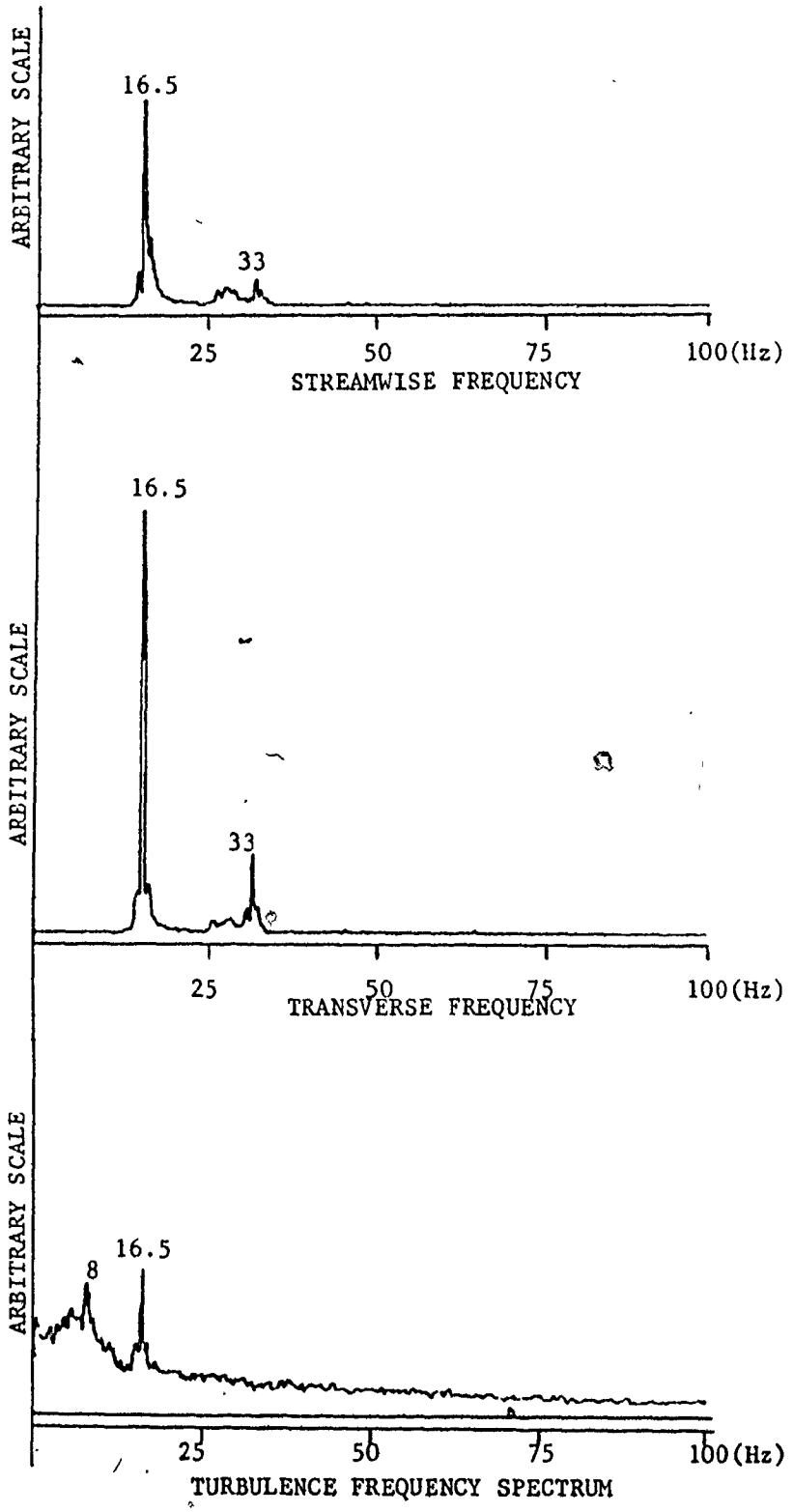

Figure 4.1.22: Amplitude and turbulence power spectra of tube no.4 at Up=0.700 m/s

as shown in figures (4.1.17), (4.1.18) (g) and (4.1.23), (4.1.24), and no dominant frequencies are observed in the turbulence spectra, until the flow is increased to 0.85 m/s where the tube undergoes large amplitude motions, as shown in figures (4.1.18) (h) and (4.1.25).

A comparison between figures (4.1.6) and (4.1.18) reveals that up to about 0.70 m/s the tubes in rows 3 and 4 during fluidelastic excitation move in a similar manner but at a relative angle of somewhat less than 90 degrees to each other, e.g., figures (4.1.6) (d) and (4.1.18) (c).

In order to generalize the results and compare them with previous data, it is desirable to nondimensionalize the parameters. In the present results the velocity parameter is defined as:

$U_p/f_{obs}\,D$ where

U_p: "pitch" velocity: m/s

f_{obs}: observed frequency of the tube at the onset of instability: Hz

D: tube diameter: m

The mass ratio is defined as:

$m/\rho\,D^2$ where

m: mass of the tube including the "added" mass per unit length: kgs/m

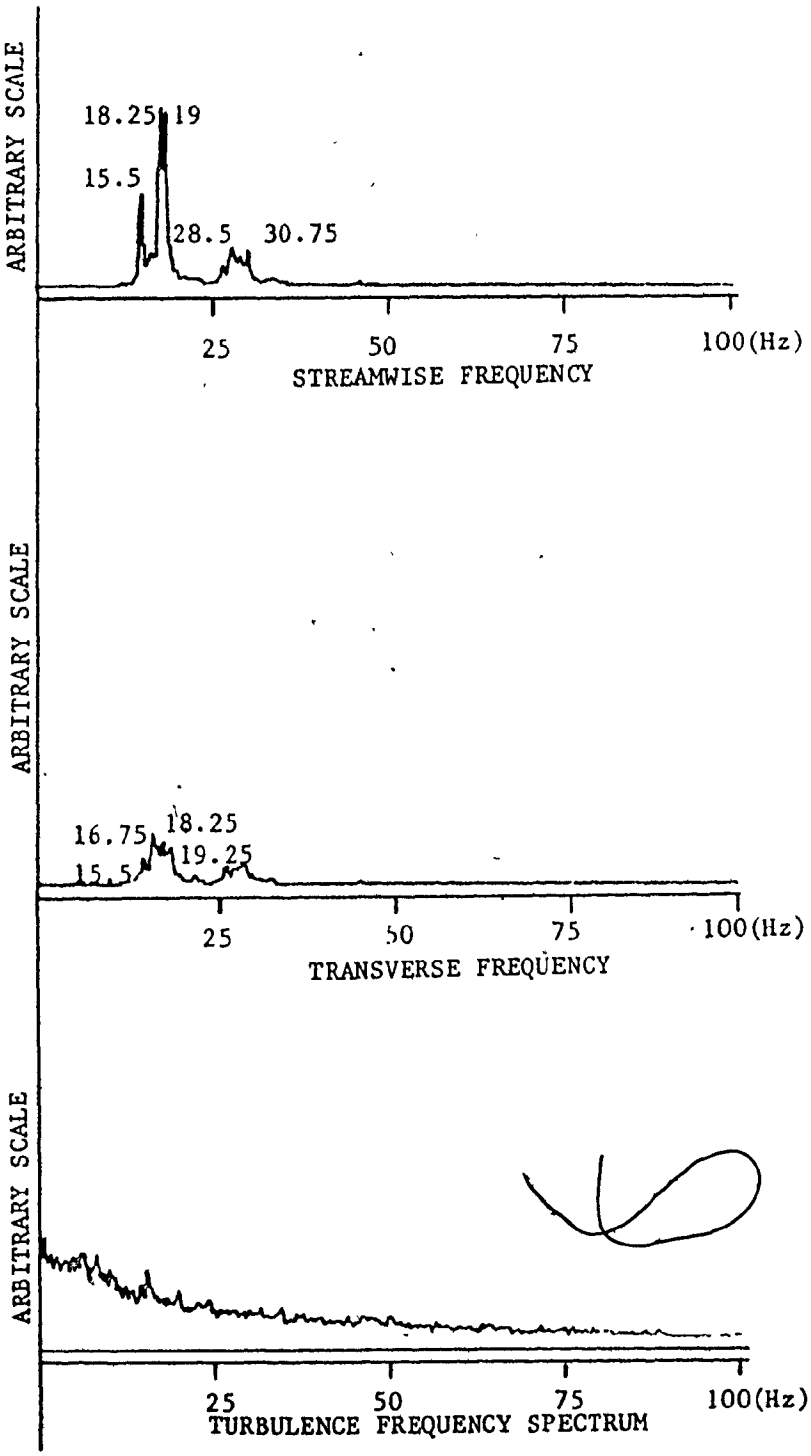

Figure 4.1.23: Amplitude and turbulence power spectra of tube no.4 at Up=0.750 m/s

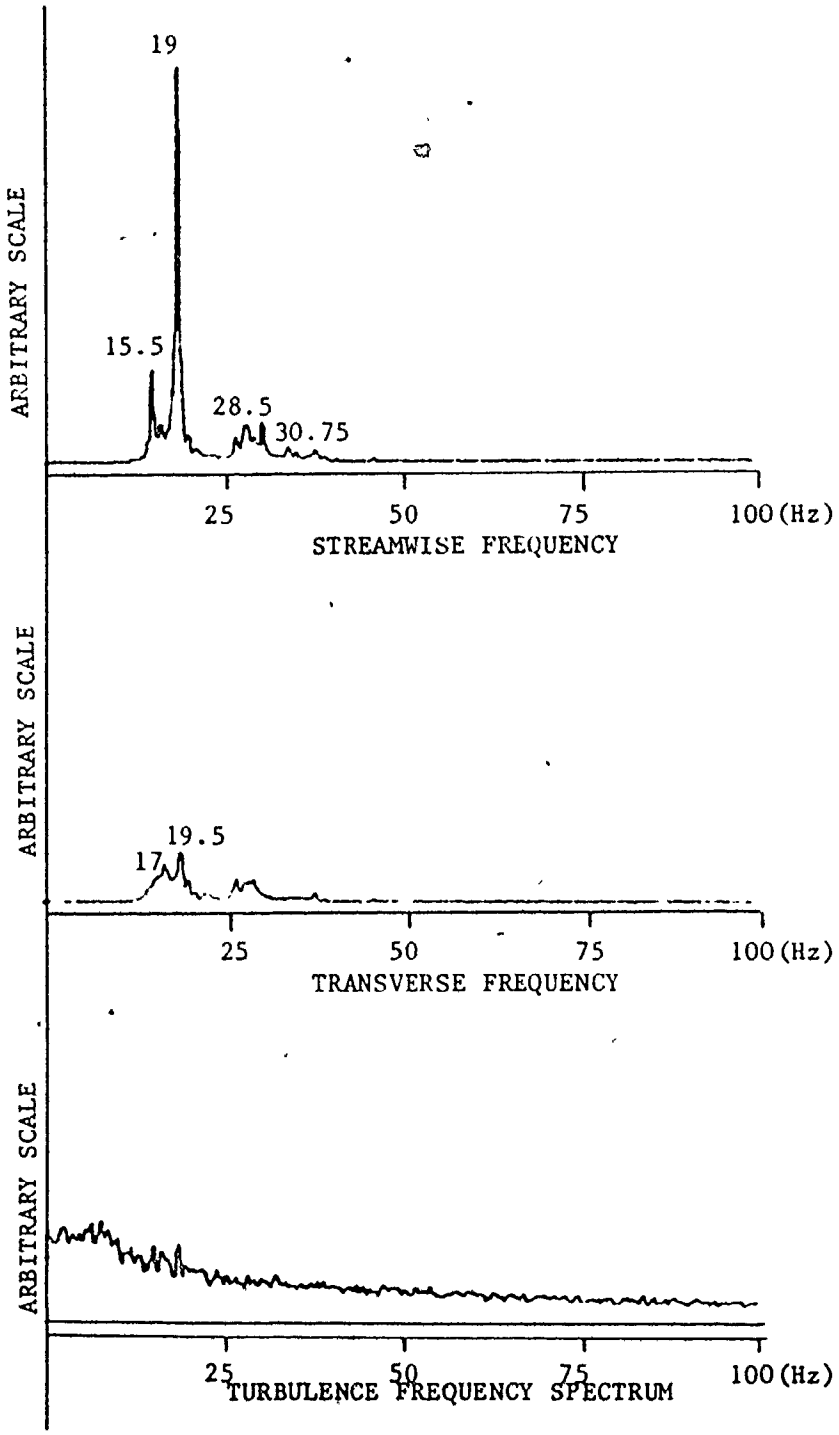

Figure 4.1.24: Amplitude and turbulence power spectra of tube no.4 at Up=0.800 m/s

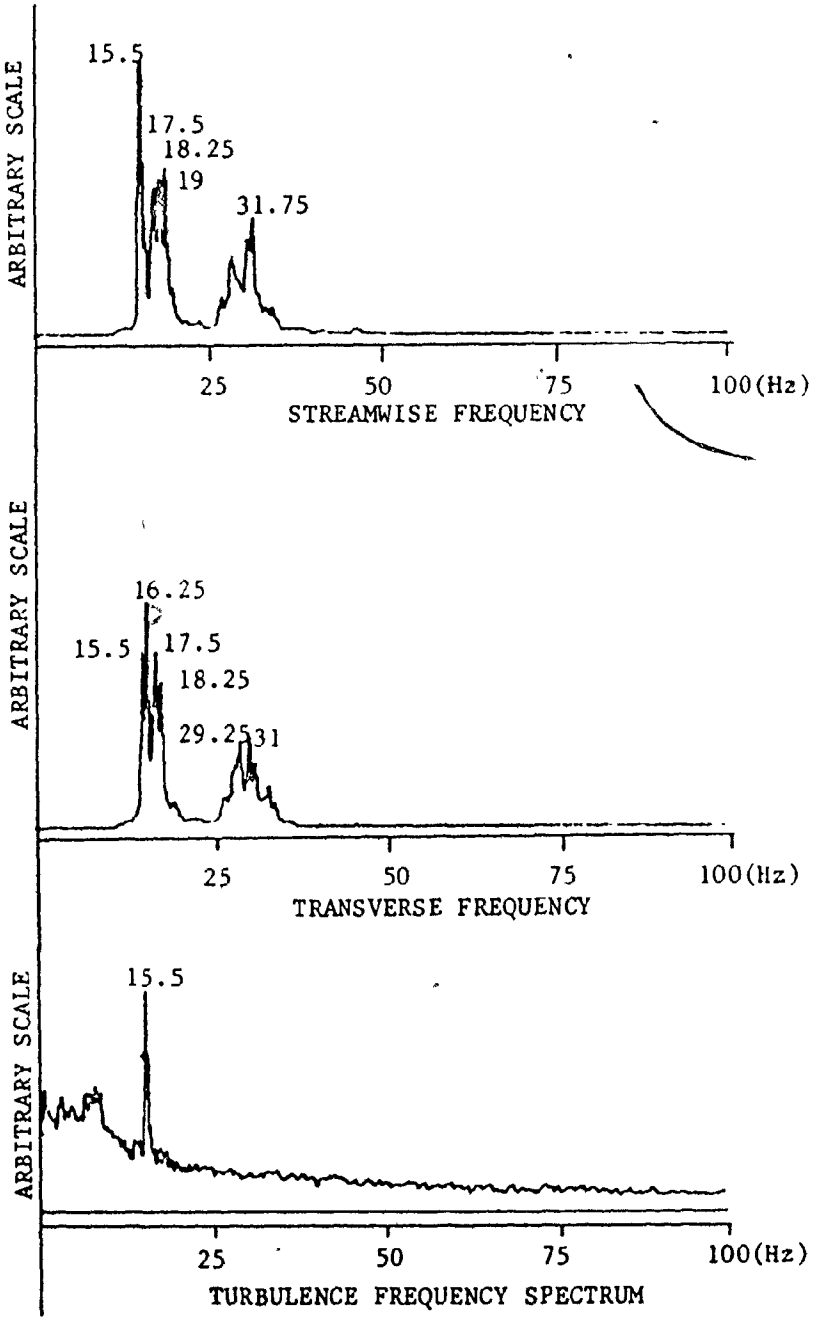

Figure 4.1.25: Amplitude and turbulence power spectra of tube no.4 at Up=0.850 m/s

ρ: density of water: kgs/m^3

D: tube diameter: m

The tube damping δ used is the one recorded in air. The tube mass per unit length is derived from the ratio of the tube's natural frequency in air to the observed tube's frequency at the onset of instability. Assuming that the added mass of the tube vibrating in air is negligible we can write:

$$f_{air} \propto (1/m_{tube})^{0.5}$$

Similarly when the tube is oscillating in water with an observed frequency f_{obs} we can write

$$f_{obs} \propto (1/m_{total})^{0.5}$$

Thus we can write:

$$f_{air}/f_{obs} = (m_{total}/m_{tube})^{0.5}$$

which reduces to

$$m_{total} = m_{tube} (fair/f_{obs})^2$$

and the mass per unit length is

$$m = m_{total}/\ell = (m_{tube}/\ell)(f_{air}/f_{obs})^2 \qquad (4.1)$$

where ℓ is the length of the tube.

The total mass of the tube oscillating in water consists of two parts: i.e.

$$m_{total} = m_{tube} + m_{added} \qquad (4.2)$$

The added mass term can be expressed as:

$$m_{added} = C_a \text{ (volume of displaced fluid)}$$

$$m_{added} = C_a \, (\rho_w (\pi D^2/4) \ell) \qquad (4.3)$$

where C_a: the added mass coefficient

ρ_{water}: density of water: kgs/m^3

D: tube diameter: m

ℓ: tube length: m

From relations (4.1), (4.2) and (4.3) we can derive a relationship for the added mass coefficient based on the tube's natural frequency in air and the observed natural frequency in water as follows:

$$C_a = 4 \, m_{tube} \, [(f_{air}/f_{obs})^2 - 1]/\rho \pi D^2 \ell \qquad (4.4)$$

As mentioned in Chapter 2, the added mass coefficient is a function of the geometry of the array. The calculated value for the added mass coefficient based on the ratio of the natural frequencies in air and quiescent water is 1.57. This value is in good agreement with the added mass coefficient

calculated by Moretti and Lowery [67] for arrays of similar geometry in quiescent water.

If the value of the observed tube frequency at the critical velocity is used, the calculated effective added mass coefficient from relationship (4.4) is 3.68. This value when compared with the theoretical value obtained by Chen [61] for a similar geometry array appears to be about 15% larger. The tube's data is summarized in Table 4.1.

Table 4.1

	Tube No. 3	Tube No. 4
f_{air}	40 Hz	40 Hz
f_{nat}	22.5 Hz	22.5 Hz
$f_{obs\ crit}$	16.25 Hz	16.25 Hz
m_{tube}	0.110 kg	0.110 kg
m	2.23 kg/m	2.23 kg/m
δ_a	0.008	0.009
δ_w	0.103	0.070
U_p	0.5 m/s	0.5 m/s
U_R	1.21	1.21
M_R	3.46	3.46
ℓ	0.298 m	0.298 m

f_{air}: natural frequency of the tube in air: Hz

f_{nat}: natural frequency of the tube in quiescent water when all adjacent tubes are rigidly fixed: Hz

$f_{obs\ crit}$: dominant frequency of the tube observed at instability: Hz

m_{tube}: mass of the tube: kg

m: equivalent total mass of tube per unit length as derived above: kg/m

δ_a: tube damping in air

δ_w: tube damping in water when all adjacent tubes are rigidly fixed.

U_p: critical "pitch" velocity: m/s

U_R: reduced threshold velocity $U_p/f_{obs\ crit}D$

M_R: reduced mass ratio $m/\rho_{water}\ D^2$

The present experimental results are plotted in figure (4.1.26) together with the results of references [39], [40], [63]. It becomes apparent that the stability boundary which is derived from wind tunnel studies ([39], [40]) and provide and excellent fit to the data yields unconservative predictions for the present results as well as those obtained in [63] for liquid flows. It is important to note that the type of array used in the above mentioned references were exactly the same geometrically.

One can conclude from the present results that the previously established stability threshold in air is unconservative for liquid flows. Further studies varying mass ratio in heavier fluids are necessary in order to establish the overall trend of the stability threshold.

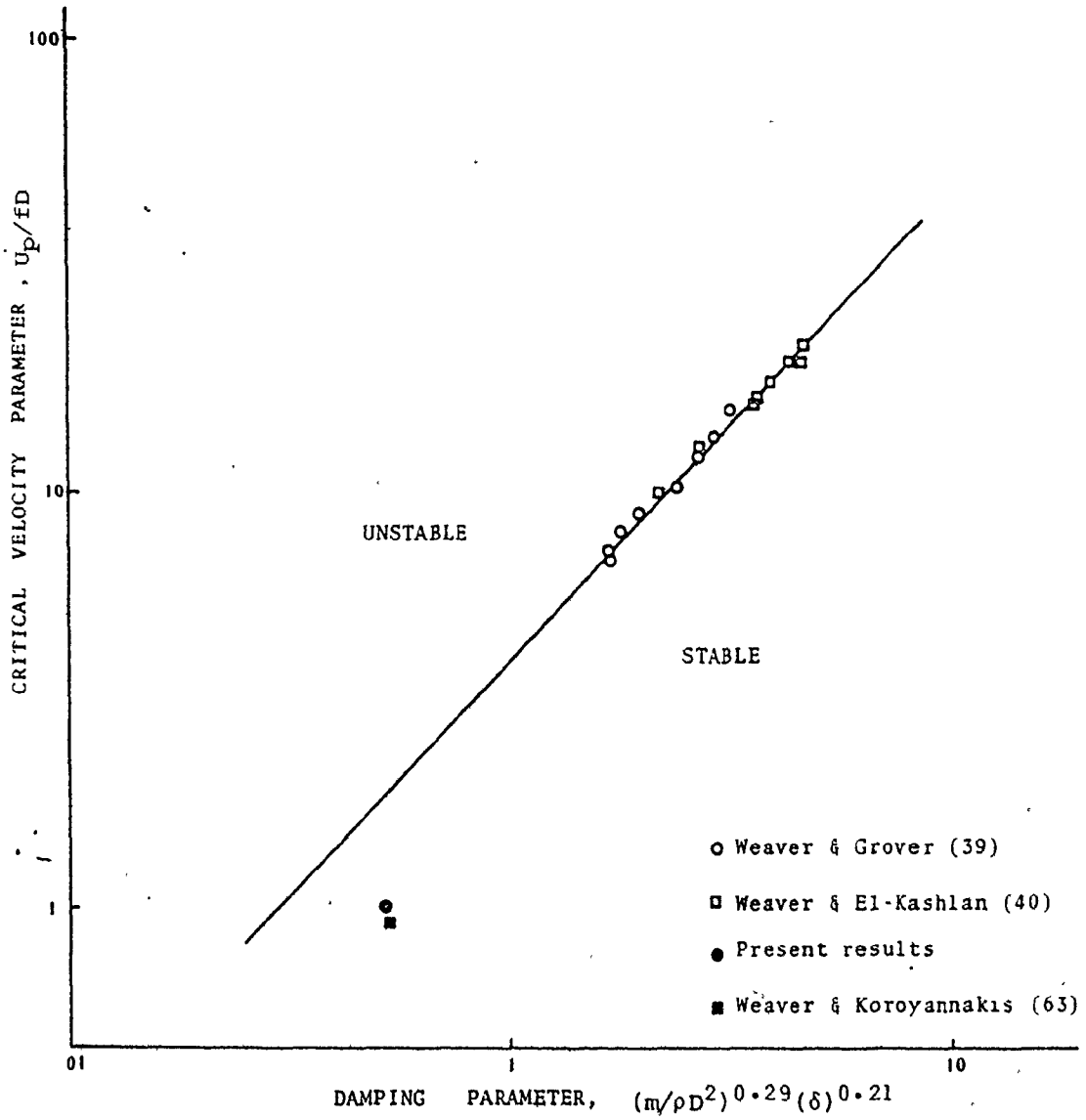

Figure 4.1.26: Plot for the threshold of fluidelastic instability of arrays of cylinders in cross-flow.

4.2 Tube Frequency Response and Flow Periodicity Measurements

The testing facility was equipped with a hot film positioned as shown in figure (3.2.5), at the wake of tube no. 4. The purpose of installing the hot film was to investigate whether or not any flow periodicities existed within array.

Careful study of the flow velocity power spectra, obtained during testing of both tube no. 3 and tube no. 4, indicated that no periodicity in the flow could be detected from the probe in the range of the flow velocities below the stability threshold. The power spectrum of the flow velocity indicate the expected turbulence spectrum and only when the tube motion becomes large enough to induce a flow periodicity a spike coinciding with the tube's frequency is observed. This frequency spike disappeared in the absence of the tubes's motion.

The tube response below the critical velocity indicates the absence of any vorticity resonances. Although in the present study we were unable to detect and identify distinct vorticity phenomena as the predominant mechanism of excitation for this type of array, it should be noted that other investigators (ref. [32], [37]), for geometrically similar arrays, reported the existence of vorticity phenomena especially at the first two tube rows. In most cases this type of excitation is not considered to result in serious vibrations.

4.3 The Effect of Detuning all Adjacent Tubes on the Stability Threshold of Tube No. 3

An interesting implication of Blevins' [64] analysis, as mentioned in Chapter 2 above, is that a significant increase in the threshold flow velocity could be achieved, if the natural frequencies of adjacent tubes relative to the monitored flexible tube are altered. Depending on the validity of this assumption, this concept could be used in the design of tube arrays. Results reported by Southworth and Zdravkovich [65] for tube rows supported this prediction. According to Blevins' analysis the fluid forces on a tube are only dependent on the relative displacements of the two nearest tubes in the same row.

To verify the validity of this assumption, an experiment was conducted in which all flexible adjacent tubes to tube no. 3 were tuned to a higher frequency of 100 ± 0.2 Hz in air, while tube no. 3 was tuned at 40 ± 0.2 Hz in air. The natural frequency monitored in water for tube no. 3 was found to be as before 22.5 ± 0.2 Hz. The adjacent tubes had a natural frequency of 55 ± 0.2 Hz which indicated that there was enough frequency separation between the monitored tube and the adjacent tubes. The test section was then inserted in the water tunnel and the response of tube no. 3 with increasing flow velocity was monitored.

The response curve is shown in figure (4.3.1) and the mode shapes of the tube motion are shown in figure (4.3.2). The tube response indicates a similar response to the one observed when the whole array was flexible. Part OA of the

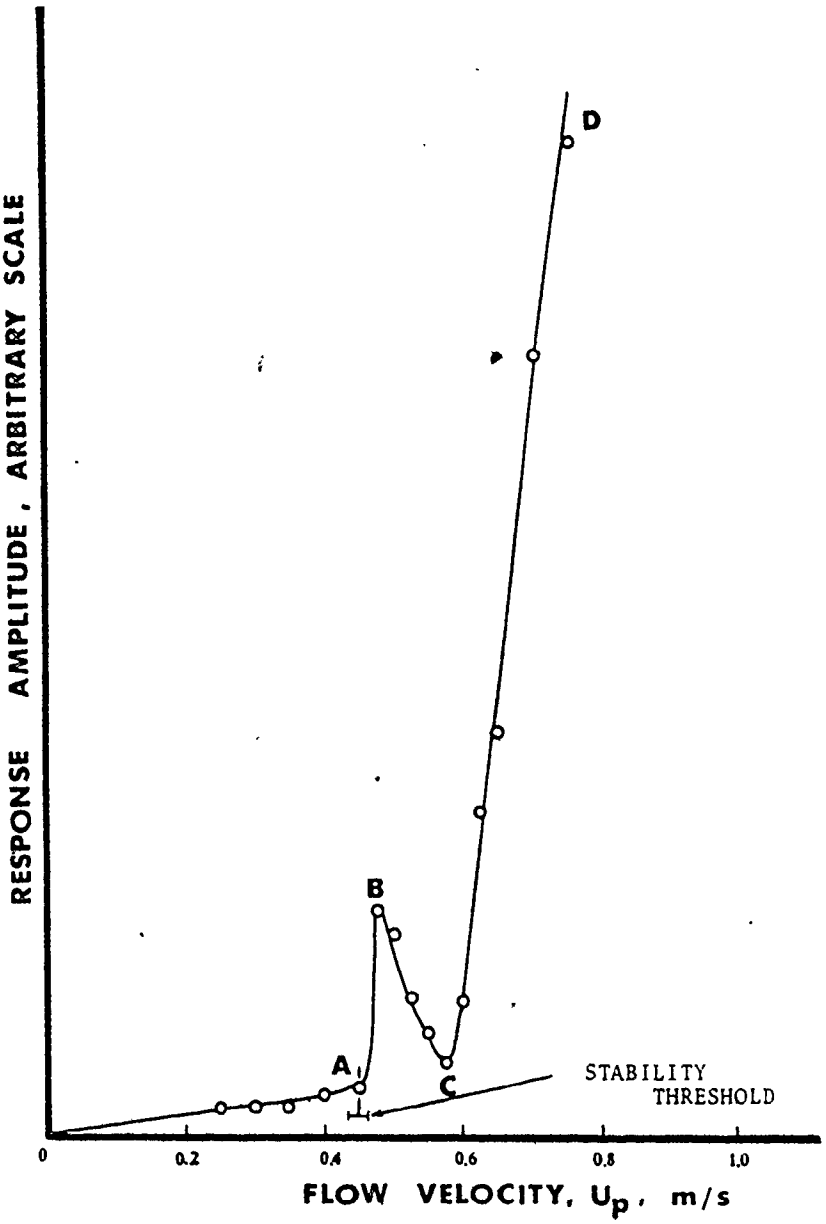

Figure 4.3.1: Amplitude response of detuned tube no. 3 with increasing flow velocity.

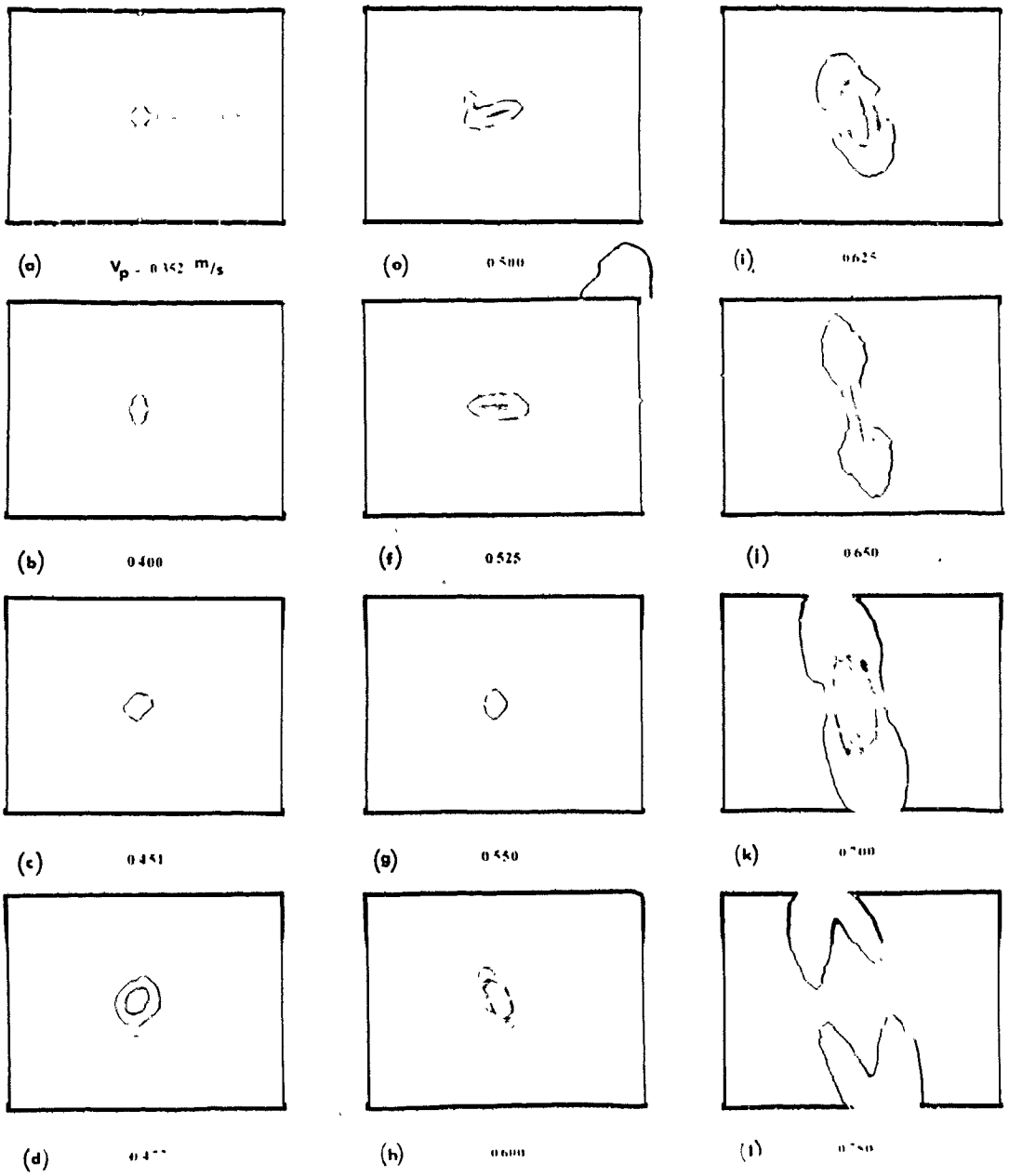

Figure 4.3.2 Oscilloscope mode shapes of detuned tube no. 3

response curve corresponds to the random response due to turbulent buffeting. The tube amplitude increases approximately linearly with the flow velocity, until the flow reaches 0.45 m/s. The mode shapes of the tube in this range are shown in figures (4.3.2) (a), (b) and (c), while the frequency spectra are shown in figures (4.3.3) and (4.3.4). An increase of the flow velocity of 0.477 m/s resulted in a sudden increase of the tube's amplitude. The mode shape of the tube at this flow was a clearly circular type as shown in figures (4.3.2) (d) and (4.3.5) at a frequency of 23.2 Hz. An overall reduction in amplitude and motion mainly in the transverse to the flow direction was observed as the velocity was further increased. Figures (4.3.2) (e) and (f) show the tube's mode shapes while the frequency spectrum corresponding to 0.5 m/s is shown in figure (4.3.6). A minimum amplitude is recorded at a flow velocity of 0.55 m/s as shown in figures (4.3.2) (g) and (4.3.7), (point C of the response curve), with a corresponding frequency of 24.4 Hz. Further velocity increase caused an increase in the tube's amplitude and the tube's motion was mainly in the streamwise direction (part CD of the response curve). The corresponding mode shapes and frequency spectra are shown in figure (4.3.2) (h) to (i) and (4.3.8) to (4.3.11) inclusive.

The motion of the adjacent tubes throughout testing was recorded through tube no. 4 and found to be negligible.

The modulating response curve of tube no. 3 in this test (noted by AC on the curve) creates some ambiguity in selecting

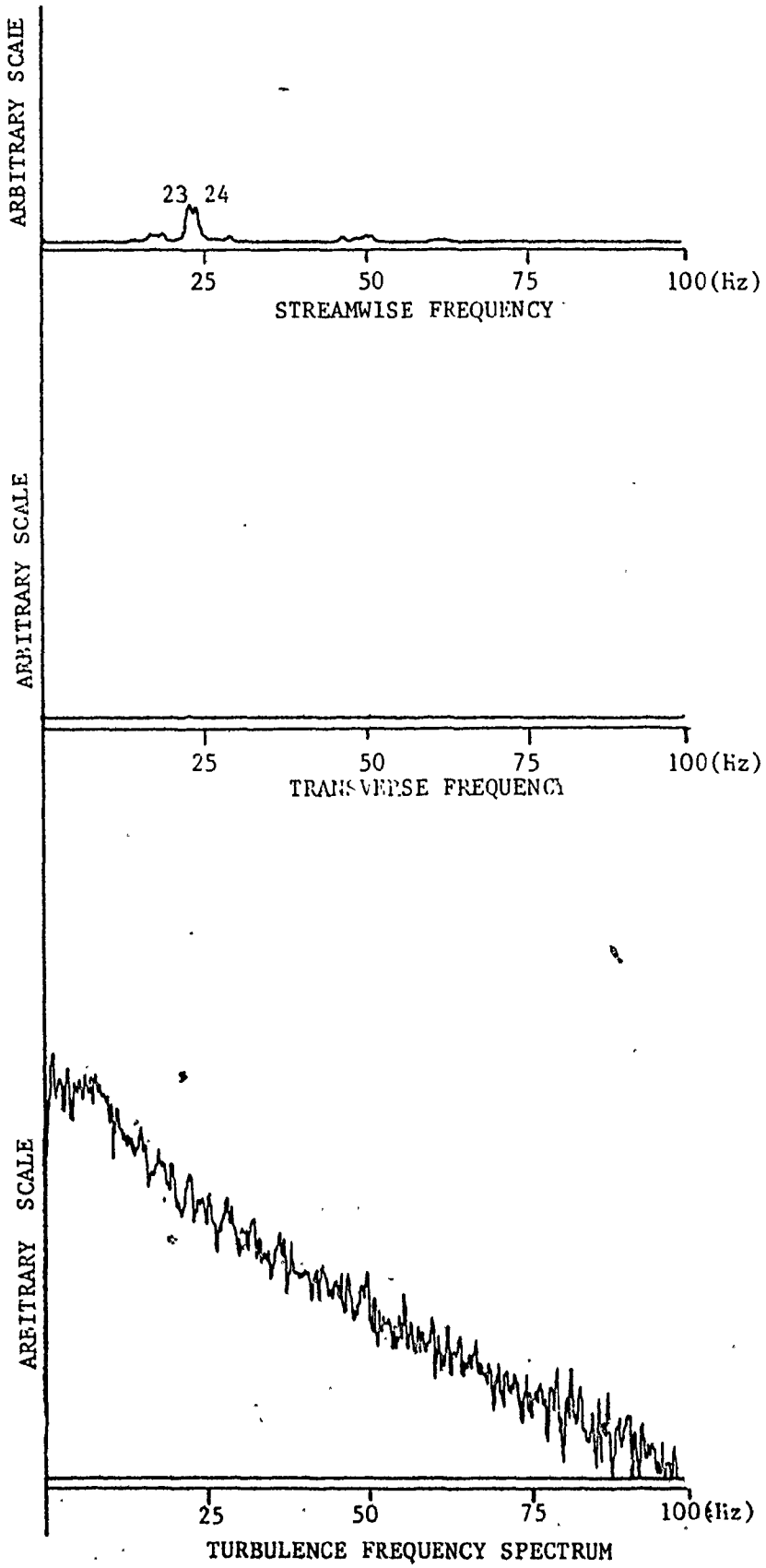

Figure 4.3.3: Amplitude and turbulence power spectra of detuned tube no.3 at Up=0.301 m/s

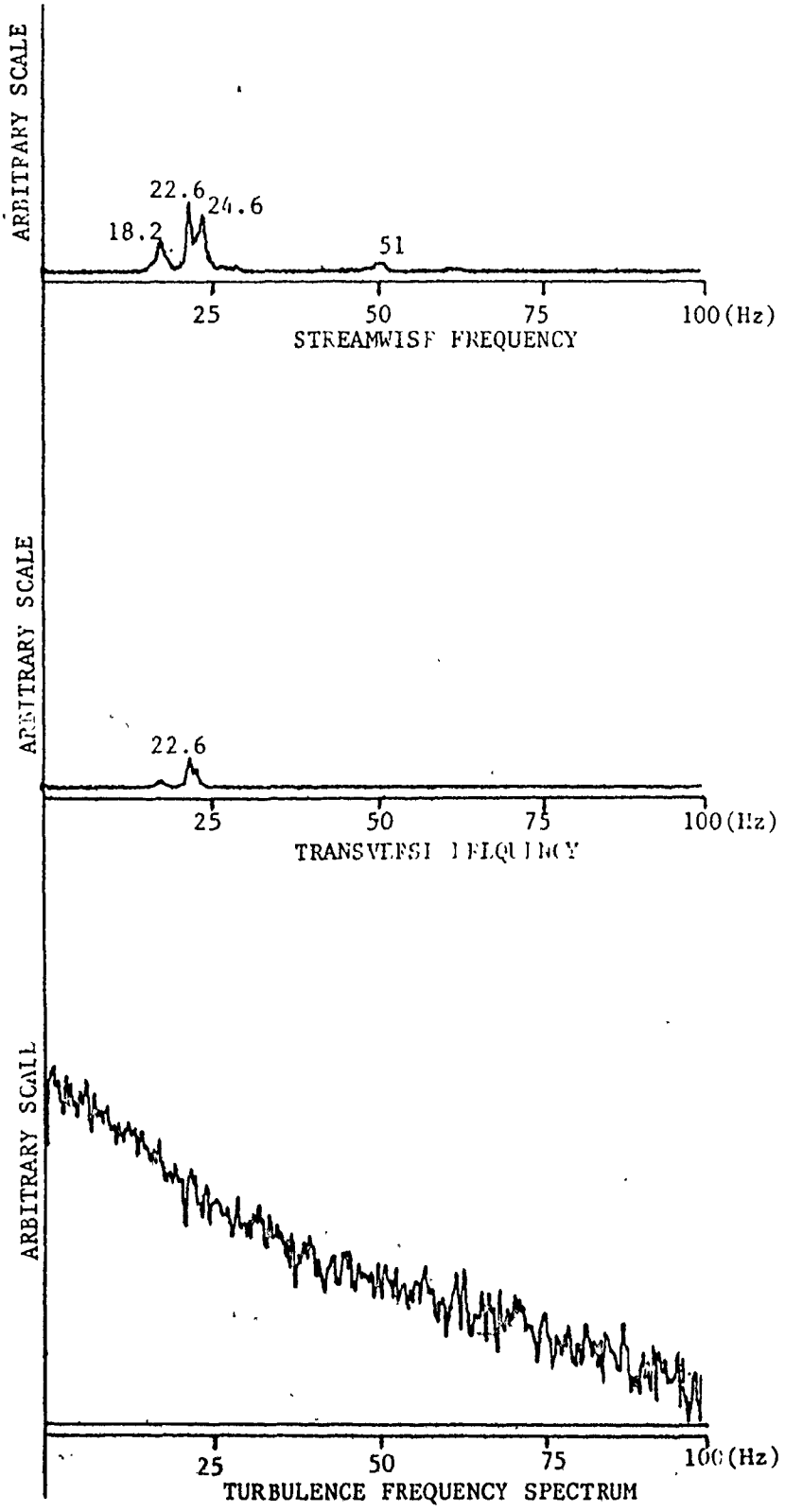

Figure 4.3.4: Amplitude and turbulence power spectra of detuned tube no.3 at Up=0.451 m/s

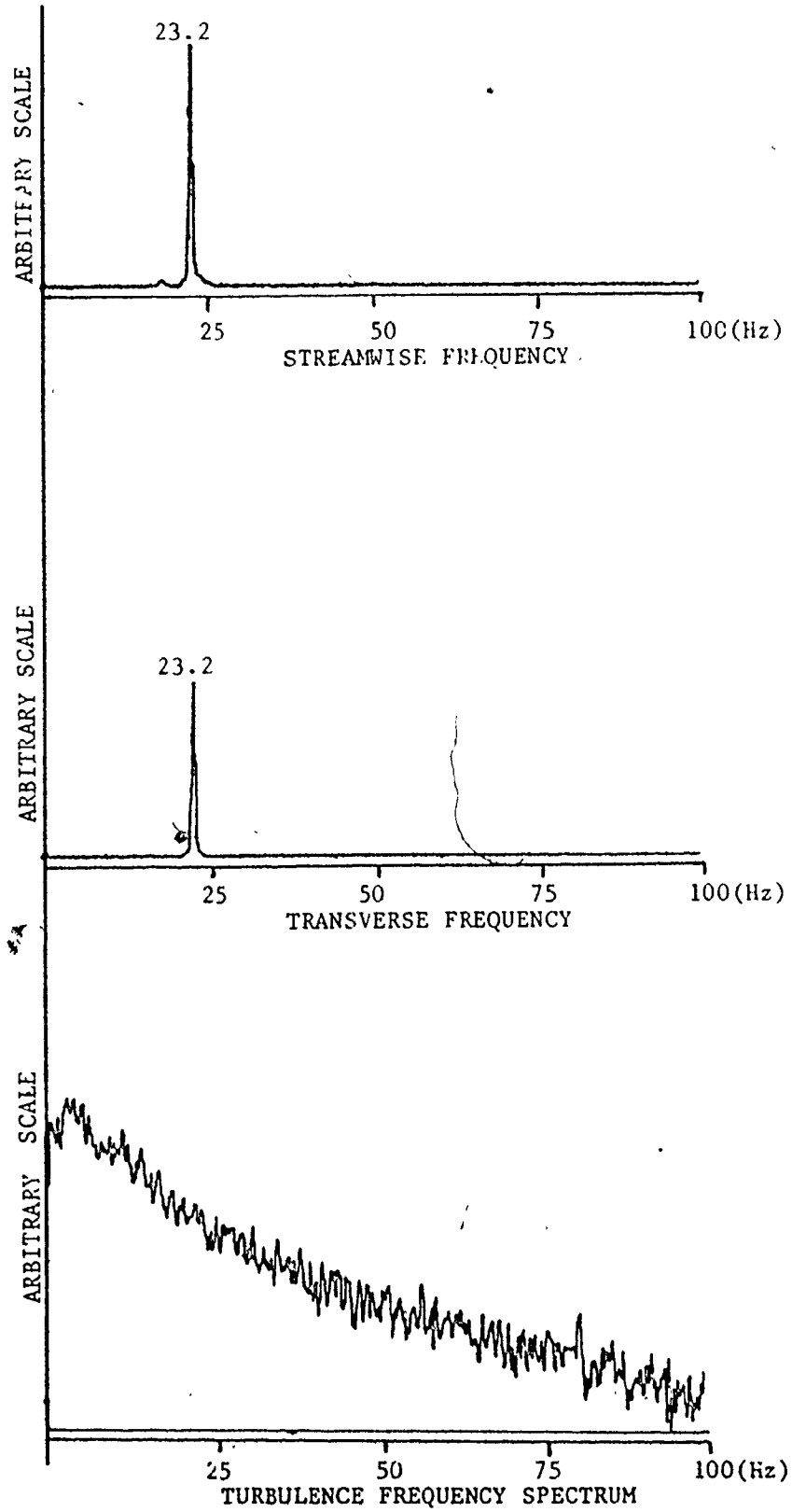

Figure 4.3.5: Amplitude and turbulence power spectra of detuned tube no.3 at Up=0.477 m/s

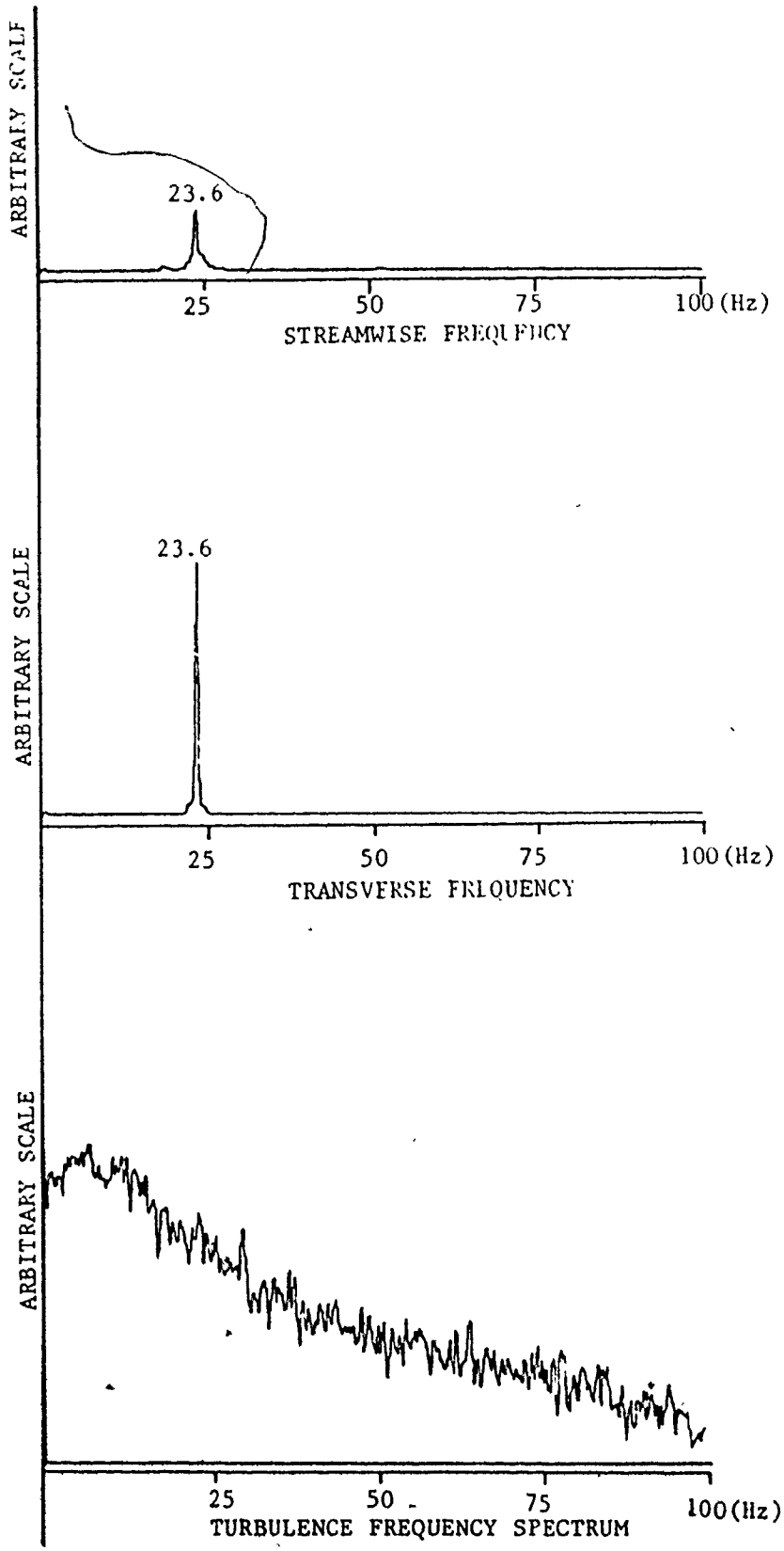

Figure 4.3.6: Amplitude and turbulence power spectra of detuned tube no.3 at Up=0.500 m/s

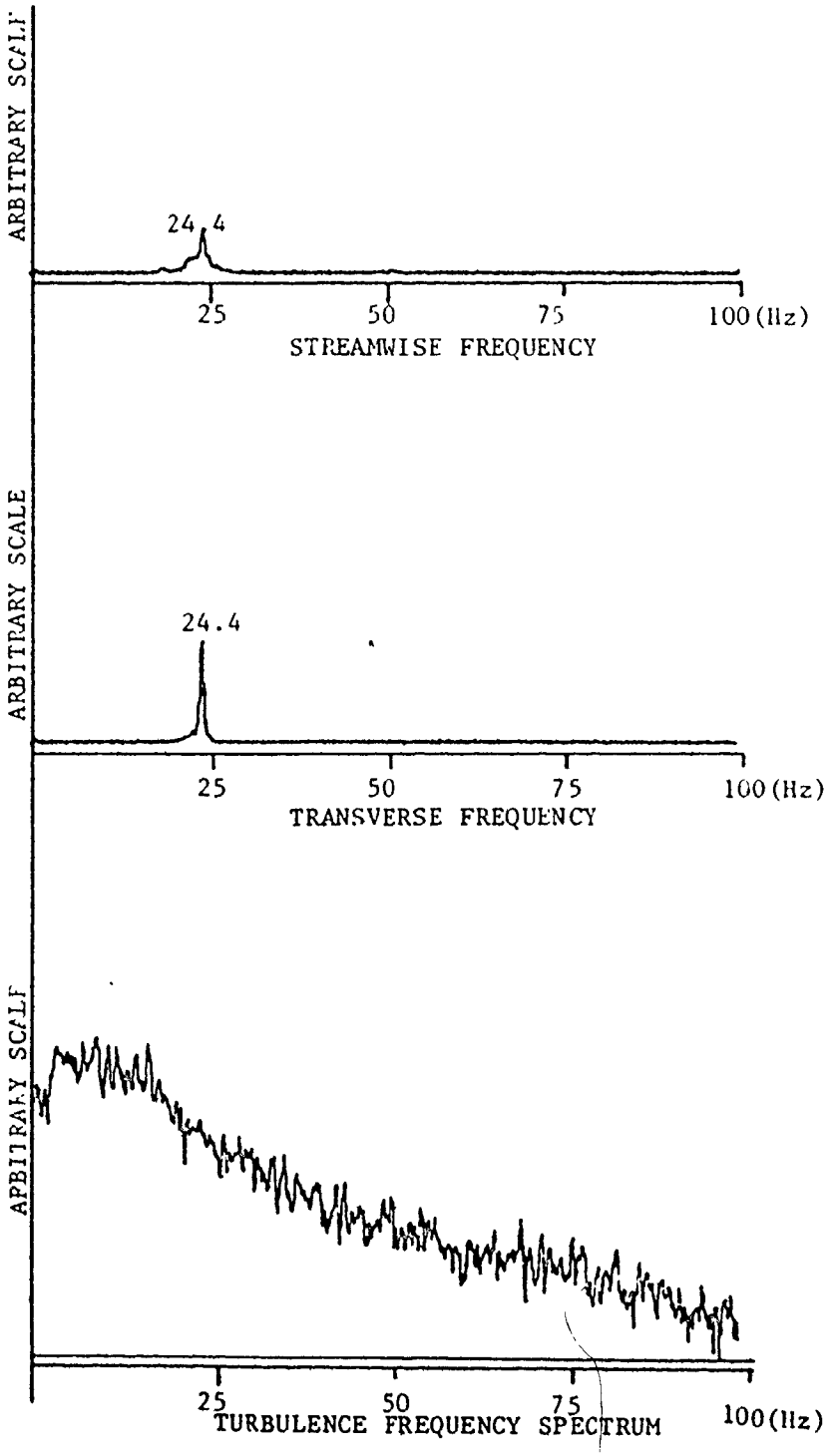

Figure 4.3.7: Amplitude and turbulence power spectra of detuned tube no.3 at Up=0.550 m/s

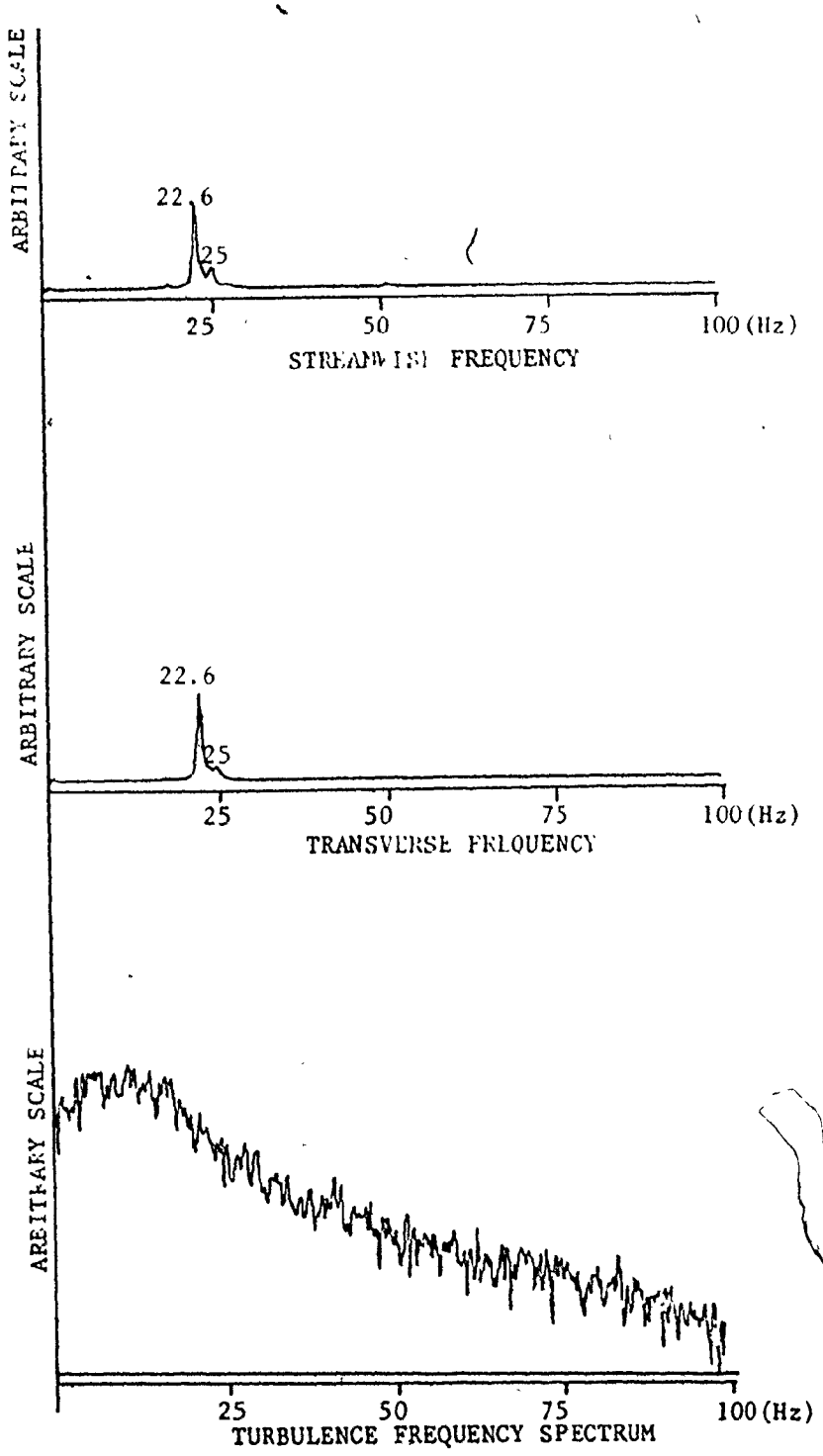

Figure 4.3.8: Amplitude and turbulence power spectra of detuned tube no.3 at Up=0.600 m/s

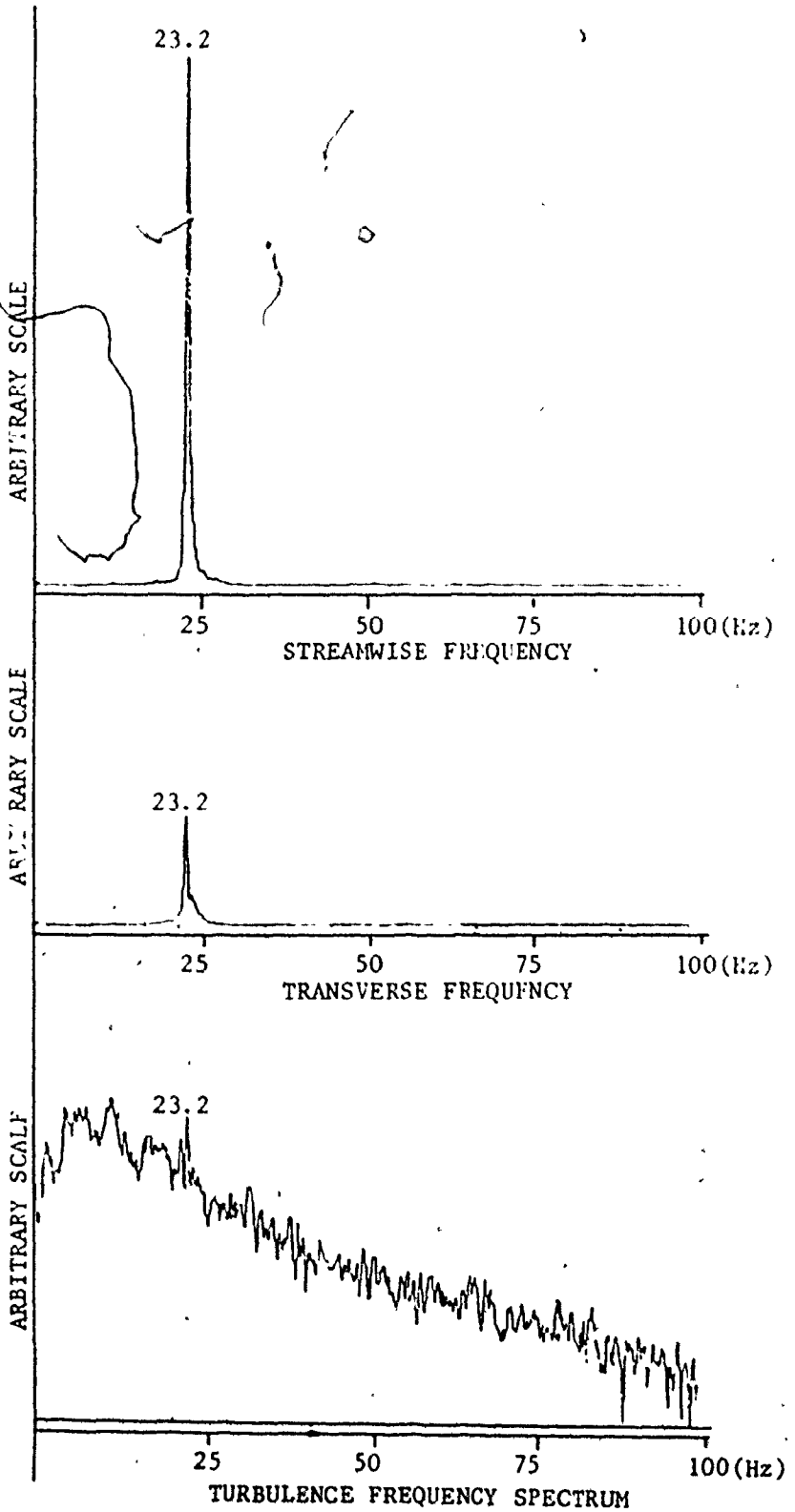

Figure 4.3.9: Amplitude and turbulence power spectra of detuned tube no.3 at Up=0.650 m/s

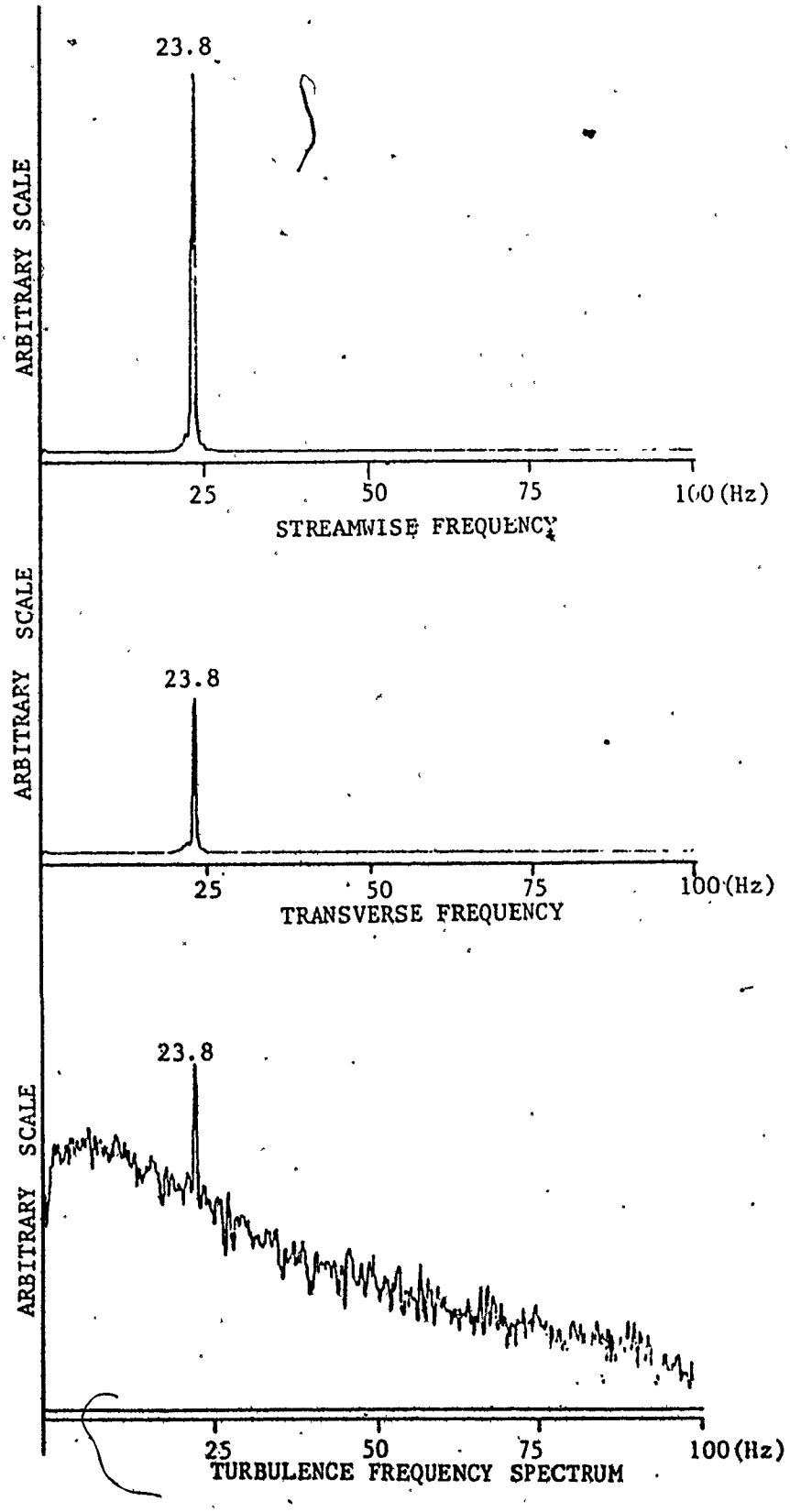

Figure 4.3.10: Amplitude and turbulence power spectra of detuned tube no.3 at Up=0.750 m/s

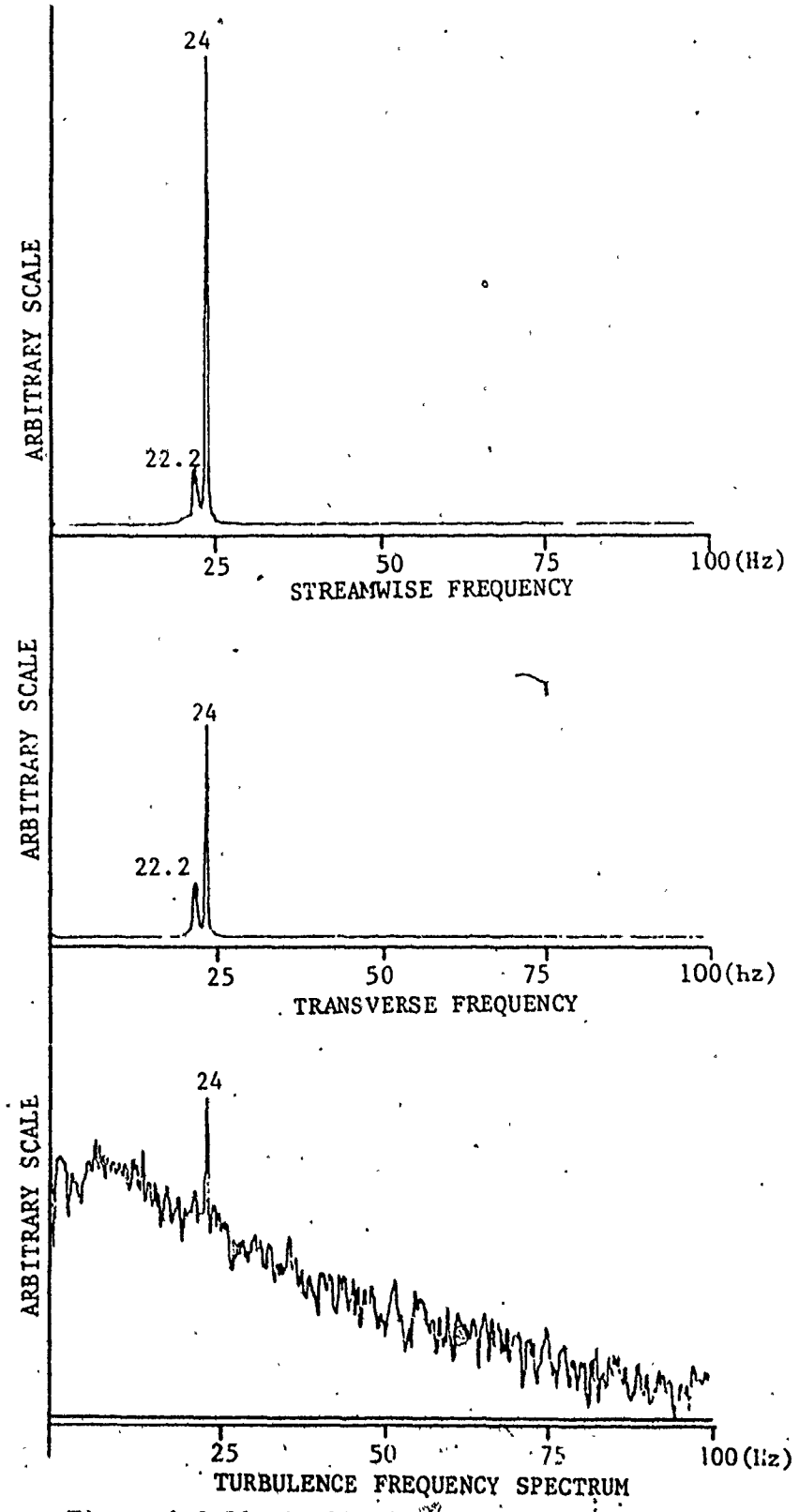

Figure 4.3.11: Amplitude and turbulence power spectra of detuned tube no.3 at Up=0.800 m/s

the stability threshold. The possibility of this response being the result of vorticity effects is excluded for the following reasons: The Strouhal number, based on the pitch velocity, corresponding to this range varies from 1.25 to 1.13 which is considerably high than previously observed, while no flow periodicity is detected in the velocity spectra. We also note the absence of any "lock-in" phenomena that are often associated with the existence of periodicty in the flow.

Since the mechanism of excitation is not well understood, one should only note the important point, that tube no. 3 vibrates close to its natural frequency in a modulated transverse oval shape before reaching very large elliptical orbits with its major axis at a small angle to the streamwise direction. This is an important observation because it indicates that the fluid coupling and displacement of adjacent tubes is not necessary for fluidelastic instabilities to occur in the tube arrays.

Following our definition of the critical velocity, it becomes clear that the onset of instability occurs at approximately 0.477 m/s, (point A' on the response curve), which is about 5% lower from the array's stability threshold for this test. The present results regarding frequency detuning are in good agreement with the results published for wind tunnel studies by Weaver and Lever [32] and the observations reported by Gorman [66] for liquid flows. We can therefore conclude that significant frequency detuning of adjacent tubes has little effect on the critical velocity of an array.

4.4 Comparison of Present Results with Previously Published

The stability threshold of a parallel-triangular array with pitch-to-tube diameter ratio of 1.375 in liquid flow was established. The response curves shown in figures (4.1.5) and (4.1.17) corresponding to tubes in the third and fourth rows yielded the same critical flow velocity, which is considered the velocity threshold for the array. The present results were compared with the published results for a similar geometry array for tests conducted in a wind tunnel. The stability threshold predicted by Weaver and El Kashlan [40] has the form:

$$U_p/fD = k\ (m/\rho D^2)^{0.29}\ (\delta)^{0.21}$$

When the present results were plotted in a similar fashion and compared to this stability boundary, it was seen that they lie somewhat below the extended boundary. Hence, the prediction of reference [40] is apparently slightly unconservative for liquid flows. Data obtained with an array of the same geometry by Weaver and the author [63] for a liquid flow, yielded results that are in good agreement with the present results. Both the present results and those obtained from reference [63] are plotted in figure (4.1.26) and compared to the proposed stability boundary by Weaver and El Kashlan [40]. It should be noted that this boundary threshold does not account for the geometry of the array. This does not affect the present comparison, since the arrays are geometrically

identical, but it will be important when considering arrays of different pitches and patterns.

As was discussed in Chapter 2, a more general stability boundary was proposed [2] in the form

$$U_p/fD = k\ (m/\rho D^2)^a\ ((P-D)/D)^b\ (\delta)^c$$

which includes the geometrical parameters of the array.

The present results and those of reference [63] are plotted in figure (4.4.1), using the stability boundary as proposed by Paidoussis [2]. The results can be directly compared with data published by a number of other investigators for the stability of arrays with various geometrical and physical characteristics, for liquid, two-phase and gaseous flows. It is clear that the results of this study are outside the lower stability boundary for the majority of the data. Only the results obtained by Nicolet et al. [31] and those of reference [63] seem to be in agreement with the present results. It should be noted however, that if an added mass coefficient of 1.0 were used, as is common in the literature, (but quite incorrect), the present results and those of reference [63] would move to the left of the stability boundary and fall within the same band as the bulk of the data. This procedure was not used in the present study as it makes no physical sense. The reason that it is common to use a value for the added mass coefficient of 1.0, is that, simply, it is easy to do so.

When the same published data and the present results

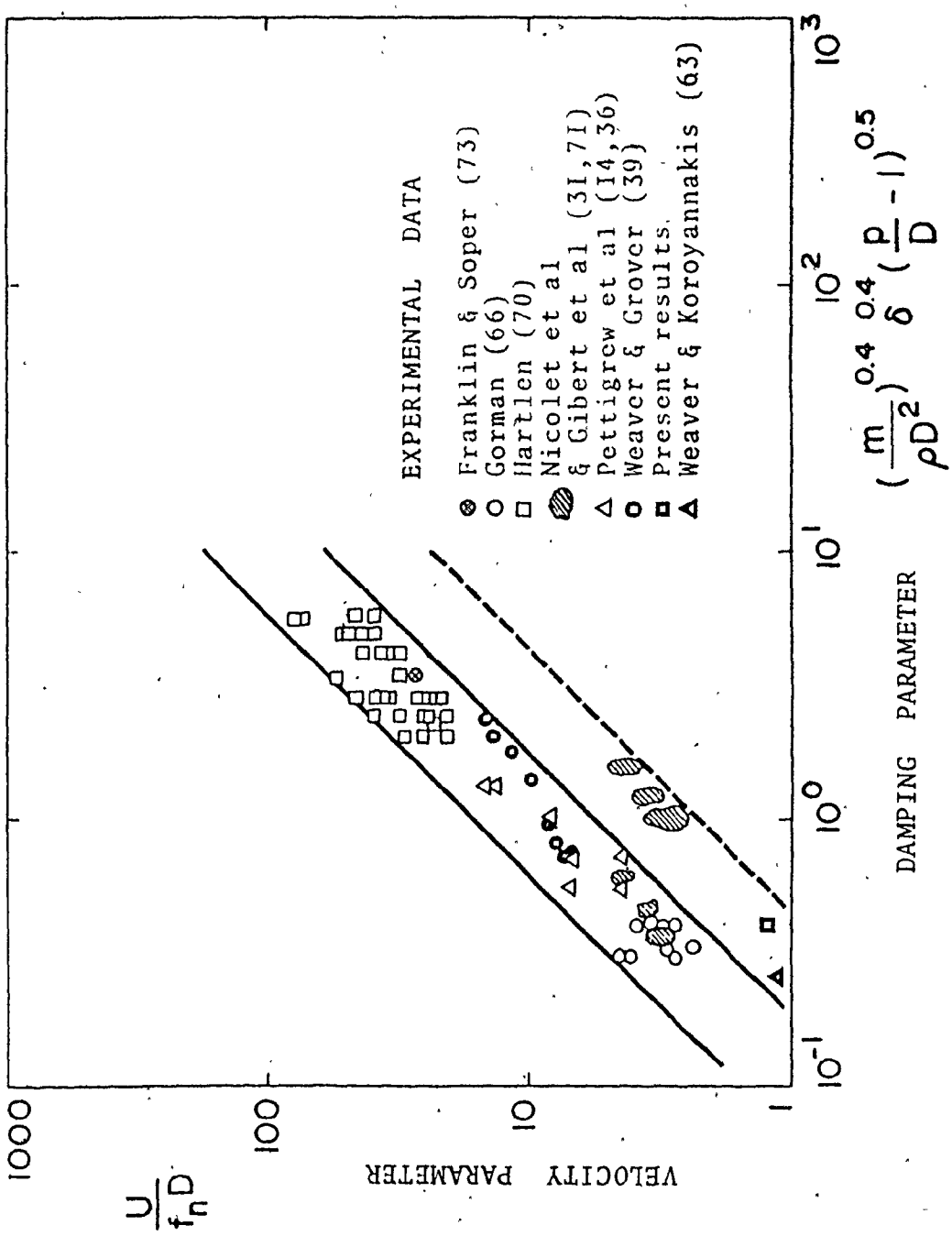

Figure 4.4.1: Comparison of present results with published experimental data.(from ref.2)

are reduced and plotted in the conventional way, as shown in figure (4.4.2), using the reduced velocity and damping parameters, the fit of the data from reference [63] seems to be in good agreement with the lower stability parameter as proposed by Pettigrew [36], but still the data obtained from the present experiments and some of the data of reference [31] is located below this stability boundary. One should be careful since this type of stability plot has already been proven to be inadequate.

The scatter observed in the published data is indicative of the inadequacy of the Connors' type relationship as well as the lack of consistent treatment of the data. Principal amongst the latter are inconsistent definitions of the stability threshold, improper accounting for added mass, and no provision for tube pattern and pitch effects. An additional problem is the measurement of damping and the question whether the damping used should be that in vacuo or in the fluid that the array is exposed to. Many more careful experiments are necessary before an adequate understanding of the phenomena involved can be achieved.

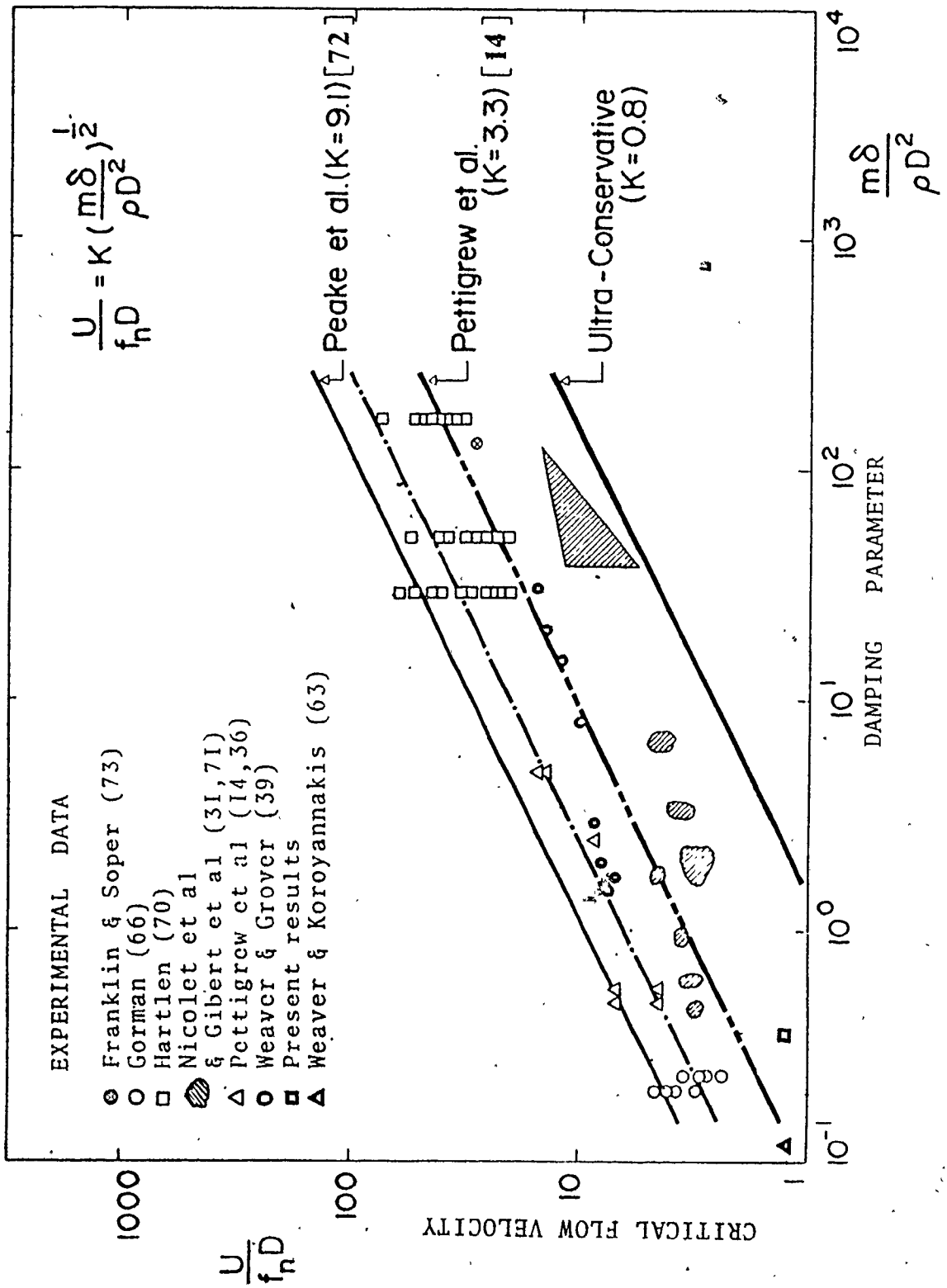

Figure 4.4.2: Comparison of present results with published experimental data.(from ref.2)

CHAPTER 5

SUMMARY AND CONCLUDING REMARKS

The aim of the present study was to design an experimental facility to study some of the phenomena associated with the liquid cross-flow-induced vibrations of a model tube-array. In particular, it was intended to determine the stability threshold of the tube-array, study the tubes' frequency response and investigate whether or not any flow periodicities can exist within the tube-array. It was also desired to examine the effect of detuning all adjacent tubes on the stability threshold of one tube in the array and finally compare the present results with previous wind tunnel results and with those published in the literature.

The experiments were conducted in a low-speed water tunnel having a 305 x 305 mm working section, designed specially for the present work. The approach flow has a low turbulence intensity (less than 0.5%) and a flat velocity profile (within 1%) outside the boundary layers.

The tube-bundle was a parallel-triangular array of tubes having a pitch to diameter ratio of 1.375. The array was six rows deep with five tubes in each row. Ten identical tubes in the middle of the tube-array were flexible and specially designed so that their natural frequency and damping could be controlled. The remaining tubes were fixed.

The amplitude response of tubes in the third and fourth

rows at different flow velocities was determined. The tubes responded randomly due to turbulence in the flow, followed by fluidelastic vibration which occurred at a 30% lower frequency than their monitored natural frequency in quiescent water. This can be explained due to the increased added mass in the fluid coupled modes of the flexible tube bundle. The stability thresholds corresponding to tubes in the third and fourth rows were found to be the same. This is considered to be the critical velocity threshold for the array.

When the present results are reduced in the form of the nondimensional velocity and damping parameters, and compared to the stability boundary which is derived from wind tunnel studies for geometrically identical arrays, we can conclude that the previously established stability threshold in air is unconservative for liquid flows.

The study of the tubes' frequency response and the flow velocity power spectra obtained during testing, indicate that no flow periodicity could be detected in the range of flow velocities below the stability threshold.

The effect of detuning all adjacent tubes on the stability of tube no. 3, located in the third row, was examined experimentally. The response of tube no. 3 was similar to that observed when the whole array was tuned at the same frequency. The tube responded to the turbulent buffeting and fluidelastic instability occurred at approximately 5% lower flow velocity than the critical flow velocity observed when the whole tube bundle was in tune. Thus we can conclude that frequency

detuning of adjacent tubes has no significant effect on the stability boundary of the tube array.

Finally, when the present results are directly compared with previously published data for the stability of arrays with various geometrical and physical characteristics, it becomes evident that they lie below the lower stability boundaries for the majority of the data, indicating that extrapolation of existing data can result in unconservative predictions of the stability boundary of an untested design.

Although the present investigation has answered some important questions, it has undoubtedly raised a number of new questions. Some of the areas where further future research is required are listed below:

(a) A comprehensive study should be undertaken to establish the stability boundary generated when the mass ratio is altered. This could be achieved by varying the tubes' mass for the same array.

(b) Since the stability boundary of an array is expected to vary with the geometrical pattern of the array, further experiments should be conducted to establish the effects of geometry on the stability threshold of arrays.

(c) A universal method for determining the stability threshold of arrays and reducing the experimental data should be developed. This would result in a reduction of the observed scatter in the published data and would yield more meaningful data comparison between the various investigators.

REFERENCES

1. International Symposium on vibration problems in industry. Keswick, England, 1973.(U.K. Atomic energy authority at Windscale, N.P.L.)

2. Paidoussis,M.P.,"Flow-induced vibrations in nuclear Reactors and Heat Exchangers, Practical experience and state of knowledge." Symposium on practical experiences with flow-induced vibrations,Karlsruhe, Germany, September 3-6,1979.

3. Shin,Y.S., Wambsganss,M.W.," Flow-iduced vibration in L.M.F.B.R. steam generators: A state-of-the art review.", A.N.L report 75-16, May 1975.

4. Oldaker,I.E., Et al.," An overview of the Canadian program to investigate vibration and fretting in nuclear fuel assemblies.",CSME paper no.73-CSME-89.

5. Weaver,D.S.,"On flow-induced vibrations in hydraulic structures and their alleviation.", Canadian J. of Civil Engg.,Volume 3, no. 1. 1976.

6. IUTAM/IAHR, 1974 Proc. of Symposium on flow-induced structural vibrations, Karlsruhe, Germany. Springer-Verlag, Berlin. Ed. E. Naudascher.

7. Sainsbury,R.N., King,D.," The flow-induced oscillation of Marine structures.", Proc. Inst. Civil Engg. pp. 269-299,1971.

8. Symposium on "Fluid-solid interaction", presented at ASME Winter annual meeting,Pittsburgh. Ed. J.E. Greenspon, Nov. 1963.

9. Proceedings of the Wind effects on buildings and structures conference,N.P.L.,Teddington,England, June 1963.

10. Naudascher,E.," From flow instability to flow-induced excitation.",ASCE, J. of Hydraulics Div. HY4, 1967.

11. Toebes, G.H.," Flow-induced stuctural vibrations" J. of Engg. Mechanics Div.,ASCE,EMG,1965 pp.39-65.

12. Savkar,S.D.," A survey of flow-induced vibrations of cylindrical arrays in cross flow.", ASME paper 75-WA/FE-21, 20pp. 1976.

13. Chen,S.S.,"Flow-induced vibration of circular cylindrical structures.Part 2: Cross-flow considerations", The shock and vibration Digest,vol.9 1977,pp. 21-27.

14. Pettigrew,M.J.,Sylvestre,Y.,Campagna,A.O.,"Vibration Analysis of Heat Exchanger and Steam Generator Designs", Nuc. Engg. and Design,Vol.48.1978 pp.97-115, also AECL report no. 5826.

15. Proceedings of IAHR/IUTAM. Symposium on Practical experiences with flow-induced Vibrations,Karlsruhe, Sep.1979, to be published by Springer-Verlag,Editors E.Naudascher and D.Rockwell,1980.

16. Blevins,R.D.,"Flow-induced Vibrations", Von Nostrand Reinhold Co. 1977.

17. Marris,A.W.," A review on Vortex streets, Periodic wakes, and induced vibration phenomena.",Trans. ASME J. Basic Engg.,86, series D, June 1964.

18. Lienhard,J.H.," Synopsis of lift,Drag and Vortex frequency data for rigid circular cylinder", Bulletin 300,College of Engg., Washinghton state Univ.,1966.

19. Chen,Y.N.," Flow-induced vibration and noise in Tube-bank Heat Exchangers due to Von Karman streets", J. Engg. Ind.,90(1),Feb.1968.

20. Putnam,A.A.," Flow-induced noise in Heat Exchangers", ASME J.of Engineering for Power,Vol.81,1959.

21. Chen,Y.N.," Excitation sources of the flow-induced vibrations and noise in tube-bank Heat Exchangers", in "Noise and Fluid Engineering",(Ed. R.Hickling) ASME, New York,1977.

22. Chen,Y.N.," Criteria for the cross-flow induced tube vibrations in tube bank Heat Exchangers", Paper 26, Inter. Conf. on Vibration in Nuclear plant,Keswick, 1978.

23. Owen,P.R.," Buffeting excitation of Boiler tube Vibration", J. of Mech. Engg. science,Vol.7,1965.

24. Fitz-Hugh,J.S.,"Flow-induced vibration in Heat Exchangers", Paper 427, Int. Symp. Vib. Problems in Industry,Keswick,1973.

25. Chen,Y.N.," The sensitive tube spacing region of tube bank Heat Exchangers for liquid-elastic coupling in cross-flow.",in" Fluid-structure Interaction Phenomena in Press. Vessel and Piping Systems", ASME 1977.

26. Grover,L.K., Weaver,D.S.," Cross-flow induced vibrations in a tube bank-Vortex Shedding",J. of sound and Vibr. Vol. 59, 1978, pp.263-276.

27. Funakawa,M.,Umakoshi,R.," The acoustic Resonance in a Tube bank", Bull. JSME,13, 57 March 1970.

28. Chen,Y.N., Young,W.C.," The orbital movement and the damping of the fluidelastic vibration of tube banks due to Vortex formation.Part3", ASME J. of Engg. in Industry, Vol. 96, 1974, pp. 1072-1075.

29. Zdravkovich,M.M.,Nuttall,J.A.," On the elimination of Aerodynamic noise in a staggered tube bank", J. of Sound and vibration 34(2),May 1972 .

30. Brunn,H.H., Davies,P.O.," An experimental investigation of the unsteady Pressure forces on a circular cylinder in a turbulent cross-flow.", J. of sound and vibration, Vol. 40(1), 1975.

31. Nicolet,J.B.,Sagner,M.,Regis,G.," Vibrations de faisceaux de tubes sous excitation aerodynamique", Revue General de Thermique, no. 128, 1976.

32. Weaver,D.S.,Lever,J.," Tube frequency effects on cross flow-induced vibrations in arrays", 5th Biennial Symp. on Turbulence,Univ. Missouri-Rolla,U.S.A. Paper IV.4 October 1977.

33. Roberts,B.W.," Low frequency, self-excited vibration in a row of circular cylinders mounted in an air stream", Ph.D Thesis, University of Cambridge,1962.

34. Connors,H.J.," Fluid-elastic vibration of tube arrays excited by cross-flow",ASME Symp. on flow-induced vibration in Heat Exchangers, New York, 1970.

35. Blevins,R.D.," Fluid elastic whirling of tube rows and tube arrays", ASME J. of Fluids Engg., Sep. 1977.

36. Pettigrew,M.J., Gorman,D.J.," Vibration of Heat Exchanger components in liquid and two-phase cross-flow",AECL report no. 6184, and British Nuc. Energy Soc.,Keswick, May 1978.

37. Gorman, D.J., "Experimental Development of Design Criteria to Limit Liquid Cross-Flow-Induced Vibration in Nuclear Reactor Heat Exchange Equipment." Nuclear Science and Engineering, Vol. 61, 1976.

38. Weaver, D.S., Grover, L.K., "Cross-Flow Induced Vibrations in a Tube-Bank - Turbulent Buffeting and Fluidelastic Instability." J. of Sound and Vibration, Vol. 59, 1978.

39. Weaver, D.S. Grover L.K., "Cross-Flow Induced Vibrations in a Tube-Bank." ASME Paper 78-PVP-25, June 1978.

40. Weaver, D.S., El-Kashlan, M., "The Effect of Damping and Mass Ratio on the Stability of a Tube-bank." Paper submitted for publication to the A.S.M.E. J. of Mechanical Engineering & Design.

41. "Hydraulic Institute Standards for Centrifugal Rotary & Reciprocating Pumps." Thirteenth Edition, Hydraulic Institute, 1975. Cleveland, Ohio. Library of Congress Card No. A56-4036.

42. Bradshaw, P., "Experimental Fluid Mechanics." Oxford New York, Pergamon Press, 1970, 2nd Edition.

43. Morel, T., "Comprehensive Design of Axisymmetric Wind Tunnel Contractions." J. of Fluids Engg., Trans ASME Series I, Vol. 97, June 1975, pp. 225-233.

44. Tsien, H.S., "On the Design of the Contraction Cone for a Wind-Tunnel." J. of Aeronautical Sciences, Vol. 10, 1943.

45. Smith, R.H., Wang, C.T., "Contracting Cones Giving Uniform Throat Speeds." J. of Aeronautical Sciences, Vol. 11, 1944.

46. Thwaites, B., "On the Design of Contractions for Wind Tunnels." ARC, R&M 2278, 1946.

47. Whitehead, L.G., Wu, L.Y., Waters, M.H.L., "Contracting Ducts of Finite Length." Aeronautical Quarterly, Vol. 2, 1951.

48. Morel, T., "Design of Two-Dimensional Wind Tunnel Contractions." J. of Fluids Engg., Trans A.S.M.E., June 1977, pp. 371-378.

49. Lighthill, M.J., "A New Method of Two-Dimensional Aerodynamic Design." ARC R&M 2112, 1945.

50. Goldstein, S., "Notes on the Design of Converging Channels." ARC R&M 2643, 1945

51. Libby, P.A., Reiss, H.R., "The Design of Two-Dimensional Contraction Sections." Quarterly of Applied Mathematics, Vol. IX, 1951.

52. Gibbings, J.C., Dixon, J.R., "Two-Dimensional Contracting Duct Flow." Quarterly J. of Mechanics and Applied Mathematics, Vol. X, Part 1, 1957.

53. Gibbings, J.C., "Flow in Contracting Ducts." AIAA Journal, Vol. 2, 1964, pp. 191-192.

54. Gibbings, J.C., "The Choice of a Hodograph Boundary for Contracting Ducts." Journal of the Royal Aeronautical Society, Vol. 68, June 1964, pp. 420-422.

55. Cohen, M.J., Ritchie, N.J.B., "Low-Speed Three-Dimensional Contraction Design." J. of the Royal Aeronautical Society, Vol. 66, 1962, pp. 231-236.

56. Rouse, H., Hassan, M.M., "Cavitation - Free Inlets and Contractions." Mechanical Engineering, March 1949.

57. Hussain, A.K.F., Ramjee, V., "Effects of Axisymmetric Contraction Shape on Incompressible Turbulent Flow." J. of Fluids Engg., Trans. A.S.M.E., Series I, Vol. 98, March 1976, pp. 58-68.

58. El-Shammaa, S.A., "On the Application of the Finite Element Method to Three-Dimensional Incompressible Potential Flow." Master's Thesis, McMaster University, 1975.

59. El Kashlan, M., "Tube Row and Damping Parameter Effects on Tube-Array Stability." Master's Thesis, McMaster University, 1980.

60. Grover, L.K., "Cross Flow-Induced Vibration Deep Inside a Closely Packed Tube-Bank." Ph.D Thesis, McMaster University, 1977.

61. Chen, S.S., Ho Chung, "Design Guide for Calculating Hydrodynamic Mass. Part I Circular Cylindrical Structures." Argonne National Laboratory, June 1976, ANL-CT-76-45.

62. Chen, S.S., Wambsganss, M.W., Jendrzejczyk, J.K., "Added Mass and Damping of a Vibrating Rod in Confined Viscous Fluids." Trans. A.S.M.E., J. of Applied Mech., Vol. 43, 1976.

63. Weaver, D.S., Koroyannakis, D., "Flow Induced Vibrations of Heat Exchanger U Tubes - A Simulation to Study the Effects of Assymetric Stiffness." Paper Submitted for publication to the Trans. A.S.M.E., J. of Mechanical Engg. and Design.

64. Blevins, R.D., "Fluid-Elastic Whirling of a Tube Row." Trans. A.S.M.E. J. of Pressure Vessel Technology, 96(4), 1974.

65. Southworth, P.S., Zdravkovitch, M.M., "Cross-Flow Induced Vibrations of Finite Tube Banks in In-Line Arrangements." J. of Mechanical Engg. Science, 17(4), 1975.

66. Gorman, D.J., "Experimental Study of Peripheral Problems Related to Liquid Flow Induced Vibration in Heat Exchangers and Steam Generators." Paper F 4/9 4th International Conference on Structural Mechanics in Reactor Technology, San Francisco, 1977.

67. Moretti, P.M., Lowery, R.L., "Hydrodynamic Inertia Coefficients for a Tube Surrounded by Rigid Tubes." Paper No. 75-PVP-47 presented at the Second National Congress on PVP, San Francisco, 1975.

68. Hartlen, R.T., "Recent Field Experience with Flow-Induced Vibration of Heat Exchanger Tubes." Paper 611 of ref. No. 1.

69. Dueck, D.G., "Major Heat Exchanger Performance in Ontario Hydro Operated CANDU Nuclear Generating Stations." Paper presented at the Canadian Nuclear Association Heat Exchanger Reliability Seminar, May 1, 1980.

70. Hartlen, R.T., "Wind Tunnel Determination of Fluid Elastic Vibration Threshold for Typical Heat Exchanger Tube Patterns." Ontario Hydro Research Division, Mechanical Research Dept. Report No. 74-309-K, 1974.

71. Gibert, R.J., Chabrerie, J. Sagner, M., "Vibrations of Tube-Arrays in Transversal Flow." Paper F 4/5, 4th International Conference on SMIRT, San Francisco, 1977.

72. Peake, C.C., Gerstenkorn, G.F., Arnold, T.R., "Some Reliability Considetations for Large Surface Condensers." Proceedings American Power Conference, Vol. 37, 1975.

73. Franklin, R.E., Soper, B.M.H., "An Investigation of Fluidelastic Instabilities in Tube Banks Subjected to Fluid Cross-Flow." U.K.A.E.A. Report AERE R-8708, H.T.F.S. R.S. 192, 1977.

74. Halle, H., Lawrence, W.P., "Cross-Flow - Induced Vibration of a Row of Circular Cylinders in Water." Trans A.S.M.E. paper 77-J.PGC-NE-4, 1977.

75. Roberts, B.W., "Low Frequency, Aeroelastic Vibrations in a Cascade of Circular Cylinders." I. Mech. E. Mechanical Engineering Science Monograph, No. 4, 1966.

APPENDIX A

FLOWMETER CALIBRATION CURVES

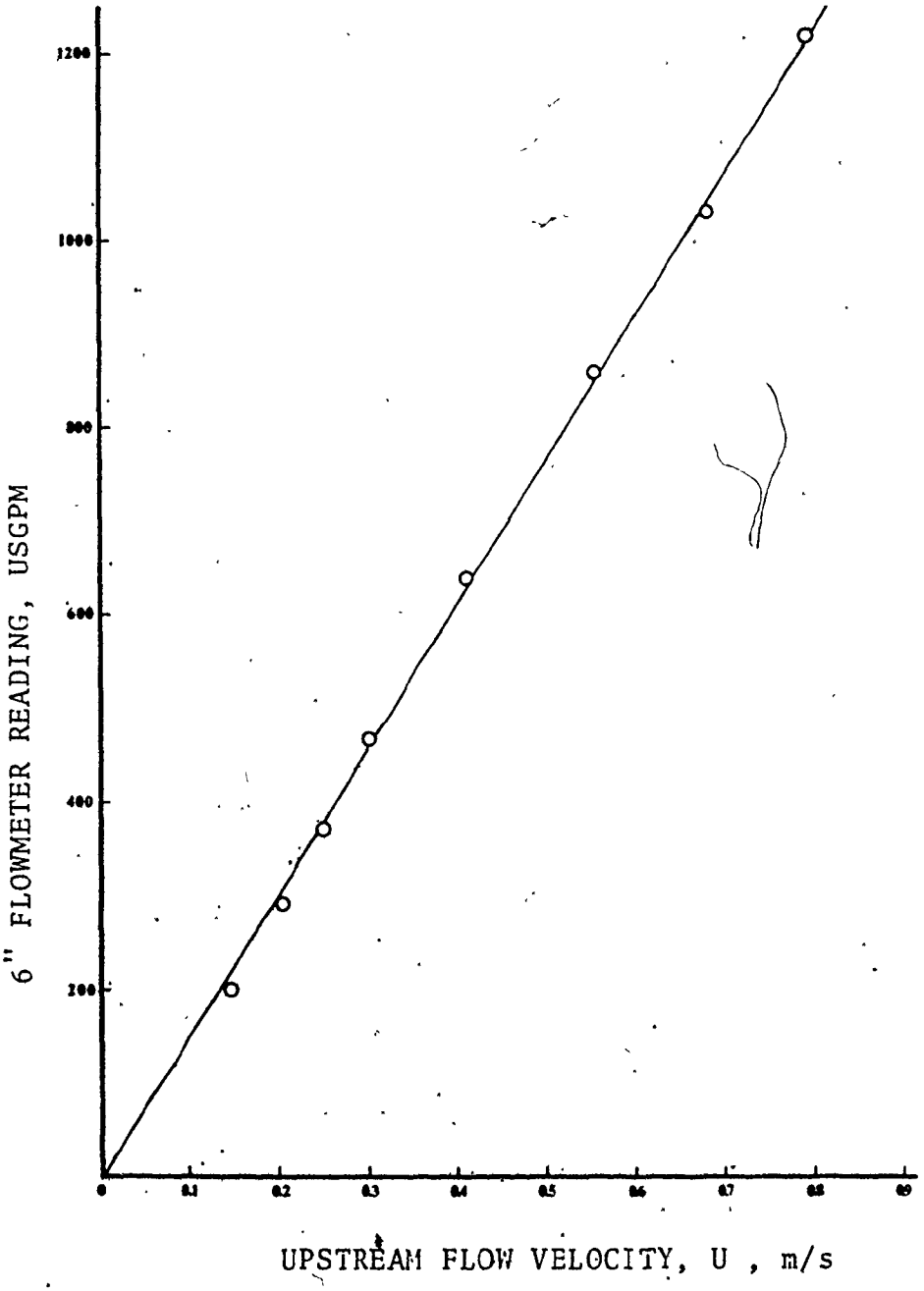

Figure A.1: 6" By-Pass line flowmeter calibration curve

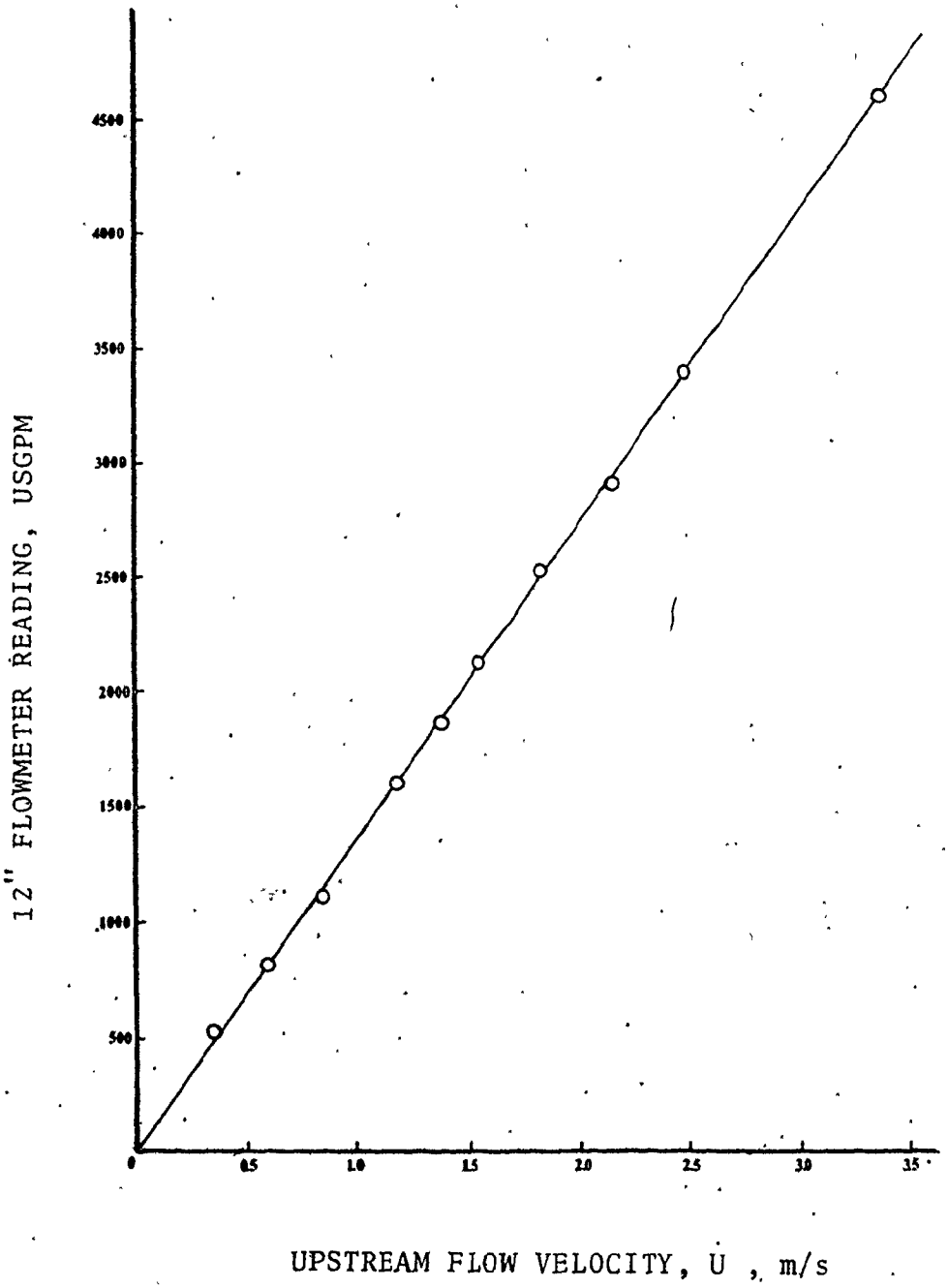

Figure A.2 : 12" Main line flowmeter calibration curve

APPENDIX B

CONTRACTION DESIGN

CONTRACTION DESIGN

A brief description of the design procedure used to obtain the contraction contour is presented below. The present approach is based on the use of design charts, published in the literature by Morel [48], which are compiled from results of a systematic series of calculations for 120 nozzles. A one-parameter family of wall shapes (fig. B.1) consisting of two matched cubic arcs, each having its apex at one end of the nozzle, and with their slopes matched in the interior, was investigated.

The primary criteria of the contraction design are:

(a) Avoidance of separation of either ends of the nozzle

(b) Maximum exit-flow uniformity

(c) Minimum nozzle length, and

(d) Minimum exit boundary layer thickness

In our design it was determined that a contraction ratio up to 4:1 should be used (see Chapter 2) for a two-dimensional contraction. By choosing the contraction ratio, the values of the inlet and outlet nozzle heights H_1 and H_2, can be determined. Based on the fact that a one foot square working section was desirable, these two parameters become $H_1 = 2$ ft. and $H_2 = 0.5$ ft. (fig. B.1) The only design parameters available, then, are the nozzle shape parameters X and nozzle length L.

The first two design criteria, i.e. avoidance of separation and exit-flow uniformity, can be satisfied by increasing the nozzle length. This however, would result in an increase in the boundary layer thickness. In order to satisfy all four design criteria, one should aim at a design in which separation is just avoided and exit-flow non-uniformities are the maximum allowable for the particular application.

In order to predict whether the flow will separate for a given application, the designer needs to be concerned with the values of the wall pressure coefficients to the point where the wall velocity within the nozzle becomes maximum (exit) and minimum (inlet), respectively.

The wall pressure coefficients are defined as:

$$Cp_e = 1 - (U_{2,\infty}/V_e)^2$$

$$Cp_i = 1 - (V_i/U_{1,\infty})^2$$

where:

Cp_e: Wall pressure coefficient at maximum wall velocity

Cp_i: Wall pressure coefficient at minimum wall velocity

$U_{1,\infty}$: Flow velocity far upstream the inlet plane: ft/s

$U_{2,\infty}$: Flow velocity far downstream the exit plane: ft/s

V_e: Maximum wall velocity: ft/s

V_i: Minimum wall velocity: ft/s

Morel [48] indicates that the values of $Cp_i \simeq 0.45$ and $Cp_e \simeq 0.1$ are good upper bounds below which boundary layer separation is unlikely to occur. Figure(B.2)demonstrates the variation of pressure coefficients for nozzles with contraction ratio of 4:1.

For our design, the particular values chosen for the wall pressure coefficients were:

$$Cp_e = 0.024 \quad \text{and} \quad Cp_i = 0.145$$

From figure(B.3),when the values of Cp_e and Cp_i are known, we can obtain the corresponding values of the dimensionless parameters F_e and F_i which are defined as:

$$F_e = \frac{m-1}{m^3} (1-X)^{-2}(L/H_1)^{-3} \qquad (1)$$

and

$$F_i = \frac{m-1}{m} (X)^{-2}(L/H_1)^{-3} \qquad (2)$$

where:

m: H_1/H_2: inlet to outlet nozzle height ratio

X: x_m/L: shape parameter (fig. B.1)

L: nozzle length; ft.

H_1: inlet nozzle height; ft.

Equations(1) and (2), when solved for X, yield to the equation:

$$X = [1 + \frac{1}{m} (F_i/F_e)^{0.5}]^{-1} \qquad (3)$$

The values of F_i and F_e are (from fig. B.3) 0.59 and 0.083, respectively. The value of m, as defined previously, is 4. Equation (3) yields to X = 0.6. By substitution of the value of the shape parameter X, into equation (1) and solving for L (nozzle length) we obtain:

$$L = 3.05 \text{ ft.}$$

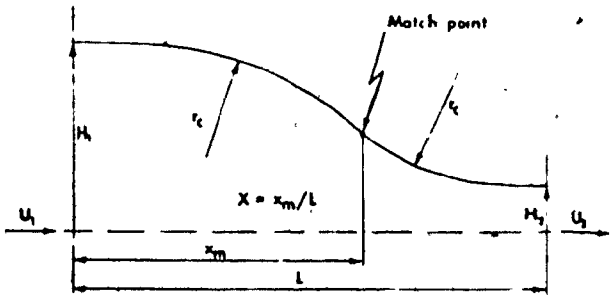

Figure B.1 Wall Shape Made of Two Cubic Arcs.

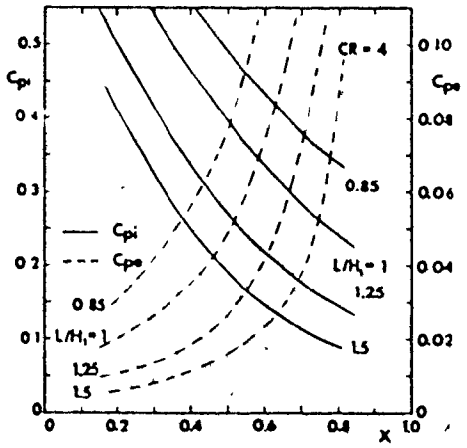

Figure B.2 Variation of Pressure Coefficients.

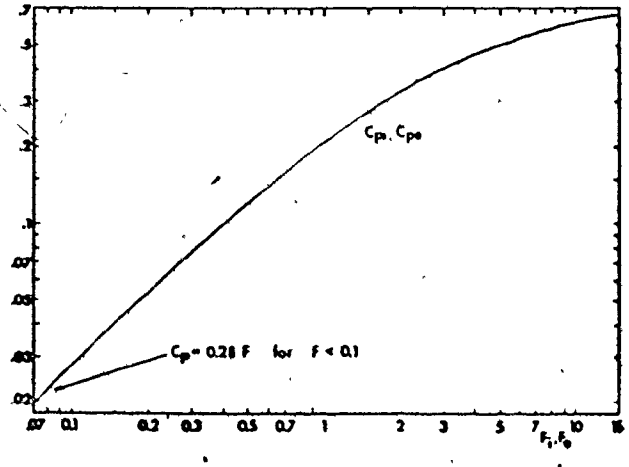

Figure B.3 Dependence of Pressure Coefficients on Dimensionless Parameters F_e and F_i.

When the values of the wall-shape parameter X and nozzle length L are known, the equation of the contour coordinates (H, x) can be obtained from the following equations:

$$(H - H_2)/(H_1 - H_2) = 1 - [(X^{-2})(x^3/L^3)] \text{ for } x/L \leq X$$

and $$(H - H_2)/(H_1 - H_2) = (1 - X)^{-2}(1 - x/L)^3 \text{ for } x/L > X$$

which yields to the final form of the contour equation:

$$H = 2 - 0.147x^3 \text{ ; for } x/L \leq 0.6 \text{ ; ft.}$$

$$H = 0.375(1 - (x/3.05))^3 + 0.5 \text{ ; for } x/L > 0.6 \text{ ; ft.}$$